AN EXPERIMENTAL INVESTIGATION OF THE NEAR-WALL FLOW STRUCTURE DURING DRAG REDUCTION

By

DAVID KENYON OLDAKER

Bachelor of Science

Oklahoma State University

Stillwater, Oklahoma

1973

Submitted to the Faculty of the Graduate College
of the Oklahoma State University
in partial fulfillment of the requirements
for the Degree of
MASTER OF SCIENCE
December, 1974

AN EXPERIMENTAL INVESTIGATION OF THE NEAR-WALL FLOW STRUCTURE DURING DRAG REDUCTION

Thesis Approved:

W. G. Tiederman, Jr.
Thesis Adviser

P. W. Morrell

Gerald Bruseuitz

D. D. Durham
Dean of the Graduate College

ACKNOWLEDGMENTS

I would like to personally thank my adviser, Dr. William Tiederman, who has made a significant contribution to my overall education and provided excellent guidance throughout this study. I would also like to thank Dr. Peter Moretti and Dr. Gerald Brusewitz for their helpful comments and discussion. I am also most grateful to my loving and patient wife, Sharon, for typing and putting up with me.

This study was financed and made possible by the National Science Foundation Grant GK-40609 which was greatly appreciated. Thanks also go to Mr. and Mrs. Sam Banks and Mr. and Mrs. Carl Oldaker for their financial assistance, Dow Chemical and Union Carbide for their generous contributions of polymer, Charlene Fries for typing the final manuscript, and Eldon Hardy for his excellent art work. The comments and suggestions of Alan Smith were helpful in the development of the new lighting technique employed in this study. The assistance of Hossein Bina and Afshin Ghajar was also greatly appreciated.

This research was conducted at the Basic Fluid Dynamics Laboratory, Department of Mechanical and Aerospace Engineering, Oklahoma State University.

TABLE OF CONTENTS

Chapter		Page
I.	INTRODUCTION	1
	The Drag-Reduction Phenomena	1
	The Turbulent Wall Structure	2
	Objectives	5
II.	EXPERIMENTAL TECHNIQUES	9
	Experimental Apparatus	9
	Preparation of Solutions	11
	Polymer Solution Characterization	12
	Channel Wall-Shear Stress Measurements	14
	Flow Visualization Techniques	16
III.	EXPERIMENTAL RESULTS	29
	Channel Qualifying Data	29
	Polymer Solution Characterization	31
	Transition in Channel Flows	33
	Qualifying Data for Streak Spacing Measurements	34
	Streak Spacing Measurements	41
	Streak Behavior in Drag-Reducing Flows	48
IV.	DISCUSSION	52
	Streak Formation	52
	Streak Spacing	55
	A Proposed Model of the Near-Wall Streak Structure During Drag Reduction	61
V.	SUMMARY, CONCLUSIONS AND RECOMMENDATIONS	65
	Summary	65
	Conclusions	68
	Recommendations	68
BIBLIOGRAPHY		70
APPENDIX A - VISUAL OBSERVATIONS IN TRANSITION FLOWS		74
APPENDIX B - COMMENTS ON STREAK BURSTING		77

Chapter Page

APPENDIX C - COMMENTS ON FLUORESCENT DYE LIGHTING TECHNIQUE . . . 85

APPENDIX D - MIXING TECHNIQUE AND SOLUTION CHARACTERISTICS 86

APPENDIX E - PRE-RUN AND DATA REDUCTION CALCULATIONS 88

APPENDIX F - UNCERTAINTY ESTIMATES 92

APPENDIX G - FIGURES AND ILLUSTRATIONS 95

LIST OF TABLES

Table		Page
I.	Polymer Characteristics	8
II.	Summary of Flow Visualization Methods	23
III.	Summary of Experimental Conditions	30
IV.	Comparison Between Methods of Data Reduction	37
V.	Summary of Flow Conditions and Major Results	42

LIST OF FIGURES

Figure		Page
1.	Schematic of Two-Dimensional Channel and Circulation System	96
2.	Line Diagram of Pipe Pressure Drop Apparatus	97
3.	Back Lighting Technique for Visualization of Low-Speed Streaks	98
4.	Side Lighting Technique for Visualization of Wall Region	98
5.	Near-Wall Flow Structure as Revealed Using the Side Lighting Technique (Water Flow, Re $\cong$ 6000)	99
6.	End-View Cross Section of the Near-Wall Streak Structure as Viewed With the Side Lighting Technique	100
7.	Control Volume for Analysis of the Outer Bounds of Dye Seeping Into a Laminar, Constant Shear Flow	100
8.	Universal Friction Correlation for Internal Turbulent Flow	101
9.	Histogram of Transverse Location of Low-Speed Streaks for a Drag-Reducing Flow (Re = 10,280)	102
10.	Longitudinal Distribution of the Spanwise Streak Spacing	103
11.	Streak Spacing Histogram for Solvent Flow (Re = 15,560)	104
12.	Streak Spacing Histogram for a Drag-Reducing Flow (Re = 10,280)	104
13.	Streak Spacing Histogram for a Drag-Reducing Flow (Re = 23,100)	105
14.	Comparison of Drag-Reducing Streak Spacing Histogram to Solvent Histogram	105
15.	Number of Samples Required to Determine $\overline{\lambda}$ in a Water Flow (Re = 15,560)	106
16.	Number of Samples Required to Determine $\overline{\lambda}$ in a Drag-Reducing Flow (Re = 23,100)	106

Figure Page

17. Non-Dimensional Streak Spacing for Non-Drag-Reducing Flows . . 107

18. Variation in Non-Dimensional Streak Spacing With Sublayer Dye Flow Rate Ratio for a Water Flow (Re = 15,200) 108

19. Effect of Sublayer-Dye Flow Rate Ratio on Non-Dimensional Streak Spacing 109

20. Non-Dimensional Streak Spacing for Drag-Reducing Solutions (Counting Technique I) $4 < M < 16$ 110

21. Comparison of Non-Dimensional Streak Spacing With Other Investigators ($4 < M < 16$) 111

22. Percentage Increase in Dimensional Spacing Between Streaks for Drag-Reducing Flows ($4 < M < 16$) 112

23. Non-Dimensional Streak Spacing for Drag-Reducing Solutions (Counting Techniques II and III) 113

24. Formation and Growth of a Streak Pair (AP-273, Re = 18,400, M = 13.6) 114

25. Growth of a Streak Pair 0.112 Seconds After Initial Disturbance to Wall Dye (AP-273, Re = 18,400) 115

26. Near-Wall Large Eddy Structure as Proposed by Bakewell et al. (2) and Sirkar et al. (34) 116

27. Proposed Near-Wall Eddy Structure Under Drag-Reducing Conditions 116

28. Expected y^+ Variation in Non-Dimensional Streak Spacing at Various Values of Drag Reduction 117

29. Proposed Near-Wall Streak Structure at Large Values of Drag Reduction 118

30. Sketch of the Relation Between Centerline Dye Bulge and Turbulent Wall Disturbance During Transition (AP-273, Re $\cong$ 7,800) 119

31. Patch of Wall Turbulence During Transition (AP-273, Re $\cong$ 8,000) 119

32. Visually Observed Flow Regimes Corresponding to Friction Factor Data 120

33. Back Lighting Technique for Dual View Visualization of Wall Region 121

Figure Page

34. Streak Ejection Distribution for a Water Flow (Re = 15,400) . . 122

35. Streak Ejection Distribution for a Drag-Reducing Flow (Re = 10,000) 122

36. Near-Wall Streak Structure as Visualized Using the Back Lighting Technique (AP-273, Re = 13,000) 123

37. Vortical Motion Associated With Newtonian Streak Bursting . . . 123

38. Viscosity-Shear Rate Dependence of the Drag-Reducing Solutions 124

39. Drag-Reducing Characteristics of 100 p.p.m, AP-273 125

NOMENCLATURE

A_c	cross-sectional area of pipe or channel
b	length or span of dye slot
D_H	hydraulic diameter, $D_H = 4\ A_c/WP$
F	spatially averaged ejection rate
f	friction factor, $f = -\Delta P\ D_H/2L\ \rho\ U^2$
k	total number of measurements of the distance between two adjacent low-speed streaks
L	distance between static pressure taps
M	mass flow rate ratio of sublayer to dye slot, $\dot{m}_s/\dot{m}_d$
$\dot{m}_d$	dye slot mass flow rate, $\dot{m}_d = \rho\dot{Q}_d$
$\dot{m}_s$	mass flow rate of dye through the viscous sublayer, $\dot{m}_s = \rho\dot{Q}_s$
N	number of occurrences
N_i	number of streaks in the i^{th} frame
n	total number of frames sampled
P	static pressure
$P(\lambda)$	probability density
$\dot{Q}$	volumetric channel flow rate
Re	Reynolds number, $U\ D_H/\nu$
T	fluid temperature
$\overline{T}_B$	mean time between bursting periods
$\overline{T}_E$	mean time between ejections
U	mass-average velocity
U_τ	wall-shear velocity, $U_\tau = (\tau_w/\rho)^{\frac{1}{2}}$

W	channel width
WP	wetted perimeter
x^+	non-dimensional longitudinal or downstream coordinate, $x^+ = xU_\tau/\nu$
y^+	non-dimensional coordinate normal to the wall, $y^+ = yU_\tau/\nu$
y_d^+	non-dimensional bounds of the dye normal to the wall, $y_d^+ = y_d U_\tau/\nu$
z^+	non-dimensional spanwise or transverse coordinate, $z^+ = zU_\tau/\nu$

Greek Letters

Δ	difference
λ_j	distance between two adjacent low-speed streaks
$\bar{\lambda}$	average streak spacing
λ^+	non-dimensional streak spacing, $\lambda^+ = \bar{\lambda}U_\tau/\nu$
ν	kinematic viscosity of the fluid
ρ	density of the fluid
ρ'	effective density of manometer fluid, $\rho' = (\rho_s - \rho_{CCl_4})$
σ	standard deviation of a sample space
τ_w	wall shear stress

Subscripts

i	frame number designation
p	polymer solution
s	solvent (water)
CCl_4	carbon tetrachloride

Special Symbols

%D.R. percentage drag reduction for a constant solvent Reynolds number,

$$\%D.R. = \frac{\Delta P_s - \Delta P_p}{\Delta P_s} \times 100$$

CHAPTER I

INTRODUCTION

The Drag-Reduction Phenomena

Drag reduction has been extensively studied over the past several years and many investigations have been devoted to the task of identifying and correlating the variables on which the level of drag reduction depends (i.e., Reynolds number, solution concentration and type, etc.). A summary of the important results from the most current drag-reduction studies are given by Hoyt (17) and Lumley (23). From these many recent investigations there are certain phenomena which now seem to be generally well established as characteristic features of drag-reducing flows. Many investigators have found that reductions in friction only occur when the flow is turbulent, but not to the extent that the flow becomes laminar again. A maximum drag-reduction asymptote is approached, independent of polymer concentration or properties, and cannot be exceeded even for high molecular weight polymers. There is some feature of the flow which even in the presence of the polymer additives prevents complete relaminarization.

Perhaps the most interesting characteristic is that drag-reduction is a wall phenomenon, that is, the polymer additives must be in the near-wall region before a decrease in the production of turbulent kinetic energy can begin. This is clearly seen in the experiments of Wells and Spangler (37) who injected a polymer solution both through a wall slot

and at the centerline of a 38 mm diameter pipe flow of water. Drag reduction did not occur until the polymer solution injected at the centerline had diffused into the wall region; however, the wall slot injected polymer yielded a reduction in friction, beginning only a short distance downstream from the slot. Therefore it was conclusively demonstrated that the polymer additives must be in the wall region to be effective. Velocity profiles measured by Reischman and Tiederman (31) indicate no increase in non-dimensional sublayer thickness from that of water flows. However, Reischman did find an extended buffer region in which the zone of maximum energy production had moved away from the wall. Recent interest has turned toward observing changes in the turbulent wall structure of drag-reducing solutions in order to gain a better understanding of how friction reduction occurs.

The Turbulent Wall Structure

The turbulent wall structure has been the subject of major experimental investigation for many years. Unlike free turbulent flows, wall flows produce as much turbulent kinetic energy as they dissipate, such that a level of turbulence is always maintained. The mechanism through which wall turbulence sustains itself is not completely understood; however, a narrow region near the wall $y^+ < 30$ appears to be the major area of interest since both the production and dissipation of turbulent kinetic energy reach their maximums near the wall.

The role of the wall structure in the production of turbulence was revealed by Kline et al. (21), in which the physical structure of the near-wall region of bound turbulent shear flows were studied. Visual studies of the viscous sublayer have revealed a longitudinal,

streaky pattern aligned in the flow direction. These patterns are made visible through either wall dye slot injection or hydrogen bubble time lines. Hydrogen bubble time lines have revealed a spanwise variation in the axial velocity component in the wall region. The regions of low velocity are associated with the longitudinal streaky pattern. In both cases the tracer collects in low-mean-speed regions. Previous investigators have reasoned that the tracer between the streaks is washed away by the high velocity regions leaving only the low-speed regions to be marked. Cross correlations from instantaneous spanwise velocity profiles, as obtained by the hydrogen bubble technique, also reveal streak spacings comparable to the spacings observed visually. The mean spacing between these longitudinal streaks depends upon the flow conditions and fluid properties. However, when the spacing of this dominant near-wall event is normalized with the proper wall (inner) variables, the structure has a characteristic non-dimensional spacing ($\lambda^+ = \frac{\lambda U_\tau}{\nu}$) of near 100. Cross correlations from measurements using laser holographic and electrochemical techniques have further supported the universality of this number for near zero pressure gradient flows. Schraub and Kline (33) have found this characteristic number to be reasonably constant over a moderate range of pressure gradients. Near relaminarization, under highly accelerated conditions the spacing approaches $\lambda^+ \cong 260$.

To orient the reader, an overview of the near-wall flow structure as observed by many investigators will now be presented. As mentioned earlier, large spanwise variations in the axial velocity component exist near the wall. The low-speed regions are visualized as a longitudinal streaky structure which periodically becomes unstable and bursts away from the wall. Kim et al. (18) have performed a detailed study of the

breakup (bursting) process of low-speed streaks. In general, as the streaks move downstream very near the wall ($y^+<10$) they lift up and begin to oscillate or wave until reaching into the buffer region where they break up in chaotic motion and move rapidly out away from the wall. Kim estimated that nearly 70% of all the production occurs during the bursting period. Investigations by Corino and Brodkey (7), Wallace, et al. (36), Lu and Willmarth (22), and Nychas, et al. (27), have shown that a sweep event involving fluid traveling toward the wall at a velocity faster than the local mean, also produces an important contribution to the Reynolds stress. Wallace estimates that the contribution from "sweep" events is also nearly 70% of the total production.

Most recently Offen and Kline (28) have shown that the interaction between bursts and the flow in the logarithmic region produces "sweeps" which, in turn, influence the generation of bursts farther downstream. Offen found a high correlation between a wallward moving disturbance and streak lift-up prior to bursting, but could not conclude that the sweep triggered the burst, although it seems highly likely. Blackwelder and Woo (4) have attempted to trigger the bursting phenomenon by a simple periodic pressure perturbation in the outer flow. They concluded that there was no correlation between applied pressure disturbance and the bursting phenomenon; however, they still suggest that bursts may be triggered from the outer flow by a more complicated pressure perturbation.

It is becoming more apparent now that the basic nature of the turbulent boundary layer energy chain is similar to a negative feedback loop. Within the total cycle, low-speed streaks come under the influence of a wallward moving disturbance, become unstable and burst

away from the wall. When the wallward moving disturbance arrives at the wall just downstream of the ejected streak it moves along the wall and is stretched out creating new streaks. Combinations of these ejected disturbances upstream gives rise to large scale turbulence in the outer flow, which "sweeps" back toward the wall triggering "bursts" from streaks just formed by the previous sweep and creating new streaks just downstream. The cycle continues endlessly with all the processes in statistical balance and equilibrium. Suppression of any process in the chain would cause the turbulent energy balance to adjust at a new equilibrium condition with lower production and dissipation.

Objectives

The overall objective of this study was to observe and quantify changes in the near-wall flow structure under drag-reducing conditions. These observations would yield a better understanding of how the polymer additives affect turbulent flows. The results obtained in the two-dimensional channel would be sufficiently general, in that they would be equally applicable to most bounded shear flow problems. The scope of such a study could be very broad and beyond the capabilities of the author to examine in detail, therefore attention was directed primarily to changes in the non-dimensional mean spacing of low-speed streaks during drag reduction. Some preliminary observations were also made of streak ejections to gain further insight into changes in the near-wall turbulent production process during drag-reducing conditions. Other observations concerning the general behavior of the wall structure during transition and fully turbulent flow were also made, but the primary objective was to focus on quantifying changes in streak spacing

during drag reduction.

At the onset of this study only three works were available in the literature which quantified changes in the near-wall streak spacing during drag-reducing conditions. Donohue, et al. (9) for 140 p.p.m. solutions of polyethylene oxide-FRA employed dye visualization techniques similar to those used in the Stanford studies. Fortuna and Hanratty (12) carried out a mass-transfer controlled electrochemical reaction to circular 0.102 mm electrodes mounted flush in a 25.4 mm pipe for 160 p.p.m solutions of SEPARAN AP-30. The mass transfer to the wall at these high Schmidt numbers is controlled by the velocity field well within the viscous sublayer. They obtain the mean spacing from time average spatial correlations of the axial velocity gradient. Eckelman, et al. (10) measured instantaneous eddy patterns from the data of Fortuna (11). The average streak spacing was obtained from the analysis of a large number of eddy patterns. Bakewell and Lumley (2) and Sirkar and Hanratty (34) have suggested that the viscous sublayer is characterized by flow-oriented eddies which have an average spacing equal to the mean spacing of low-speed streaks. In these three investigations, either the method of data reduction or the technique used to detect and sense the streaks varies significantly. In addition, the results obtained using the electrochemical technique are seen to differ significantly from those obtained using the wall dye slot technique. The data of Donohue, et al. (9) show that the spacing increases nearly linearly with drag reduction while results obtained from the electrochemical technique show a faster than linear increase at higher values of drag reduction. The differences were noted by Donohue, et al. (9) and were believed to be due to either polymer type and/or technique

employed in detecting the streaks. It was therefore the objective of this study to resolve these differences in results as obtained by the various investigations and obtain the correct dependence between non-dimensional streak spacing and the level of drag reduction.

This objective was achieved by (1) varying the flow conditions and, (2) the counting technique used to detect and sense the streaks. The flow conditions were changed by independently varing both the type and concentration of the polymer solutions over a wide range of flow rates. The counting technique used to identify the streaks was also varied to determine if the differences between Donohue et al. (9) and Eckelman et al. (10) were due to technique employed in sensing the streaks.

The experimental objectives were to: (1) Identify low-speed streaks in the near-wall region of a fully developed two-dimensional turbulent channel flow during drag-reducing conditions. (2) Obtain from films data concerning their average spacing. (3) Correlate the results and test for universality of the correlation. These objectives were realized through the use of flow visualization techniques. Visualization of the effects of drag-reducing additives on the near-wall structure was made possible by seeping dilute dye solutions into the viscous sublayer of a two-dimensional turbulent channel flow. The dye moves downstream along and very close to the wall, marking longitudinal low-velocity regions. Movies taken of these dye-marked low-velocity streaks were analyzed to obtain the mean streak spacing.

Two polyacrylamides and a single polyethylene oxide were chosen for use in this study. Polymer characteristics as advertised by manufacturer are given in Table I.

TABLE I

POLYMER CHARACTERISTICS

Polymer	Molecular Weight[1]	Manufacturer
Magnifloc 837-A (polyacrylamide)	15×10^6	American Cyanimid
Separan AP-273 (polyacrylamide)	7.5×10^6	Dow
Polyox WSR-301 (polyethylene oxide)	4×10^6	Union Carbide

[1]Advertised.

High molecular weight solutions were needed to obtain drag reduction in the two-dimensional channel at wall-shear velocities low enough that flow visualization techniques could be employed. The level of drag reduction was obtained through measured pressure drop in the channel during each experiment.

During the course of this study, a new lighting technique was employed for the visualization of the near-wall region. The advantage of this new lighting scheme is that it yields more information concerning the physical behavior of the near-wall flow while permitting observation of the structure in three dimensions. A summary of the flow conditions may be found in Table III with a summary of experimental results given in Table V. Major results concerning streak spacing data are found in Figures 17 and 19 through 23 of Appendix G. Discussion of results is given in Chapter IV with conclusions and recommendations presented in Chapter V.

CHAPTER II

EXPERIMENTAL TECHNIQUES

This chapter presents the details of the flow facility, and experimental procedures used for data acquisition and reduction.

Experimental Apparatus

The two-dimensional channel used in this study was a modified and rejuvenated version of the channel originally constructed by Donohue (8). It is nominally 38 mm wide, 454 mm tall, and 2.54 m long. Two pressure taps were added to the channel so that the wall-shear stress could be measured in the fully developed flow of the test section. These taps were located 457 mm apart with the first tap 1.78 m downstream from a two-dimensional bell mouth entrance. The second tap is eight channel widths upstream from the end of the channel where the flow enters a constant-head weir tank. These locations were chosen so that the upstream tap was far enough downstream for the flow to be fully developed and the downstream tap was far enough from the end of the channel for it to be uneffected by the sudden expansion of the flow area at the end of the channel.

To insure that the channel width was constant, a Plexiglas gauge block was milled to a width of 38.1 $\pm$ .08 mm and the width between the channel walls set to these dimensions. However, additional complications could have arisen from a longitudinal variation in the degree of bowing

of the channel walls by hydrostatic pressure. To solve this problem the walls were supported from bowing over the last 1.07 m of the channel by three spanwise Plexiglas blocks 25.4 mm wide, 63.4 mm thick and spaced 305 mm apart. These were complemented by two sets of longitudinal bracing blocks 12.7 mm wide and 50.8 mm thick. All bracing was milled flat before construction. As a final check the channel inside width was gauged at the top and bottom using a micrometer. The maximum longitudinal variation in channel width was 1% while the maximum longitudinal variation in channel height was 0.1% over the last 0.8 m of the channel. As a further check the channel was gauged at the top, middle and bottom while water was flowing at approximately 6.3×10^{-3} m^3/s. There was some slight bowing due to hydrostatic pressure. The top and bottom gauged at 38.23 mm and the middle at 39.24 mm. This is about a 2.5% variation in the channel width. The excess area over that of a uniform 38.1 mm width was then calculated yielding a cross-sectional area of 175.81 cm^2 and a hydraulic diameter of 71.67 mm. These values were then used for calculation of the mass-averaged velocity and Reynolds number, since they are the best estimate of the channel cross-sectional area and hydraulic diameter.

The upstream settling chamber consists of two sets of flow straighteners which redistribute the inlet flow evenly before the entrance. Probing the flow field with needle dye injection indicates that this is the case. It should be emphasized here that the entire flow system is constructed from Plexiglas, PVC, and stainless steel only, hence minimizing the possibility of degradation by contamination from the system itself.

The experiments in this study were conducted using the flow system constructed by Reischman (30) and shown in Figure 1. Experiments with water were carried out in a closed loop system utilizing a centrifugal pump with a maximum continuous capability of 1.26×10^{-2} m^3/s. Experiments with dilute polymer solutions were made without the use of the pump and hence mechanical degradation of the solutions was minimal. To carry out these experiments a 13.63 m^3 upstream stainless steel tank was pressurized, forcing the fluid through the channel. The maximum flow rate from the pressurized tank was approximately 1.26×10^{-2} m^3/s. Fluid leaves the channel through a 305 mm x 305 mm overflow, constant-head tank. After passing over the weir, solutions were caught in the open-top 2.27 m^3 tank and drained through the system drain. None of the polymer solutions were reused or recirculated.

Preparation of Solutions

The polymer solutions were prepared by first mixing a concentrated (1000-2000 ppm) solution and then diluting to the desired (50-200 ppm) concentration. The first step in the solution preparation was heating the water in a 0.38 m^3 stainless steel open-top mixing tank with an immersion heater to approximately 30°C. Either 700 or 1400 grams of polymer crystals were then added to approximately 0.008 m^3 isopropanol alcohol and suspended by continuous stirring. The mixing tank was stirred vigorously and the alcohol-polymer suspension was quickly added to the heated water. At this point continued gentle stirring and thorough mixing are essential. This step is an important one, since thorough dispersion of the particles allows a viscous envelope to surround each of the crystals. This is essential for supressing

agglomerations or so-called "fish-eyes" and obtaining a homogenous well mixed solution. The concentrated solutions were occasionally stirred during the 1.5 to 2 hours that was provided for polymer hydration before dilution. This method of mixing yielded homogenous solutions without any visible agglomerations.

The second step consisting of dilution and mixing was carried out in the 2.27 m^3 open-top catch tank. Water was passed through 5 μm filters before entering the catch tank into which the concentrated solution was slowly gravity drained and mixed to the proper concentration for the experiment. After mixing, each solution was clear and visibly free of "fish-eyes." The solution was then gravity drained to the 13.63 m^3 storage tank for later use. Experiments conducted with 100 p.p.m AP-273 show that the drag-reduction levels off and reaches a maximum about 24 $\pm$ 6 hours after mixing. Experiments with 100 and 200 p.p.m AP-273 were run approximately 18-24 hours after the solutions were mixed and 50 p.p.m. AP-273, 12-18 hours after mixing. The 837-A solution was run after remaining in the 2.27 m^3 storage tank for 3 hours while the Polyox WSR-301 solution was run only 20 minutes after mixing, due to its fast rate of degradation.

Polymer Solution Characterization

Drag Reduction

A characterization of the drag-reducing solutions was performed after each data run. This characterization yielded the drag-reduction as a function of solvent wall-shear stress, and gave a means of testing the consistancy between each batch of polymer solution mixed.

The pipe pressure drop apparatus used in this study is shown in Figure 2. The system is constructed from stainless steel, flexible rubber hose, and contains no pumps. A 0.265 m^3 stainless steel tank was filled by gravity draining solution from the channel immediately after each data run. All manometer lines were cleared of air and a manometer "zero" reading was taken both before and after running each pipe. The two pipes used were gauged at 10.9 mm and 21.2 mm inside diameter using a micrometer. Test section lengths were 1.45 m and 2.88 m respectively with a distance to the first tap of 1.38 m and 2.12 m. The 0.265 m^3 tank was then pressurized to force the fluid through the pipes. The flow rate was determined from a calibrated flowmeter located at the system exit. None of the solutions were recirculated or reused.

Viscosity

The viscosity at the wall-shear rate of each experiment is needed for the non-dimensionalization of data. Solution samples were taken from the downstream head tank during each run or immediately after each run. Two Couette viscometers (Brookfield Synchro-Electric Model LVF with UL adapter and a Fann Model V-G) were used to obtain the shear-rate dependence of viscosity over a range from 15 to 1022 sec^{-1}. Wall shear rates for the channel experiments, were in the 70 to 280 sec^{-1} range. Viscosity samples taken from the top and bottom of the storage tank indicated that solutions were homogeneously distributed in concentration.

Channel Wall-Shear Stress Measurements

The wall-shear stress during each run was calculated from the pressure difference measured between two 3.18 mm diameter wall taps located 83 mm from the "floor" of the channel and 457 mm apart. A two-fluid micromanometer using carbon tetrachloride and water, which was rigidly mounted to the channel frame, was used to measure the pressure difference. Chromic acid was used periodically for cleaning the inside of the glass manometer. The micrometer dial has 0.25 mm divisions and the stainless steel needle indicator was cut to a long sharp point on a lathe and polished with 400 grit emery paper.

Pressure drop measurements were made during each run only after the manometer had reached equilibrium. Mass average velocities were calculated from flow rates which were obtained during each run by timing the collection of a measured volume of fluid caught in a 0.152 m^3 rectangular stainless steel container.

A commonly used procedure for measuring flow rate is to simply detour the flow into a container for a measured period of time. However, deflecting fluid from over the weir into a container was not practical in this case. Instead a stainless steel container was mounted on wheels and placed in the 2.27 m^3 open-top catch tank where it could be quickly rolled under the weir for fluid collection and quickly removed when full. Level indicators with 1 mm divisions were placed in each of the four corners of the collection bucket and the bucket was calibrated with a known volume of fluid. After collection, the fluid level in each of the four corners was recorded and then averaged to obtain the collected volume. Volumes collected were accurate to about 3%, and the collection

time was accurate to approximately 0.4 sec. or 2%. The fluid temperature during each run was recorded with an accuracy of $\pm$ 0.1°C. and a solvent Reynolds number based on hydraulic diameter was calculated from which a solvent based friction factor was obtained from Figure 8. This was the primary method used to determine the channel mass-average velocity during the experiments.

For setting the channel flow conditions, the rectangular weir at the exit of the head tank was used for approximate flow rate measurements. To obtain accurate weir height measurements, Tygon tubing was connected to the bottom of the constant head tank and run alongside a vertical scale with 0.397 mm divisions which was secured to the downstream tank. In this section of tubing, a short orifice element approximately 0.8 mm in diameter served to dampen out the effect of small scale surface fluctuations on the weir measurement caused by turbulent mixing in the constant head tank. Weir height measurements were made during each run and the calibration was used as a secondary standard for flow measurement. The weir height calibration was uneffected by the polymer additives.

With the wall-shear stress calculated from pressure drop measurements and the mass-average velocity calculated from the flow rate measurements, a friction factor for the drag-reducing flows was obtained through the relation:

$$f = 8 \left(\frac{U_\tau}{U}\right)^2$$

The reduction in drag, defined through the following relation was then calculated for each flow condition.

$$\frac{\text{Percent Drag Reduction}}{100} = \left(\frac{\Delta P_s - \Delta P_p}{\Delta P_s}\right)_{Re_s = \text{Const.}}$$

Details regarding the calculation of wall-shear stress and level of drag reduction are given in Appendix E.

Flow Visualization Techniques

Wall Dye Slot

Visualization of the near-wall region is accomplished by seeping dye through the two wall dye slots previously used by Donohue (8). These slots are 0.127 mm in the streamwise direction and 178 mm in the spanwise or transverse direction. The slot locations are 1.78 m and 2.06 m downstream from the two-dimensional entrance. It should be pointed out, however, that since the channel walls were constructed from a single continuous sheet of Plexiglas and the slots made free of any burrs, disturbances produced by the wall were minimized. Each dye slot could be masked off to allow, on the average, only a specific number of low-speed streaks to be marked. This was accomplished using masking tape and modeling clay on the inside of the dye slot. No tape or obstructions were on the flow side of the dye slot.

To insure that the dye flow was not disturbing the near-wall flow an estimate of the dye flow rate through the slot was essential. In initial experiments, the dye flow rate through the slot was controlled by the elevation of the dye pot reservoir above the weir tank. The dye flow rate had previously been calibrated as a function of the dye pot elevation for the specific solutions used in this study and with water flowing in the channel at approximately 4×10^{-3} m^3/s. The volume

flow rates from the dye pot reservoir were calculated by measuring the volume of dye which flowed out of the reservoir over a given period of time. Later experiments utilized a series of three Matheson rotameters to monitor dye flow rates ranging from 0.004 ml/s to 2.0 ml/s. Dye from the dye pot reservoir flows through one or more of the rotameters before passing through the dye slot. Dye flow rate was controlled by the use of a valve located at the exit of the dye pot reservoir. Each rotameter was calibrated for each type of dye solution.

In order to interpret results of the dye visualization studies, it is necessary to estimate the region in the near-wall flow which dye marks. The dye near the wall is bounded in the z-direction by the span of the dye slot, both at the slot and further downstream since near the wall the transport of dye in the spanwise direction is small. The bounds of the dye normal to the wall are, however, not as easily defined. The following analysis is only a first approximation to a very complex problem. The problem may be better understood with the aid of Figure 7. Consider dye seeping into a laminar, constant shear flow. The outer edge of the dyed region is located at y_d. A control volume is drawn from the wall to $y^+ = 8$, over a long enough length (x) that the dyed fluid has taken on the character of the flow (i.e., linear velocity gradient), and extends across the span a distance equal to the slot length (b). The dye seeping through the slot turns downstream and aligns itself with the mean flow in a very short distance. The mass flow rate in the sublayer ($\dot{m}_s$) is then expressed as,

$$\dot{m}_s = b\rho \int_{y=0}^{y=8\nu/U_\tau} u\,dy = 32\, b\rho\nu$$

and the mass flow through the dye slot ($\dot{m}_d$) equals $\rho\dot{Q}_d$. From considerations at control surface 3 we may express $\dot{Q}_d$ as,

$$\dot{Q}_d = b \int_{y=o}^{y=y_d} u\,dy = \frac{b(U_\tau y_d)^2}{2\nu}$$

rearranging, the bounds of the dye normal to the wall (y_d) is given as:

$$y_d = \frac{1}{U_\tau} \left(\frac{2\nu\dot{Q}_d}{b}\right)^{\frac{1}{2}}$$

and in non-dimensional units as:

$$y_d^+ = \frac{y_d u_\tau}{\nu} = \left(\frac{2\dot{Q}_d}{\nu b}\right)^{\frac{1}{2}} = 8.0\ M^{-0.5}$$

The ratio of sublayer to dye mass flow rate is given the value M. The flow rate leaving control surface 2 is simply $\dot{Q}_d$. Turbulent flow in the viscous sublayer, however, is NOT laminar, or two-dimensional. Dye collecting into streaks is displaced from the wall by an amount dependent on the magnitude of the fluid motions which influence their formation and by the amount of dye locally available to collect into a streak (i.e.--the local dye flow rate). The influence of turbulence within the channel acts to increase the value of y^+ marked by the dye, hence the preceding estimates of the distance normal to the wall marked by the dye are somewhat low for the experimental conditions.

The thickness of the viscous sublayer was taken at $y^+ = 8$, based on the observation of Reischman (30), that there is no detectable difference in non-dimensional sublayer thickness between solvent and drag-reducing flows. The reader should remember that increasing values of M are associated with decreasing values of dye flow rate.

Dye Solutions

Two types of dye were used to visualize low-speed streaks. The first was a 0.25% solution of Methylene Blue and water. This dye was used only in initial water flow experiments.

The second dye used was a 0.25% solution of Rhodamine B base, a fluorescent dye made by J. T. Baker Chemical Company. The spirit soluable powder was mixed with anhydrous isopropanol alcohol in the proportion of 5g/50ml. This mixture was then added to two liters of water where it was mixed and filtered before use. A second fluorescent dye used was Rhodamine B (practical), a water soluable powder made by Eastman Kodak Company. A 0.12% solution (with no alcohol) yielded essentially the same dye color as the Rhodamine B base.

The two dye solutions were burgandy in color, though in natural powder state their color was different. The B base is a redish lavender while the B is a dark olive green similar to Fuchsine, another water soluable fluorescent dye. The molecular composition of these two dyes varies only by a chlorine and hydrogen atom.

For the polymer experiments, the dye solution was made from the same polymer solution used in the experiment. This was done to insure validity of the dye flow rate calibrations which were obtained with freshly mixed solutions. Also injection of dye mixed with either a degraded polymer solution or water into the near-wall region was not desirable. The prepared dye was maintained at the temperature of the solution in the storage tank, to insure that the viscosity of the dye solution was the same as the fluid into which it was injected. Before use, the dye was slowly filtered through a 150 mesh stainless steel

screen to eliminate any possible molecular aggregates or foreign material that might become lodged in the dye slot during the experiment. There was no measurable difference in viscosity of the filtered and non-filtered solutions.

Lighting Arrangements for Visualization of Low-Speed Streaks

Basically two lighting schemes were employed to study the near-wall streaks. The first was a back light arrangement utilizing a 160 watt tungsten light source covered by a frosted Plexiglas plate as shown in Figure 3. The camera was located approximately two meters from the channel on the opposite side. Dye seeping into the flow through the wall dye slot was silhouetted by a diffuse light source. In water flow experiments, the dye collected into streaks almost immediately after leaving the slot and proceeded only a short distance before bursting away from the wall in chaotic motion. The scene is the same as that visualized by Runstadler et al. (32), Donohue et al.(9), and Halleen and Johnston (15).

The second lighting technique was a side light arrangement (Figure 4) with Rhodamine dye seeping into the flow through the wall dye slot. Here, the light from four 500 watt photo flood lamps was projected down through the top of the channel. The lamps were evenly distributed over the last 0.75 m of the channel. The top of the channel was masked off to allow the light source to enter only across the channel width, eliminating internal reflection within the Plexiglas walls which would otherwise have to be filtered out by a polaroid lens. The camera was located about one meter from the channel, viewing the streaks in the

near-wall region from the "top" rather than the underneath side. This technique was most effective when the wall next to the dye was contrasted against a dark background and surrounding room lights were minimal.

Because of the dye's unique feature, in that it fluoresces, the near-wall structure appears self-illuminating. The result is a three-dimensional view of the dye marking the near-wall flow (Figure 5). The dye emitts light which is yellowish-gold in color. In laminar flow the dye is in the plane of the wall and fluoresces a uniform intensity yellowish-gold light. As the dye collects into a longitudinal structure it bulges out from the wall a small amount. Any disturbance to the dye or variations in displacement of the dye from the wall appear quite distinctively as "streaky protrusions" on the surface of the dye. Figure 6 shows an end-view cross-section of the near-wall streak structure as revealed using the fluorescent dye lighting technique. The streaks appear as a longitudinally oriented structure with finite volume and dimensions.

When back lighted, the streaks appear as longitudinally oriented dye structures which are much darker than the surrounding dye between the streaks. This coupled with the observation that dye marked streaks bulge out from the wall, strongly suggests that the absence of dye between low-speed streaks is a result of its collection into adjacent streaks and not the consequence of higher velocity fluid between the streaks washing the dye downstream.

Keep in mind that the dye fluoresces a three-dimensional view which depicts the motions of the fluid in the near-wall flow structure which it marks. The longitudinally oriented "peaks" in the dye are highlighted

on the side facing the external light source and appear more brightly illuminated than the dye in the plane of the wall. The side facing away from the external light source will appear as a shaded region compared to its surroundings. The effect is similar in principle to dark field illumination in that displacements from the wall are discriminated from their surroundings. This lighting technique offers a high resolution picture of the near-wall region. Contortions in the dye, on the order of the normal distance from the wall where dye marks ($\simeq$0.2 mm) could be detected. In principle, any fluorescent dye when properly lighted should produce the same effect, but will most likely yield a different color. The probability of streaks over-shadowing neighboring streaks and eliminating them from view was small, since some light was internally reflected from the channel walls hence minimizing the possibility. When back lit, the dye appears burgandy in color, and yields a two-dimensional silhouette of the near-wall structure.

No precise measurements were made of the normal distance from the wall (thickness) of these low-speed streaks. However, it is estimated that in both the water and drag-reducing flows the streak thickness seldom exceeded a y^+ of 10 before lifting into the buffer region where it was ejected away from the wall.

Photographic Techniques

Motion pictures were taken using a super 8 mm Beaulieu movie camera with an f-1.8, 25 mm lens. Kodak Ektachrome type A film was used without daylight filter at 24 frames per second. Higher flow rates required the use of Kodak 4-X Reversal film without filter at 36 frames per second. A limited number of 16 mm movies were made with a Bolex H-16

Reflex (f-1.8, 25 mm lens) at 24 frames per second. The 8 mm Ektachrome film gave excellent color rendition without the use of a daylight filter. Filtering should be used when photographing with 16 mm film of both the high-speed Ektachrome tungsten (7242) and daylight (7241) type. Ektachrome 35 mm film photographed at ASA 400 and $1/125^{th}$ second exposure without filters yielded excellent quality pictures. High-speed Ektachrome daylight film (ASA 160) photographed at ASA 400 and push processed gave excellent high resolution pictures. Ektachrome-X (ASA 64) rendered the colors slightly warmer and also produced an excellent picture. Typical duration of 8 mm real time filming was 100-200 sec. A summary of the lighting arrangements and dyes utilized for streak visualization is given in Table II.

TABLE II

SUMMARY OF FLOW VISUALIZATION METHODS

Lighting Technique	Dye	Film
Side light	Rhodamine B	8 mm & 16 mm Ektachrome
(Figure 4)	Rhodamine B Base	8 mm 4-X Reversal
Back light	Rhodamine B Base	8 mm & 16 mm
(Figure 3)	Methylene Blue	Ektachrome

Low-Speed Streak Counting Techniques

Films were analyzed using an MFS-8 Ektagraphic Super 8 mm projector. A limited number of 16 mm movies were analyzed using a Bell & Howell model 173 Time & Motion Study projector. Movies were viewed once or twice before beginning data reduction, giving observers time to examine the general character of the near-wall structure, and allowing time for the observers to adjust to the new surrounding light level. Play back speed was generally six frames per second (fps) for water flow experiments and 24 fps for polymer experiments. By randomly stopping the film, streak spacing data was obtained from approximately 15-20 frames per run. The time interval between two samples was kept long enough so that each measurement was independent and not correlated with its predecessor. Practically speaking, a sufficient time interval is three to four times the apparent bursting period of an individual streak. Polymer and water streak-spacing data were taken downstream from the dye slot at an approximate non-dimensional distance $x^+ = 1000$. The length of the dye slot typically was 102 mm for solvent flows and 150 mm for drag-reducing flows. The camera field of view extended about 200 mm downstream from the dye slot.

A specified set of rules was developed for the detection of low-speed streaks. A streak was defined as a single longitudinal structure which was distinct enough to stand out and be identifiable from its surroundings, and which had a length of at least four times the apparent spacing of neighboring streaks. This amounted to neglecting any short branches which were part of the main streak structure.

Since the method of streak detection has varied between different investigations, three different counting techniques were developed which represent three threshold levels of detection. These threshold levels will be used to determine the maximum and minimum number of streaks which might be identified using any detection scheme and to determine if differences in detection level account for the differences between Eckleman et al. (10) and Donohue et al. (9). All three techniques were applied to the same film only for a limited number of experiments.

Counting Technique I. Observers taking data were located 3.0-4.5 m in front of the viewing screen. The projected viewing area was approximately 1 m x 1 m. Each observer counted the number of streaks across the span (b) of the dye slot at a prescribed (x) location downstream and parallel to the dye slot. A streak was counted provided it was distinct enough to stand out and be identifiable from its surroundings as a single longitudinal structure of length greater than approximately four times the apparent spacing of neighboring streaks. It is important and consequently it is restated that this definition for a streak remained unaltered in all three counting techniques. The observers viewed across the span (b) of the slot applying the above criterion and identifying all streaks in a given frame. This technique might be referred to as a "normal" or "standard" technique since observers were located at a normal viewing distance from the screen and counted all visible streaks which satisfied the above definition for a streak. It is also believed that this method is consistent with that of Runstadler et al. (32) and Donohue et al. (9). This method is believed to yield the best estimate of mean streak spacing.

Counting Technique II. When viewing movies obtained using the side-lighting technique, the longitudinal streaks were highlighted, and this makes them readily identifiable from their surroundings. In Newtonian flows, all streaks were highlighted to about the same degree of brightness. However, in drag-reducing flows, some streaks were more brightly lit than others and in general appeared to be larger in both width and extent normal to the wall. These streaks were defined to be dominate streaks and in Counting Technique II only dominate streaks were counted. Estimates of an average spacing obtained using this technique represent an upper bounds for the mean spacing which could be obtained by other detection schemes.

Counting Technique III. The rules for streak identification are again the same as in Counting Technique I, except that observers taking data are located very close to, and at a distance of less than 1 m from the viewing screen. The purpose of this technique was to identify all possible streaks even those only barely visible in the movie. These estimates represent a lower bounds for the mean spacing which might be obtained by other detection schemes.

When the streaks in any given frame are identified, the mean spacing may be computed using two methods. The first method takes the number of streaks in the i^{th} frame (N_i) and divides into the span (b) over which the count was made forming the following expression for the mean value of streak spacing ($\overline{\lambda}$):

$$\overline{\lambda} = \frac{1}{n} \sum_{i=1}^{n} b/N_i$$

The second method is a little more tedious and involves measuring distances between adjacent streaks (λ_j) to form a histogram from which

the moments of the distribution may be calculated. The mean spacing is defined through the following relation:

$$\bar{\lambda} = \frac{1}{\kappa} \sum_{j=1}^{\kappa} \lambda_j$$

Similarly, the second central moment ($\bar{\lambda}^2$) or variance (σ^2) which is a measure of the relative width of the histogram may be calculated from,

$$\sigma^2 = \bar{\lambda}^2 = \frac{1}{k-1} \sum_{j=1}^{k} (\lambda_j - \bar{\lambda})^2$$

For the case of a discrete random variable, histograms were obtained by simply counting the number of λ_j values in a specified $\Delta\lambda$ interval. The probability density $P(\lambda)$ is defined as the probability of finding λ_j between λ and $\lambda+\Delta\lambda$. The mean value in each $\Delta\lambda$ increment is given as λ_q and s is the number of increments in the histogram. The third moment of the distribution yields a measure of the asymmetry of the histogram distributions and is normally non-dimensionalized with σ^3 to form the skewness factor $S = \bar{\lambda}^3/\sigma^3$. The kurtosis or flatness factor is obtained from non-dimensionalization with the fourth moment and is expressed as $K = \bar{\lambda}^4/\sigma^4$. The higher central moments were calculated from histogram approximations through the following relation:

$$\bar{\lambda}^r = \sum_{q=1}^{s} (\lambda_q - \bar{\lambda})^r P(\lambda)$$

where r is the degree of the moment and s is the total number of increments in the histogram. These distributions may be compared to a Gaussian distribution by calculation of the skewness and flatness factors. The Gaussian is that distribution approached by the sum of a large number of independent random samples. Deviations from Gaussian are due to some correlation between λ_j values or reflect the presence

of some phenomena associated with the streaks. For a Gaussian distribution S=0 and K=3. Positive skewness indicates more values are less than the mean than greater, while kurtosis less than three indicates the distribution is "flatter" than normal, where most of the tails of the histogram are within the limits of the standard deviation. Histograms of measured distances between streaks were formed for one solvent flow and two drag-reducing flows with essentially the same friction velocity U_τ, using the side-lighting technique.

CHAPTER III

EXPERIMENTAL RESULTS

This chapter presents the results of data obtained during both water and polymer flow experiments. The results are classified into three major categories: (1) channel qualifying data; (2) qualifying data for streak spacing measurements; and (3) streak spacing data.

Flow visualization studies were made in water at eight flow rates, and in 17 polymer flows at 13 levels of drag-reduction ranging from 13% to 62%. A summary of the experimental conditions for each run is shown in Table III and a quantitative outline of the results are given in Table V.

Channel Qualifying Data

The two-dimensional channel configuration remained essentially unaltered from the experiments of Donohue (8). He concluded using laser velocimeter techniques that mean velocity profiles measured at 47 channel widths (1.70 m) from the entrance were in good agreement with the universal turbulent velocity profile.

In this study pressure drop measurements were made in both a pipe and the channel to ensure that the two-fluid manometer was yielding correct results. The pipe system was constructed for temporary use by connecting the 13.63 m^3 upstream tank to a pipe running parallel to the channel. The exit of the pipe was connected to the channel settling

TABLE III

SUMMARY OF EXPERIMENTAL CONDITIONS

Solution Type	Conc. (p.p.m)	U (m/s)	Lighting, S-side B-back	$\dot{Q}x10^3$ (m^3/s)	T °C	Re UD/ν_s	Re UD/ν_p
Solvent	0	0.174	S	3.04	29.0	15,200	-
Solvent	0	0.180	S	3.10	23.6	13,210	-
Solvent	0	0.250	S	4.39	23.6	18,360	-
Solvent	0	0.260	B	4.73	12.8	15,400	-
Solvent	0	0.287	B	5.05	9.6	15,560	-
Solvent	0	0.287	S	5.05	9.6	15,560	-
Solvent	0	0.311	S	5.47	23.6	22,800	-
Solvent	0	0.335	B	5.87	9.4	18,100	-
Solvent	0	0.360	S	6.24	23.6	26,400	-
Polyox Coagulant	50	0.169	S	2.97	20.8	12,200	11,150
AP-273	50	0.232	S	4.01	23.8	17,000	13,000
837-A	100	0.238	S	4.18	26.7	16,700	19,750
Polyox WSR-301	100	0.248	S	4.36	26.7	16,700	20,600
AP-273	50	0.334	S	5.87	23.8	25,000	10,280
AP-273	50	0.401	S	7.05	28.0	33,600	22,900
AP-273	100	0.311	S	5.47	23.4	23,300	13,000
AP-273	100	0.360	S	6.31	13.2	21,500	13,850
AP-273	100	0.465	S	8.18	23.4	34,800	19,400
AP-273	100	0.445	B	7.82	13.0	26,600	16,400
AP-273	100	0.445	S	7.82	13.0	26,600	16,400
AP-273	50	0.557	S	9.78	28.0	46,700	31,800
AP-273	200	0.720	S	12.65	23.6	53,900	17,600
AP-273	200	0.620	S	10.90	26.7	51,300	18,400
AP-273	100	0.474	S*	8.33	27.2	39,800	23,100
AP-273	100	0.481	S*	8.45	26.7	39,900	21,800
AP-273	100	0.575	S	10.12	14.0	35,350	22,200
AP-273	100	0.637	S	11.18	26.7	52,800	33,400

*16 mm movies.

chamber inlet. The 6.1 m long PVC pipe was gauged at 62.3 mm inside diameter. Both the pipe and channel data are plotted in Figure 8, along with the well known Prandtl universal law of friction for smooth pipes and indicate that the micromanometer yields the correct results. Since the channel data falls slightly below the Prandtl relation, a line drawn through the two-dimensional channel data and parallel to the Prandtl relation was used to determine solvent pressure drop. The difference from the Prandtl relation was only 4%. The channel results are in agreement with Hartnett, Koh and McComas (16) who found that the circular tube correlation accurately predicts the friction coefficient for flow through rectangular ducts of any aspect ratio for Reynolds numbers based on hydraulic diameter between 6×10^3 and 5×10^5.

Pressure drop data from the 10.9 mm and 21.2 mm pipes obtained using an inverted u-tube manometer are also shown in Figure 8. They are also in agreement with the Prandtl relation.

Polymer Solution Characterization

Drag Reduction

As mentioned previously a careful characterization of each drag-reducing solution was performed after each data run. The results and a discussion of the drag-reducing solution's capabilities are presented in Appendix D.

Viscosity

The polymer solution Reynolds number was based on solution viscosity at the wall-shear rate of each run. The viscosity corresponding to the wall-shear rate of each run was obtained from a plot of the

viscosity-shear rate dependence for each solution, such as those shown in Figure 38. It is interesting to note the degree of non-Newtonian behavior for these fluids. The polyacrylamides are somewhat pseudoplastic while the polyethylene oxide is more Newtonian in behavior. However, the Magnifloc 837-A solution displayed Newtonian behavior, possibly the result of nearly 18 months of storage, since 12 months earlier the same dry stock batch yielded a much higher viscosity with slightly non-Newtonian behavior.

For "dilute" solutions, polymer molecules exist as isolated "regions" or segments separated extensively from each other by pure solvent. However, in reality it is doubtful that the polymer molecules exist as isolated "regions" in the highly sheared near-wall region. The maximum polymer concentration allowed for a thermodynamically dilute solution could not accurately be estimated using the method of Merrill, et al. (24), due to large uncertainties in the estimates of rms radius of gyration. Departure from Newtonian behavior is not a good indication of a concentrated solution, since as mentioned earlier polyacrylamides are more pseudoplastic and polyethylene oxides are more Newtonian in behavior. Virk, et al. (35) have pointed out that practically speaking, "dilute" solutions exhibit viscosity ratios less than about 2. The viscosity ratio being the ratio of polymer viscosity to that of water at the same temperature. The 100 p.p.m AP-273 solutions yielded approximate viscosity ratio of 1.75 at 37 sec^{-1} and were only slightly non-Newtonian, as was expected for the high molecular weight polyacrylamides. The 200 p.p.m solutions yielded a viscosity ratio of approximately 3.3 at 37 sec^{-1} and displayed quite non-Newtonian characteristics. The 100 p.p.m AP-273 solutions are therefore near the limit of being classified

as "dilute," while the 200 p.p.m solutions are most assuredly "concentrated."

Transition in Channel Flows

In order to correctly interpret the effects of drag-reducing macromolecules on the Newtonian near-wall structure, it is essential that comparisons be made only when "fully turbulent flow" exists. Turbulent activity must occur continuously in the near-wall region. The requirement of fully developed flow is not as critical since the wall structure is not influenced much by weak pressure gradients.

Considerable question has been raised as to effect of drag-reducing additives on transition, with a majority of the discrepancy between investigators due largely to the criteria used to distinguish fully turbulent flow. For this reason 8 mm movies were taken of the near-wall region utilizing the side-lighting technique, during channel flows of water; 50, 100, and 200 p.p.m AP-273 solutions, covering a wide range of flow rates from laminar to fully turbulent flow.

In channel flows, the structure of the near-wall during transition is more like that observed in a boundary layer, in that turbulent spots [Kline (19)] which form near the wall in early stages of transition spread and contaminate a larger portion of the flow as Reynolds number is increased. Near the end of transition, intermittent quiescent spots in the dye may appear. In this study "fully turbulent flow" was considered to exist when the visually observed near-wall was completely and continuously active (i.e., no intermittent appearance of quiescent spots).

For the water flow, the first evidence of a longitudinal wall structure was at about Re $\cong$ 2,000 with the appearance of groups of long "lazy" streaks, while the last evidence of intermittent quiescent spots occurred at Re $\cong$ 8,400. This value corresponds to Re $\cong$ 4,500 based on channel width.

In general, for drag-reducing solutions of 50, 100, and 200 p.p.m AP-273 the near-wall region was completely and continuously active in the Reynolds number range 4500-5400 based on channel width and solution viscosity. Centerline injected dye had diffused by turbulent action before reaching the vicinity of the dye slot. For all data runs in this study, a Reynolds number of 10,000 (5400 based on width) was chosen as the lower limit for continuously turbulent flow. Further comments regarding visual observations during transition are given in Appendix A.

Qualifying Data for Streak Spacing Measurements

This section serves to examine and specify some of the conditions under which streak spacing data will be taken and reduced. The location downstream from the dye slot where streaks are to be counted will be specified as well as the method of data reduction, once the streaks have been identified.

Streak Sampling Location

The streaks were found to occur at random locations across the span. Figure 9 shows no evidence of any spanwise variation in streak spacing and further indicates that the flow is two-dimensional.

For Newtonian flows, virtually all the dye injected through the slot had been transported and diffused away from the wall (except for a

small amount transported back to the wall) at $x^+ = 1500$. For drag-reducing flows, increased spacing between streaks and decreased values of eddy diffusivity [Reischman (31)] result in dye persisting near the wall for exceptionally long distances.

Longitudinal distributions of the spanwise streak spacing obtained from three flows are presented in Figure 10. By moving the camera downstream of the dye slot, it is seen that the value of $\overline{\lambda}$ is nearly constant over the limits observed $600 < x^+ < 3900$. This does not imply a streak length, but shows that due to the persistence of the dye close to the wall, nearly all the streaks were marked in the limits of viewing. In all drag-reducing runs, dye persisted near the wall to some degree, all the way to the end of the channel ($x^+ \cong 8000$). The location downstream from the slot where streaks are to be counted was then set at approximately $x^+ = 1000$.

In the 100 p.p.m run, back lighting and side lighting techniques were compared in a drag-reducing flow where the only parameter varied was lighting technique. The two techniques yielded nearly the same value of λ^+.

Data Reduction Methods

When the streaks in any given frame are identified, the mean spacing may be computed using either of the two methods described earlier. The first method takes the number of streaks in the i^{th} frame (N_i) and divides into the span (b) over which the count was made, forming the following expression for the mean value of streak spacing:

$$\overline{\lambda} = \frac{1}{n} \sum_{i=1}^{n} b/N_i .$$

The second method involves measuring the distance between adjacent streaks (λ_j) from which a histogram is formed and moments of the distribution may be calculated. The mean spacing by this method, for j=k measurements may be expressed through the following relation:

$$\overline{\lambda} = \frac{1}{k} \sum_{j=1}^{k} \lambda_j$$

where

$$k = \left(\sum_{i=1}^{n} N_i\right) - n$$

A comparison between these two methods of reduction, utilizing Counting Technique III with the side lighting arrangement is given in Table IV, along with calculated non-dimensional moments of the distributions. Since the observer measuring the distance between adjacent streaks was located within 1 m of the viewing screen, Counting Technique III best describes the conditions under which the streaks were identified. For a given sample size, the deviation between the two methods is shown in Table IV for average spacings of 8% and 11% of the dye slot length. Each pair of entries represents the average streak spacing from a selected frame, applying the two methods of reduction. Applying the appropriate statistical "t-test" for comparison of the means for the water and 50 p.p.m flow, showed that at the 95% level of confidence there was no difference between the two methods of reduction. For the 100 p.p.m flow, there was approximately a 10% difference; however, examination of Figure 21 shows that this difference is not significant in terms of the general results and conclusions which will be reached. The method of averaging the number of streaks in the span was therefore chosen to be used for the reduction of all data.

TABLE IV

COMPARISON BETWEEN METHODS OF DATA REDUCTION

A

$$\overline{\lambda} = \frac{1}{n} \sum_{i=1}^{n} b/N_i$$

B

$$\overline{\lambda} = \frac{1}{k} \sum_{j=1}^{k} \lambda_j$$

where $k = \sum_{i=1}^{n} N_i - n$

Counting Technique III

	Water Flow U_τ = 0.0156 m/s		AP-273 50 p.p.m U_τ = 0.0157 m/s		AP-273 100 p.p.m U_τ = 0.0165 m/s	
	n=15	k=175	n=11	k=120	n=14	k=97
i	A	B	A	B	A	B
15	7.8	8.0	-	-	-	-
14	7.8	8.7	-	-	16.6	12.8
13	8.5	8.7	-	-	18.6	14.3
12	8.5	8.0	-	-	18.6	16.3
11	7.3	8.2	9.9	9.9	16.6	16.0
10	7.8	8.0	12.4	12.6	24.9	20.1
9	8.5	9.3	12.4	13.3	24.9	21.0
8	6.8	7.5	13.6	11.7	18.6	15.7
7	7.8	7.8	13.6	13.1	21.3	21.4
6	10.2	9.4	14.9	13.0	18.6	16.7
5	9.3	9.6	14.9	15.1	21.3	16.3
4	7.3	7.1	13.6	13.3	16.6	14.6
3	7.8	8.1	13.6	12.8	18.6	16.0
2	8.5	7.3	11.5	11.3	14.9	14.5
1	8.5	8.4	9.9	8.8	18.6	20.0
$\overline{\lambda}$(mm)	8.14	8.27	12.52	12.04	18.82	16.51
λ^+	96.40	97.80	151.00	145.00	208.00	183.00
$\sigma/\overline{\lambda}$	-	0.39	-	0.36	-	0.34
S	-	0.78	-	0.51	-	0.30
K	-	3.58	-	2.36	-	2.51
$\overline{\lambda}/b$	-	0.08	-	0.08	-	0.11
$\frac{1}{n} \sum_{i=1}^{N} N_i \cong$	13	-	12	-	8	-

Histograms of the measured distance between adjacent streaks are shown in Figures 11, 12 and 13. The three flows have essentially the same friction velocity. The distributions are not exactly Gaussian. For the drag-reducing flows, estimates of the skewness and flatness factors are decreased from that of the water flow, showing more symmetry and a "smearing out" of the distributions. These values are a rough comparison since accurate estimates of skewness and flatness factors require a much larger number of samples. For the one solvent and two drag-reducing flows in which streak spacing distributions were examined, the ratio of standard deviation to mean was approximately 36%. Schraub and Kline (33) obtained a value of 30% with 450 samples, in a zero pressure gradient boundary layer.

The drag-reducing distributions are not simply a Newtonian distribution shifted to a higher mean value. If the constant A is added to all points on the Newtonian distribution, then the mean is shifted by the constant A, while the standard deviation is unaffected. If all points on the distribution are multiplied by the constant A, then the mean is multiplied by the constant A as well as the standard deviation so that the ratio of the two is constant. The distribution is shifted as well as "smeared out." This appears to be more the case as seen from Figure 14. Skewness in the water distribution might be explained by the observed pairing of streaks before bursting. The increased standard deviation for drag-reducing distributions might also be explained by the observed disappearance of some streaks prior to their bursting. These observations will be discussed later in Chapter IV.

Estimates of the mean spacing from counting the number of streaks in a given span approaches the value obtained by measuring individual

distances between streaks, provided that there is a fairly even distribution of streaks about the mean of any given frame. When measuring the distance between streaks, the span should be large enough that at least two streaks are in the field of view at any given time. This means that the span must be at least 1.5 times the maximum spacing as obtained from the streak spacing histograms. As seen from Figure 14, there is a 95% probability that at least one streak exists at all times in a span of approximately 1.7 $\overline{\lambda}$. Therefore, at 20:1 odds a span of at least 2.6 $\overline{\lambda}$ is required when measuring the distance between two streaks. If the span is less than 2.6 $\overline{\lambda}$, then there is a 5% probability that only one streak will be observed; hence, measuring the distance between streaks will be biased toward a lower value of $\overline{\lambda}$. The limiting value of the number of streaks in the span at any time is two when measuring the distance between streaks, and one when counting the number of streaks. For these reasons it is desirable to count over as large a slot width as possible.

Required Sample Sizes

The question regarding the number of samples or frames required to obtain a stable mean must be answered. The mean must be at an acceptable tolerance, yet excessive film footage should be minimized. The number of samples and frames required to determine $\overline{\lambda}$ for a water flow is shown in Figure 15 for the two methods of averaging. For the water flow, there were approximately 13 streaks on the average, in the 102 mm span. A good estimate of the mean spacing is realized after about 30 individual measurements of the distance between adjacent streaks, and for a relatively small number of frames. For drag-reducing flows, the number of

samples required to determine an accurate estimate of $\overline{\lambda}$ is increased from the Newtonian case. For the 56% drag reduction run (Re = 23,100), estimates of the number of samples and frames required using the two methods of averaging was obtained from Figure 16. Approximately 50 samples and eight frames were required to obtain an accurate value of $\overline{\lambda}$, when on the average approximately eight streaks were in the 150 mm span. As $\overline{\lambda}/b$ becomes small the number of frames required for an accurate mean becomes less.

The same values can be obtained from statistical arguments assuming a normal distribution in streak spacing. An estimated 207 samples are required for a 5% uncertainty in the mean, while only 52 samples are needed for a 10% uncertainty. These values correspond to the sampling of approximately 10 to 20 statistically independent movie frames for these experiments. Details regarding these calculations are given in Appendix F. Sample sizes for the data shown in subsequent figures were sufficient to yield estimates of $\overline{\lambda}$ with an uncertainty of 7%.

In summary, the counting location was set at approximately x^+ = 1000, and the number of streaks in a given frame were averaged across the span to obtain the mean spacing. The sample size was set at approximately 15-20 movie frames. Generally, two observers (not necessarily the same for each film) viewed each film, identifying streaks. Values from independent observers differed by less than about 10% and were averaged. Results presented in the next section were obtained with these conditions specified. The remaining variables were: (1) channel flow conditions; (2) sublayer to dye flow rate ratio; and (3) counting technique employed to detect the streaks.

Streak Spacing Measurements

Newtonian Flows

Estimates of mean spacing between low-speed streaks in the near-wall region were made from movie films using the counting techniques described earlier.

In order to compare the back lighting and side lighting techniques a run was made in which the only parameter varied was the lighting technique. The non-dimensional value of streak spacing was 96 and 89, respectively. Applying the "t-test" for comparison of the means showed no significant difference between results obtained using the two lighting techniques at the 95% confidence level. The side lighting technique, however, yields more information regarding the physics of the near-wall flow, and was consequently the primary method utilized in observing changes to the wall structure during drag-reducing conditions. At higher flow rates black and white 4-X Reversal film was used at 36 frames per second. The black and white film provided a higher degree of contrast between the streaks and their surrounding background. As shown in Figure 17 it was concluded that the change in film type did not yield non-dimensional spacings significantly different from the well accepted Newtonian value of $\lambda^+ \tilde{=} 100$. The two highest Reynolds number runs yielded a slightly larger spacing due primarily to the fact that the spacing decreases proportional to the inverse of the wall-shear velocity, yielding poor resolution in this higher velocity environment. When the spacing between adjacent streaks becomes very small at higher friction velocities, one might expect to get higher values of $\overline{\lambda}$, since two adjacent streaks might appear as a single streak. It is therefore

TABLE V

SUMMARY OF FLOW CONDITIONS AND MAJOR RESULTS[1]

Solution Type	Conc. (p.p.m)	U (m/s)	U_τ (m/s)	Percent D.R.	$\nu \times 10^6$ (m^2/s)	$\bar{\lambda}$ (mm)	λ^+	M	$\dot{Q}_s$ (ml/s)	Run No.
Solvent	0	0.174	0.0102	0	0.82	7.62	95	6.8	0.40	SL-6
Solvent	0	0.174	0.0102	0	0.82	7.61	95	9.6	0.28	SL-6
Solvent	0	0.174	0.0102	0	0.82	7.07	88	16.6	0.16	SL-6
Solvent	0	0.174	0.0102	0	0.82	7.24	90	26.7	0.10[2]	SL-6
Solvent	0	0.180	0.0106	0	0.92	7.67	89	7.7	0.36[2]	SL-5
Solvent	0	0.250	0.0139	0	0.92	6.58	99[6]	7.7	0.36[2]	SL-5
Solvent	0	0.260	0.0158	0	1.21	7.77	102[6]	13.0	0.30[2]	SL-1
Solvent	0	0.287	0.0156	0	1.32	8.14	96	11.9	0.36[2]	SL-4
Solvent	0	0.287	0.0156	0	1.32	7.58	89	11.9	0.36[2]	SL-4
Solvent	0	0.311	0.0170	0	0.92	6.30	116	7.7	0.36[2]	SL-5
Solvent	0	0.335	0.0186	0	1.33	7.49	105	15.3	0.28[2]	SL-3
Solvent	0	0.360	0.0190	0	0.92	5.61	116[5]	7.7	0.36[2]	SL-5
Polyox Coagulant	50	0.169	0.0118	0	1.08	10.21	93[5]	9.8	0.33[2]	HB-4
AP-273	50	0.232	0.0123	13	1.30	12.83	121	11.7	0.53[2]	AP-14
837-A	100	0.238	0.0125	17	1.11	12.75	143	15.1	0.35	MG-1
837-A	100	0.238	0.0125	17	1.11	13.28	149	67.6	0.06	MG-1
Polyox WSR-301	100	0.248	0.0129	18	1.11	11.96	139	15.1	0.35	PL-3
Polyox WSR-301	100	0.248	0.0129	18	1.11	10.70	124	33.8	0.15[2]	PL-3
AP-273	50	0.334	0.0157	24	1.30	12.60	152	11.7[7]	0.53[2]	AP-14
AP-273	50	0.401	0.0165	40	1.25	12.80	168	11.6[7]	0.35[2]	AP-20
AP-273	100	0.311	0.0124	44	1.63	21.40	163	17.2	0.44[2]	AP-12
AP-273	100	0.360	0.0140	52	1.86	23.90	180	20.1	0.44[2]	AP-2
AP-273	100	0.465	0.0164	54	1.58	17.70	184	17.2	0.44[2]	AP-12
AP-273	100	0.445	0.0165	55	1.95	23.20	195	21.2	0.44[2]	AP-3
AP-273	100	0.445	0.0165	55	1.95	22.80	192	21.2[7]	0.44[2]	AP-3
AP-273	50	0.557	0.0286	56	1.25	13.20	200	11.6[7]	0.35	AP-20
AP-273	200	0.720	0.0239	56	2.93	58.20	474	48.0	0.29	AP-13
AP-273	200	0.620	0.0211	56	2.32	24.30	220	13.6	0.85	AP-18
AP-273	200	0.620	0.0211	56	2.32	35.80	324	40.0	0.29	AP-18
AP-273	200	0.620	0.0211	56	2.32	-	-	240.0	0.05	AP-18
AP-273[3]	100	0.474	0.0165	57	1.49	18.82	208	15.6	0.46	AP-19
AP-273[3]	100	0.474	0.0165	57	1.49	19.53	216	15.6	0.46	AP-19
AP-273[3]	100	0.481	0.0166	57	1.49	19.79	220	6.7	1.07[2]	AP-16
AP-273	100	0.575	0.0188	59	1.86	20.41	207	20.1	0.44[2]	AP-9
AP-273	100	0.637	0.0198	62	1.39	18.06	255[4]	4.1	1.58	AP-15
AP-273	100	0.637	0.0198	62	1.39	17.80	-[4]	4.5	1.46	AP-15
AP-273	100	0.637	0.0198	62	1.39	16.94	240	5.5	1.18	AP-15
AP-273	100	0.637	0.0198	62	1.39	17.68	251	11.8	0.55	AP-15
AP-273	100	0.637	0.0198	62	1.39	23.57	335	25.2	0.26	AP-15

[1] All polymer runs with 150 mm dye slot and solvent runs with 102 mm slot unless otherwise specified. 8 mm movies taken unless otherwise specified. Data in Table V obtained using counting Technique I.

[2] Estimated values, M $\pm$ 5.

[3] 16 mm movies.

[4] Solvent dye.

[5] 94 mm dye slot.

[6] 109 mm dye slot.

[7] 102 mm dye slot.

desirable to control the flow conditions so that there are from 12 to 15 streaks on the average across the span.

The average value of mean spacing for the seven flow rates is $\lambda^+ = 102$. The results are shown in Figure 17 along with the results of various other investigators using a variety of techniques, and the agreement is very good. Counting Technique I was used to reduce the solvent data since in the Newtonian flow dominant streaks could not be discriminated, hence eliminating Technique II. Utilizing Technique III yielded a non-dimensional spacing of 96 as compared to 89 using Technique I. The two techniques are not significantly different at the 95% confidence level. However, a limiting case, and one to be avoided, is when counting 20 or more streaks in the span where poor resolution would obviously lead to higher values of $\bar{\lambda}$ using Technique I.

The effect of varying flow rate of dye on streak spacing for a water flow was investigated using the back lighting technique. The back lighting technique would provide a critical test since there is a possibility for streaks to be "washed out" at low dye flow rates, a problem not associated with the side-lighting technique. The only parameter varied during the experiment was the flow rate of dye through the 102 mm slot. The results shown in Figure 18 indicate that the characteristic non-dimensional streak spacing for a water flow has not changed over the dye flow rate range $7 < M < 27$. If the concept is adopted that increasing dye flow rate marks fluid further away from the wall, then this result is consistent with the observations of Fortuna (11) and Schraub and Kline (33), that the non-dimensional value of streak spacing is constant for $0.5 < y^+ < 7$.

Drag-Reducing Flows

The streak spacing results for drag-reducing flows will be presented in two segments. First the counting technique used to detect the streaks will be specified and the value of M will be varied, then for a specified range of M the counting technique will be varied.

The effect of sublayer-dye flow rate ratio on the non-dimensional streak spacing is shown in Figure 19 for both water and drag-reducing flows. Approximate y^+ locations for the distance normal to the wall where dye marks fluid are also shown, using the estimates presented in Chapter II. These streak spacing results were obtained using Counting Technique I, since it was believed to best represent the actual number of streaks present. The other two techniques deviate significantly in method from Technique I, which might be referred to as a "normal" or "standard" technique. The non-dimensional streak spacing in drag-reducing flows was found to be dependent on the ratio M, at large values of drag reduction. As seen from Figure 19 the non-dimensional spacing was essentially unaffected at high values of drag reduction over the range $4 < M < 16$. The region where the mean spacing is unaffected by the ratio M will be referred to as the "plateau region." For drag-reducing flows in the 56-62% range, the non-dimensional mean spacing is constant and independent of dye flow rate for this range. When M is greater than about 16, only the fluid very close to the wall is marked by dye. In this region the non-dimensional mean spacing is no longer a single function of the level of drag reduction. At the 56-62% drag reduction level the value of M has an influence on the mean spacing. With increasing values of M, λ^+ increases toward values obtained by Eckelman

et al. (10) in the 60% drag reduction range. The drag-reducing flows near the 18% level show no apparent change in streak spacing when $15 < M < 68$. For Newtonian flows the non-dimensional streak spacing is not a function of dye flow rate over the range $7 < M < 27$ and appears to have a characteristic value of near 100 in the range $0.5 < y^+ < 7$, as stated earlier. The water data of Schraub and Kline (33) is from a hydrogen bubble wire located at $y^+ = 3.3$ while the data of Eckelman et al. (10) is at essentially $y^+ = 0.5$, since the high Schmidt number mass transfer boundary layer formed by the electrochemical reaction is within these limits. Therefore, both the water and drag-reducing flows near the 18% level show no apparent change in streak spacing when dye flow rate is varied. However, at the 56-62% drag reduction level, the streak spacing is unaffected by M only over a specified range of M.

Attention will now be focused on the plateau region or results which are unaffected by the value of M. Specifically, results obtained when the dye flow is in the range of $4 < M < 16$. Again applying Counting Technique I the non-dimensional streak spacing characteristic of the near-wall flow was found to be a monotonically increasing function of drag reduction (Figure 20). For the Re = 23,100, 56% drag reduction run, values obtained using Techniques I and III were $\lambda^+ = 216$ and 208, respectively. This result shows that the number of streaks detected by observers located close to the viewing screen was approximately the same as the number detected by observers located 3-4.5 m from the screen.

Applying the "method of linear least squares," the data in Figure 20 is represented by the relation:

$$\lambda^+ = 1.90 \text{ (\% DR)} + 99.7$$

Based on this data alone, one would conclude that the non-dimensional spacing for non-drag-reducing flows should have a value near 100, which is in fact the case, as observed by many investigators. The data in Figure 20 indicate this relationship is independent of polymer type and concentration since the results are in good agreement with (Figure 21) Donohue et al. (9) for Polyox-FRA at 140 p.p.m, and Achia et al. (1) for AP-30 at 50 p.p.m. The results are also in agreement with Eckelman et al. (10) for values of drag reduction less than about 35%. The data of Fortuna and Hanratty (12) and Fortuna's (11) predicted values obtained from a simplified Newtonian model of the near-wall eddy structure, involving various simplifications and ad-hoc assumptions, are not in quantitative agreement.

At larger values of drag reduction, data from this study approaches the streak-spacing measurements of Kline et al. (21) for strongly accelerating flows. Their findings indicate that the flow has very nearly relaminarized when,

$$K = \frac{\nu}{u_\infty^2} \frac{du_\infty}{dx} = 3.25 \times 10^{-6}$$

yielding $\lambda^+ = 256$ and $\overline{T}_B = 5.8$ s/burst. The heat transfer experiments of Moretti and Kays (26) show "laminar-like" Stanton numbers for $K > 3.7 \times 10^{-6}$.

During drag reduction, the percentage increase in dimensional streak spacing from that of a water flow at the same flow rate and temperature was found to be a monotonically increasing function of drag reduction, in which the viscosity was not a parameter. The data shown in Figure 22 represents four concentrations from six different polymer types for values of drag reduction to 62%. Solvent streak spacing

values were computed using a characteristic non-dimensional spacing of 100. The results are in good agreement with both Donohue et al. (9) and Achia et al. (1), except for the concentrated 200 p.p.m AP-273 run at Re = 18,400. Applying the "method of linear least squares" the data may be represented by the relation,

$$\frac{\lambda_p - \lambda_s}{\lambda_s} = 0.069 \ (\% \ DR)$$

which for dilute solutions also appears to be independent of polymer type and concentration.

For the single non-drag-reducing polymer solution a value of λ^+ = 93 was obtained. Although it seems likely, further study is needed to verify the hypothesis that non-drag-reducing polymer flows attain the characteristic Newtonian spacing of near 100.

The use of solvent dye for polymer experiments was not found to significantly affect the observed mean spacing, although for obvious reasons it was undesirable to use. Back lit films did, however, indicate more contrast between the streaks and surrounding dye when solvent dye was used. The streaks were darker, since more dye between streaks had collected into streaks, indicating that the polymer additives have an influence on the amount of dye that collects into streaks.

For dye flow rates in the range $12 < M < 20$, estimates for the non-dimensional spacing of dominant streaks were also made for the higher values of drag reduction using Counting Technique II. The data in Figure 23 indicate that using Counting Technique II, the non-dimensional spacing between dominant streaks has increased to values in the range of Fortuna's (11) results. Note that using Counting Technique I, Figure 19, λ^+ for these experiments was about 200. At higher levels of drag

reduction the spacing between dominant streaks is in agreement with the results of Eckelman et al. (10).

For dye flow rates in the range 13 < M < 48, Counting Technique III was applied to obtain the average spacing of all observable streaks. As shown in Figure 23 this technique yielded values consistent with those obtained using Technique I when the dye flow rate was in the range 4 < M < 16. When the dye flow rate ratio was greater than 16, however, close examination of the films yielded average spacings less than values obtained using Technique I and consistent with results obtained when dye marks fluid farther away from the wall (4 < M < 16). Close examination of the viewing screen reveals that the dimension of these "extra" streaks normal to the wall is very small. These extra streaks are not seen to burst in the field of view, but form randomly over the surface and slowly migrate downstream before losing their identity or passing out of the field of view. They are not seen to involve momentum transport away from the wall. It was also seen that for the Re = 17,600 run with M = 48 the average spacing from Technique II was nearly equal to that obtained using Technique I, indicating that only the dominant streaks are clearly marked very near the wall. These results strongly suggest that influences immediately adjacent to the wall involving streak formation are more strongly influenced by the polymer additives than those influences farther from the wall.

Streak Behavior in Drag-Reducing Flows

This section will describe some of the major observed differences in streak behavior as compared to a water flow at the same wall shear stress. Comparisons made at equal flow rates are even more dramatic

since the solvent wall-shear stress is much higher. The physical thickness of the sublayer is also much larger, while at the same wall-shear stress they are nearly the same. This is one reason why the comparison is at the same wall-shear stress. Comparison will be made between the SL-4 and AP-19 runs.

As previously mentioned, turbulence production in a non-drag-reducing flow occurs through a sequence of events whose important aspects are: formation, growth, lift-up, and breakup of low-speed streaks; also associated are interactions with large scale inrushes or sweeps originating in the logarithmic region. A qualitative description will be made to assess the effect of the polymer additives on streak formation and growth. These are only preliminary observations and further studies should explore changes in the overall production cycle in more depth.

Under non-drag-reducing conditions nearly all the dye collects into streaks a short distance downstream from the slot. For the drag-reducing flow, dye was readily available for collection at considerable distances ($x^+ \cong 4000$) from the slot. At no time did the streaks collect all the dye between them. It appears as though the outermost layers of dye are mainly involved in marking streaks.

In the drag-reducing flow, some streaks that formed were dissipated without bursting, while some were seen to form, subside, reform and burst. The most predominant streaks did not subside. The polymer additives act to resist the formation and bursting of some streaks, while dominant streaks do not seem affected. Utilizing the back lighting technique revealed that a local accumulation of dye indicating a local fluid deceleration usually preceded the observed wall disturbances and

streak formation. This observation is consistent with the findings of Corino and Brodkey (7) and Offen and Kline (28).

The relative dimenisons of the streaks are not precisely known; however, they are much wider and thicker than the solvent streaks. The increased width is probably due to a "smoothing out" of the spanwise velocity gradients near the wall. Achia and Thompson (1) have noted this feature using laser holographic techniques. The dimension normal to the wall of these streaks is difficult to estimate. An outstanding characteristic of the side-lighting technique is its ability to yield a sense of depth. This coupled with an approximate 30% magnification of the wall structure, resulting from two changes in refractive index, yield an exaggerated estimate of the streak thickness. Viewing from the downstream end of the channel, the streaks are seen to have very little thickness. An estimate of the streak thickness before lift-up for both flows would be $y^+ < 10$, since ejections and breakup of the streaks are usually initiated in the buffer region. The average length of drag-reducing streaks from formation to breakdown is dimensionally much larger than the water flow. However, the AP-20 run at the same wall-shear stress but lower drag reduction, was somewhere between the two. The average time from formation to complete breakdown of these streaks is much longer, as some streaks persist for a considerable length of time. Streamwise vorticity associated with these streaks is also greatly reduced but not completely eliminated. The streaks are seen to periodically sweep from side to side a small amount while displaying a lateral waving motion. The drag-reducing streaks showed less wavy motion when compared to the water flow, as also noted by Donohue (8). Periodic lateral sweeping of the streaks was sometimes seen to

result in combining of two or more streaks into one, and was noted in both water and drag-reducing flows. By observing the films through only a width of $3\bar{\lambda}$, two streaks combined into a single one, approximately 15% of the time for both the water and drag-reducing flows. Some streaks were seen to only lift-up in the field of view, proceeding downstream as they gradually lifted away from the wall. Also seen were some streaks that lifted and then returned to the wall. Donohue (8) has also observed this behavior in 140 p.p.m polyethylene oxide solutions.

CHAPTER IV

DISCUSSION

The major goals of this study were to (1) quantify and correlate changes in the near-wall streak structure under drag-reducing conditions, resolving the differences between the results of Donohue et al. (9) and Eckelman et al. (10); and (2) gain further insight into changes in the near-wall turbulent production process. Discussion of these results and other observations will be made in this chapter. A model of the near-wall streak structure during drag-reducing conditions will be postulated. The model is consistent with observations of various other investigators. Differences in the behavior of the near-wall structure will also be discussed.

Streak Formation

In most water flow studies, the time scale of events in the wall region require the aid of high-speed photography. The slowing down and spacing out of events in this region during drag reduction has brought to light a well defined event. This event is an apparent disturbance to the wall dye, presumably from the outer flow field, and it will be described initially from observations using the side lighting technique. The events will be described as seen in drag-reducing flows only because they are most easily visualized under those conditions. The same

sequence of events appears to occur in water flows where it has been observed at low flow rates.

The sequence of events begins with a local initially undisturbed region of dye in the near-wall region where the flow appears to be locally laminar. The initiation of the wall dye disturbance is seen as an oval shaped crater-like depression in the dye, aligned in the flow direction. This is seen to be a depression in the dye since the center is darkly shaded. This depression then begins to elongate in the downstream direction with the longitudinal sides raising up above the plane of the dye to become more brightly lit than the surrounding fluid. The elongation continues, as an apparent streak pair beings to grow. Similar depressions and events may occur within this streak pair during its growth. The streaks are seen to oscillate laterally before bursting. The growth of a streak pair following an initial wall disturbance is shown in Figure 24. The depressions in the wall dye correspond to an event traveling in the downstream direction at 0.75 U. Using the velocity profile data and drag reduction correlation of Reischman (30), the event is traveling near the mean velocity at $y^+ = 40$. Initially, the rate of elongation of these streaks is half this velocity. A photograph of the initial growth of a streak pair is shown in Figure 25. Several such disturbances usually occur at about the same time and within a local region, resulting in the formation of several streaks at nearly the same time. They usually occur just downstream of and following the bursting of streaks marked farther upstream. Offen and Kline (28) also found that nearly 3/4 of the observed sweeps reached the wall, downstream and ahead of the bursting wall dye. The fact that streaks form downstream of the dye slot, as seen in Figures 24 and 25, lend further

evidence that streaks are not caused by the presence of the slot.

The event just described also was seen in a different perspective using the back lighting technique. The dye near the wall provides a nearly uniform color background. The streaks appear as dark longitudinal dye structures while the wall disturbances appear as local spots, lighter than the surrounding dye. At low flow rates these disturbances are very gentle and extend over a relatively long distance while at higher flow rates they are more violent and abrupt in nature.

The question now arises concerning the connection between the observed wall disturbance and some feature of the flow which might cause such a disturbance. The fact that the sequence of observed dye depressions (Figure 24) corresponds to an event traveling much faster than the local mean velocity near the dye strongly suggests that the disturbances are due to a "sweep" type event. The presence of an initial crater-like depression in previously undisturbed flow suggests that the disturbance also has a velocity component toward the wall. A sweep is an event where a finite volume of fluid moves toward the wall from somewhere in the logarithmic region. The event is convected at a velocity faster than the local mean and has a velocity component toward the wall. The result is an event which contributes to the production of turbulent energy. These events having been investigated by Corino and Brodkey (7), Nychas et al. (27), and others have been found to contribute about 70% to the overall energy production. Sweeps have been observed by Nychas et al. (27) to have transverse vortical motion. As these sweeps move toward and strike the wall, their vortical motion may be stretched out in the streamwise direction, resulting in longitudinally-oriented wall-eddies which collect dye into the adjacent low-speed regions. It is

therefore postulated that "sweep" type events are associated with streak formation. If the proposed model for the complete bursting cycle from Offen and Kline (28) is adopted and modified, then a wallward moving sweep is associated with both a burst and the formation of a streak pair immediately downstream from the burst.

In drag-reducing flows, not all of these dye disturbances developed into streaks. Some degenerated immediately following their occurrence. The 200 p.p.m runs at the maximum drag reduction asymptote clearly show a large number of disturbances being dissipated. The wall layer is seen to be very "passive" in nature with a very large number of wall disturbances occurring and degenerating as compared to the number of bursts observed in the field of view. As seen from the films, many disturbances are imposed on the wall. These disturbances either form into streaks or are dissipated immediately after their occurrence. The streaks which do form either burst away from the wall or degenerate and are no longer identifiable. The films suggest that the existence of these wall disturbances are the one feature not greatly affected by the polymer additives at the maximum drag reduction asymptote.

Streak Spacing

The results shown in Figure 19 obtained using Counting Technique I indicate that at the 56-62% level of drag reduction the non-dimensional streak spacing is constant over the range of dye flow rates $4 < M < 16$, and for $M > 16$ increases with M toward values obtained by Eckelman et al. (10) at the same level of drag reduction. A few brief comments are in order which support this observed dependence. One might argue that the dye flow rate was too large for the range $4 < M < 16$, hence creating a

larger number of streaks than might actually exist. This is highly unlikely for the following reasons:

1. The non-dimensional spacing is constant in this region.

2. One might intuitively expect to see the streak spacing change with dye flow rate at the lower values of drag-reduction (flow rates) because the flow should be less stable to disturbances induced by the dye flow at lower values of drag-reduction (flow rates). This is not the case.

3. For an excessive dye flow rate, one would expect to see a larger number of streaks near the slot as created by the disturbing dye flow. This is not the case, as can be seen from Figure 10. Movies also indicate that as many streaks form downstream of the slot ($x^+ \cong 1500$) as near the slot.

4. Within the range of experimental uncertainty, there was no effect of varying dye flow rate on the non-dimensional streak spacing of a water flow for the range $7 < M < 27$.

Conversely, one could argue that for $M > 16$ the observed increase in streak spacing is the result of an insufficient amount of dye needed to mark all the streaks. This also is highly unlikely for the following reasons:

1. The physical volume flow of dye into the sublayer is roughly twice that of water flows for the same value of M.

2. There is no observed increase in streak spacing at the 18% drag-reduction level, or in water flows for the same values of M.

3. Movies show that a sufficient amount of dye is always present in the wall region for collection into visually observable streaks.

Therefore, it is postulated that the observed changes in structure at the 56-62% level of drag reduction are the result of dye marking fluid at various levels normal to the wall. The exact distance normal to the wall where λ^+ begins increasing is not known. A reasonable estimate would place it within the viscous sublayer. It is, however, in a region where influences of the mechanism (s) which is (are) responsible for streak formation are strongly influenced by the polymer additives. Some streaks are more predominant than others in that they appear to be larger and more brightly lit than most streaks. The thickness normal to the wall of these streaks is larger and their apparent length is longer than most streaks. As dye marks fluid closest to the wall, dominant streaks appear to be the only streaks present and are usually single structures. However, close examination of the viewing screen reveals a larger number of streaks to exist which are barely observable and whose detection is due only to the lighting technique's ability to discriminate the most minute changes in dye contour. Within the field of view these barely observable streaks are seen to form randomly over the surface, slowly migrating downstream and then losing their identity without bursting. The dimension of these streaks normal to the wall is very small.

Accounting for these extra streaks using Counting Technique III yielded results which were consistent with results obtained using Counting Technique I, when the dye flow rate was in the range $4 < M < 16$. These streaks, which are barely observable when dye marks only the fluid very close to the wall, may have a much greater influence farther away from the wall. These streaks, which are barely observable when M is greater than 16, should not be counted in estimating the mean spacing

since their detection is at the threshold of visual observation. This data suggests the presence of a larger number of streaks above the marked dye and whose influence on the marked fluid nearest the wall is greatly affected by the presence of the polymer additives. The author suggests an analogy with a real life physically observed occurrence. A tornado (fluid motions which influence streak formation) which has not touched ground passes over a group of trees (dye closest to the wall) in which only the leaves and a few branches are removed (minute streak observed whose distance normal to the wall is very small). A second tornado, touching the ground, passes through the same group of trees leaving only the roots (distinct marking of all streaks which are influenced). The influence of the tornado depends on its location relative to the trees.

Changes other than in streak spacing occur when dye is injected at other than normal flow rates. For the Re = 33,400 run with M = 4.0, the dye flow rate was probably too high as indicated by an apparent excessive amount of bursting as compared to scenes when M = 5.5. The interesting observation is that the average spacing seems unaffected at this high dye flow rate. This suggests that the mechanisms involved in streak formation are much more dominant than disturbances induced by an excessive dye flow rate. Scenes at the M = 5.5 and 11.7 levels are nearly identical; however, at the 25.2 level major changes occur. Associated with a 34% increase in mean spacing, streaks marked in this region are longer than in the previous scenes. Nearly all streaks extend well outside the camera's field of view. The most noticeable change that occurs when the mean spacing increases in this case is a 66% decrease in the number of bursts per unit area-time. For M = 5.5 and 11.7 nearly every

streak began to burst in the field of view, while for M = 25.2 many left the field of view without bursting.

When dye marks the outer regions of the viscous sublayer, the effect of drag-reducing additives on the non-dimensional streak spacing is shown in Figure 20 as a function of the level of drag reduction. The agreement with Donohue et al. (9) for a 140 p.p.m polyethylene oxide solution is quite good. However, the data of Fortuna and Hanratty (12) obtained from long-time average spatial correlations using wall mounted electrochemical probes in a 2.54 cm pipe is not. Averaging over too long of a time tends to "smear out" the positive correlations produced by adjacent streaks, and thus may detect only the largest scales and most predominant streaks. It is noteworthy to observe that the non-dimensional spacing between dominant streaks (Figure 23) is in agreement with Fortuna (11) and at higher values of drag reduction, the results of Eckelman et al. (10).

The data of Eckelman et al. (10) was obtained by measuring instantaneous eddy patterns from the data of Fortuna (11) and is in agreement with this work to about the 35% level of drag reduction. It should be pointed out that due to the high Schmidt number mass transfer boundary layer over the wall mounted electrochemical probes, this technique only correlated fluid motions inside $y^+ \cong 0.5$. Preliminary results from the work of Achia and Thompson (1) were published near the conclusion of this study. In their study, the wall structure of 50 p.p.m solutions of AP-30 were visualized in a 2.63 mm pipe through the use of real-time laser holographic interferometry. The flow patterns in the near-wall region of the pipe flow were made visible by infusing a refractive index enhancer into the flow through a 0.2 x 14 mm slot. Variations in the

concentration of the enhanced layer caused movement of the fringe patterns when the test section was viewed through a hologram. Measured fringe shifts were used to compute the spatial spanwise correlation of the streamwise concentration fluctuation. Their results are in good agreement except for the 44% drag reduction point. It is not clear why this point is high, although several potential problems associated with the wall dye slot method will be discussed. As seen earlier, a dye slot length of approximately 2.6 $\overline{\lambda}$ is required to obtain a spatial correlation at any time. The data from this investigation indicates that the 44% drag reduction point does not satisfy this latter condition. For a slot length of 2 $\overline{\lambda}$ only one streak was seen in the field of view approximately 20% of the time. It would be interesting to compare visual counts to spatial correlation measurements from their movies. However, based on their published data, it is seen from Figure 22 that the dimensional increase in spacing is in good agreement with the results of this study and of Donohue et al. (9). This could possibly indicate a problem in the measured pressure drop.

Since measurements made in the four investigations were essentially under the same type flow (i.e., near zero pressure gradient bounded turbulent shear flow), one might expect the mechanism of drag reduction to be the same. An interesting analogy can be drawn from the conflicting observations seen by Corino and Brodkey (7) and Kim et al. (18), both in near zero pressure gradient bounded shear flows. It might be expected that the actual processes of turbulent production were the same in both cases. However, the method of flow visualization applied in both cases was not the same, and each brought forth phenomena the other could not easily detect. Only by applying a third flow visualization scheme

[Offen and Kline (28)] were these two conflicting observations found to be related. Possibly a similar case exists here in that the electrochemical technique detects only the streaks within $y^+ \tilde{=} 0.5$, while the wall dye slot technique detects streaks which are much farther away from the wall. In the next section a postulated model of the near-wall streak structure during drag reduction will provide a tentative explanation for the apparent discrepancy between the investigations discussed earlier.

A Proposed Model of the Near-Wall Streak Structure During Drag Reduction

The formulation of this model is based on the recent investigations of Bakewell and Lumley (2) and Sirkar and Hanratty (34), who suggest that the large eddy structure in the viscous sublayer is characterized by flow-oriented eddies. Based on these observations, Fortuna (11) has developed a model of the near-wall flow structure consisting of counter-rotating eddy pairs (Figure 26). Between these eddy pairs exists a low axial velocity and fluid "updrafts." These regions are associated with the low-speed streaks observed by Kline et al. (21) and many others. Fortuna's model spaces the regions of "updraft" by the non-dimensional distance between streaks ($\lambda^+ = 100$) as obtained by many investigators (Figure 26). The analysis predicts reasonably well the velocity profile in the near-wall region when compared to previous experimental results. Fortuna's extension of a Newtonian Model to drag-reducing flows, however, is not so encouraging, particularly because it is based on an observed Newtonian structure.

For Newtonian flows, the wall structure proposed is the same as described by Fortuna (11), and remains nearly the same to approximately the 30% level of drag reduction, except for the increased streak spacing. Increasing the flow rate further produces a variation in streak spacing with distance normal to the wall, as weaker eddies are unable to maintain their existence immediately adjacent to the wall (Figure 27). At yet higher values of drag reduction medium strength eddies are not longer able to exist, leaving only the strongest eddies at the wall. This accounts for Eckelman's faster than linear increase in λ^+ at larger values of drag reduction as observed from their data taken inside $y^+ = 0.5$. The circles in Figure 27 represent the low-speed streaks which would normally be detected and counted by most techniques. At the higher values of drag reduction it is uncertain whether weaker streaks actually exist at or have a marginal influence at the wall. Figure 28 shows the expected y^+ variation in non-dimensional streak spacing at various values of drag reduction. The work of Achia and Thompson (1) cannot be further compared until more results are published.

The variation in streak spacing with y^+ may be associated with the polymer solution's ability to resist spanwise vortex stretching which is a phenomenon believed to be associated with streak formation (see Kline et al. (21)). As the wall-shear stress is increased, the effect of polymer additives on the level of turbulent production is increased. Thus, in a drag-reducing flow, the effect of the polymer additives appears to increase as the wall is approached.

As also observed in this study, the dominant streaks appear longer than most other streaks. A representation of the proposed streak structure at high values of drag reduction is shown in Figure 29. As

mentioned earlier, for larger values of drag reduction, when only fluid closest to the wall is marked, the values of λ^+ increase with an even larger decrease in the rate of streak bursting per unit area. Based on these arguments it will be postulated that at higher values of drag reduction the average streak spacing, time between streak ejections or bursts, and length of streak from formation to breakdown are all functions of y^+ over some finite distance normal to the wall. This model differs from those of Fortuna (11) and Black (3), where these phenomena do not vary with distance normal to the wall. It is also doubtful that Black's model is correct, since it is based on the stability of a thickened sublayer. A recent investigation by Reischman and Tiederman (31) has shown that only the buffer region (elastic sublayer) is thickened.

The proposed description of the streak structure during drag reduction has been explained in terms of previously published and generally accepted results. If the postulate discussed in the previous section is accepted, that one of the mechanisms of streak formation involves a "sweep" type event onto the wall as observed by Offen and Kline (28), then the proposed model may also be explained in these terms. As the drag reduction begins to increase, weak sweeps with low momentum either do not move into close proximity of the wall, or if they do streak formation is inhibited due to the solution's resistance to axisymmetric straining. At higher wall-shear rates the moderate strength sweeps are restricted from forming streaks leaving only the dominant sweeps with high momentum, which create dominant streaks. Visual observations, however, indicate that the dominant streaks are single structures. Possibly the dominant sweep exerts more influence in one direction. More information has to be obtained regarding the interrelation between sweeps and

newly formed streaks before this question can be resolved. This speculation is supported by the recent work of Carpenter (5) in a 2.54 cm pipe, who employs the same flow visualization technique as Corino and Brodkey (7). At low values of drag reduction, Carpenter found a sequence of events consisting of sweeps, ejections and other fluid interactions occurring near the wall and similar to those described by Corino and Brodkey (7) and Nychas et al. (27) in a Newtonian flow. As the drag-reduction is increased the frequency and magnitude of these events were decreased. Also the events occurred farther from the wall as the drag-reduction was increased. The limiting behavior of the proposed model at the maximum drag reduction asymptote is unclear. For the Re = 18,400 run with M = 240, the structure was very undefined, with only one or two dominant streaks appearing periodically.

CHAPTER V

SUMMARY, CONCLUSIONS AND RECOMMENDATIONS

Summary

As stated earlier the objective of this study was to quantify and correlate the non-dimensional mean spacing of low-speed streaks in the near-wall region of drag-reducing flows. This objective was achieved by varying (1) the flow conditions, and (2) the counting technique used to detect the streaks. The flow conditions were changed by independently varying both the type and concentration of the polymer solutions over a wide range of flow rates. The counting technique used to identify the streaks was also varied to determine if the differences between past investigations were due to technique employed in identifying the streaks.

Experimentally, the objectives were to:

1. Identify low-speed streaks in the near-wall region of a fully developed two-dimensional turbulent flow during drag-reducing conditions.

2. Obtain from films data concerning their average spacing.

3. Correlate the results and test for universality of the correlation.

Two polyacrylamides and a single polyethylene oxide were chosen for use in this study.

The unique lighting technique applied in this study revealed that in both Newtonian and drag-reducing flows, the dye which collects into a streak identifies it as a longitudinal structure of finite volume.

The dimension of this structure normal to the wall is much larger than the normal distance marked by undisturbed dye. When back lighted the streaks appear as longitudinally-oriented dye structures which are much darker than the dye marked regions between the streaks. This suggests that the dye between streaks collects into adjacent streaks rather than being swept downstream by faster moving fluid. After formation and just before breakdown, a low-speed streak attains a maximum finite length. The length of these streaks was seen to increase with increasing drag-reduction and/or polymer concentration. In drag-reducing flows the longitudinal length scale of the low-speed streaks is increased from that of a Newtonian flow at the same solvent Reynolds number.

Considerable data was taken over a wide range of flow conditions, limited only by transition and the channel's maximum attainable flow rate. It was seen that the presence of the polymer in the near-wall region acts to increase the average spacing (both dimensional and non-dimensional) between low-momentum streaks as compared to a Newtonian flow, at the same solvent Reynolds number. When dye marks the outer portions of the viscous sublayer such that $4 < M < 16$, the non-dimensional average spacing was found to increase nearly linearly with drag reduction. This relation appears to be independent of polymer type and concentration. For dilute polymer flows, the dimensional increase in average spacing from that of a Newtonian flow (at the same solvent Reynolds number) was also found to be a nearly linear function of drag reduction, independent of polymer type and concentration.

At the 56-62% drag reduction level, marking only the fluid closest to the wall by adjusting $M > 16$ showed that the non-dimensional average spacing increased toward values obtained by electrochemical techniques

at the same level of drag reduction. Close examination of these films shows the faint existence of a larger number of streaks with an average spacing nearly equal to that obtained when dye marks fluid farther away from the wall. The extra streaks observed are seen to only form and dissipate in the field of view without bursting. However, these barely observable streaks should not be counted when estimating the mean streak spacing since they are near the threshold of visual observation and are not believed to be an important part of the turbulent process. The non-dimensional spacing between dominant streaks increased toward values obtained by Fortuna (11) and Eckelman et al. (10) at the higher levels of drag reduction. Both data and movies indicated that dominant streaks are the main feature when dye marks only the fluid closest to the wall. Adjusting $M > 16$ for Newtonian and drag-reducing flows in the 17-18% range of drag reduction yielded no change in the non-dimensional spacing despite the fact that the physical volume flow of dye through the slot was nearly half that of the 56-62% drag reducing flows at the same value of M.

Periodic disturbances, believed to be "sweeps," were imposed on the near wall dye, randomly over the surface and many times were associated with the inception of a streak pair, while some were dissipated immediately after their occurrence. Some streaks formed were observed to only "lift-up," indicating a break in the chain of events which lead to bursting. Movies indicate that in drag-reducing flows, the number of ejections per unit area-time is lower than that corresponding to a Newtonian flow at the same wall-shear stress. The increase in both the longitudinal and transverse length scales associated with low-speed streaks results in a decrease in the number of bursts per unit area-time

and hence a lower production of turbulent kinetic energy. This is consistent with the conclusions of Donohue (8).

Based on the observations of this and previous studies, a model of the near-wall streak structure is postulated. The validity of the model is strengthened by the observations of other investigations. The polymer additives are seen to periodically modify or terminate the cycle of events at various stages, which are associated with turbulent energy production from low-speed streaks.

Conclusions

It is concluded from this study that at higher values of drag reduction, there is a variation normal to the wall, in the non-dimensional streak spacing. In the outer regions of the viscous sublayer the non-dimensional streak spacing increases nearly linear with drag reduction, and within the inner portion of the sublayer, the non-dimensional spacing increases at a faster than linear rate. These conclusions offer a tentative explanation for the observed differences in the results of Donohue et al. (9) and Eckelman et al. (10).

Recommendations

Based on observations made during this study, the following recommendations are made.

1. Due to limitations of the flow facility, the maximum drag reduction asymptote for dilute polymer flows proposed by Virk et al. (35) could not be reached. Future experiments should be designed to attain this level providing a critical test of the proposed near-wall streak structure model.

2. Problems encountered in obtaining the period between wall ejections for drag-reducing flows are discussed in Appendix B. Future studies should continue in this area and experiments should be designed to overcome these problems and resolve the question concerning the effect of polymer additives on the time period of wall ejections.

3. The effects of polymer additives on the production of turbulent kinetic energy should be examined in depth. Such a study should look closely at the trajectory angles of ejected low-speed streaks. Streaks observed to only lift-up may not be reaching the zone of maximum interaction within the extended buffer region.

4. Wall disturbances associated with streak formation were postulated to be the result of a "sweep" event onto the wall. Further studies should verify this statement and provide a qualitative description of the interactions between the outer flow and wall region in drag-reducing flows.

5. The processes involved in collection of dye into streaks could be resolved using the side lighting technique. Superimposed on the fluorescent dye would be equally spaced lines of blue dye also introduced at the slot. Lateral displacements in the wall region could easily be detected.

BIBLIOGRAPHY

(1) Achia, B. U., and D. W. Thompson. "Laser Holographic Measurement of Wall-Turbulence Structures in Drag-Reducing Pipe Flow." Presented at BHRA Inter. Conf. on Drag Reduction, St. John's College, Cambridge, England, 1974.

(2) Bakewell, H. P., and J. L. Lumley. "Viscous Sublayer and Adjacent Wall Region in Turbulent Pipe Flow." The Physics of Fluids, Vol. 10 (1967), p. 1880.

(3) Black, T. J. "Viscous Drag Reduction Examined in the Light of a New Model of Wall Turbulence." Viscous Drag Reduction. Wells, ed. New York: Plenum Press, 1969.

(4) Blackwelder, R. F., and H. H. W. Woo. "Pressure Perturbation of a Turbulent Boundary Layer." The Physics of Fluids, Vol. 17, n. 3 (1974), p. 515.

(5) Carpenter, C. N. "Drag Reduction Visual Study." (Ph.D. thesis, Ohio State University, 1973.)

(6) Castro, W., and W. Squire. "The Effect of Polymer Additives on Transition in Pipe Flow." Appl. Sci. Res., Vol. 18 (1967), p. 81.

(7) Corino, E. R., and R. S. Brodkey. "A Visual Investigation of the Wall Region in Turbulent Flow." J. of Fluid Mechanics, Vol. 37 (1969), p. 1.

(8) Donohue, G. L. "The Effect of a Dilute, Drag-Reducing Macromolecular Solution in the Turbulent Bursting Process. (Ph.D. thesis, Oklahoma State University, 1972.)

(9) Donohue, G. L., W. G. Tiederman, and M. M. Reischman. "Flow Visualization of the Near-Wall Region in a Drag-Reducing Channel Flow." J. of Fluid Mechanics, Vol. 56, part 3 (1972), pp. 559-575.

(10) Eckelman, L. D., G. Fortuna, and T. J. Hanratty. "Drag Reduction and the Wave Length of Flow-Oriented Wall Eddies." Nature, Vol. 236 (1972), p. 94.

(11) Fortuna, G. "Effect of Drag-Reducing Polymers on Flow Near a Wall." (Ph.D. thesis, University of Illinois, 1971.)

(12) Fortuna, G., and T. J. Hanratty. "The Influence of Drag-Reducing Polymers on Turbulence in the Viscous Sublayer." J. of Fluid Mechanics, Vol. 53 (1972), p. 575.

(13) Gupta, M. K., A. B. Metzner, and J. P. Hartnett. "Turbulent Heat-Transfer Characteristics of Viscoelastic Fluids." Int. J. of Heat Mass Transfer, Vol. 10 (1967), pp. 1211-1224.

(14) Giles, W. B., and W. T. Pettit. "Stability of Dilute Viscoelastic Flows." Nature, Vol. 216 (1967), p. 470.

(15) Halleen, R. M., and J. P. Johnston. "The Influence of Rotation on Flow in a Long Rectangular Channel--An Experimental Study." Report MD-18. Stanford University: Thermosciences Div., Dept. of Mech. Engr., 1967.

(16) Hartnett, J. P., J. C. Y. Koh, and S. T. McComas. "A Comparison of Predicted and Measured Friction Factors for Turbulent Flow Through Rectangular Ducts." Trans. ASME, J. of Heat Transfer, Vol. 84 (February, 1962), pp. 82-88.

(17) Hoyt, J. W. "The Effects of Additives on Fluid Friction." Freeman Review, presented at the ASME Winter Annual Meeting, Washington, D.C., 1971.

(18) Kim, H. T., S. J. Kline, and W. C. Reynolds. "An Experimental Study of Turbulence Production Near a Smooth Wall in a Boundary Layer With Zero Pressure Gradient." Report No. MD-20. Stanford University: Thermosciences Div., Dept. of Mech. Engr., 1968.

(19) Kline, S. J. "Observed Structure Features in Turbulent and Transitional Boundary Layers." Fluid Mechanics of Internal Flow, Sovran, ed. New York: Elsevier Pub. Co., 1967.

(20) Kline, S. J., and F. A. McClintock. "Uncertainties in Single-Sample Experiments." Mechanical Engineering, Vol. 75 (January, 1953), pp. 3-8.

(21) Kline, S. J., et al. "The Structure of Turbulent Boundary Layers." J. of Fluid Mech., Vol. 30 (1967), p. 741.

(22) Lu, S. S., and W. W. Willmarth. "Measurements of the Structure of the Reynolds Stress in a Turbulent Boundary Layer." J. of Fluid Mech., Vol. 60 (1973), pp. 488-511.

(23) Lumley, J. L. "Drag Reduction in Turbulent Flow by Polymer Additives." J. Polymer Sci.: Macromolecular Reviews, Vol. 7 (1973), pp. 263-290.

(24) Merrill, E. W. et al. "Study of Turbulent Flows of Dilute Polymer Solutions in a Couette Viscometer." Trans. of the Soc. of Rheology, Vol. 10, No. 1 (1966), p. 335.

(25) Metzner, A. B., and M. G. Park. "Turbulent Flow Characteristics of Viscoelastic Fluids." J. of Fluid Mech., Vol. 20 (1964), pp. 291-303.

(26) Moretti, P. M., and W. M. Kays. "Heat Transfer Through an Incompressible Turbulent Boundary Layer With Varying Free-Stream Velocity and Varying Surface Temperature." Report No. PG-1, Stanford University: Thermosciences Div., Dept. of Mech. Engr., 1964.

(27) Nychas, S. G., H. C. Hershey, and R. S. Brodkey. "A Visual Study of Turbulent Shear Flow." J. of Fluid Mech., Vol. 61 (1973), pp. 513-540.

(28) Offen, G. R., and S. J. Kline. "Combined Dye-Streak and Hydrogen-Bubble Visual Observations of a Turbulent Boundary Layer." J. of Fluid Mech., Vol. 62 (1974), p. 223.

(29) Patterson, R. W., and F. H. Abernathy. "Transition to Turbulence in Pipe Flow for Water and Dilute Solutions of Polyethylene Oxide." J. of Fluid Mech., Vol. 51 (1972), pp. 177-185.

(30) Reischman, M. M. "Laser Anemometer Measurements in Drag-Reducing Channel Flows." (Ph.D. thesis, Oklahoma State University, 1973.)

(31) Reischman, M. M., and W. G. Tiederman. "Laser Doppler Anemometer Measurements in Drag-Reducing Channel Flows." Accepted for publication in the J. of Fluid Mech., October, 1974.

(32) Runstadler, P. W., S. J. Kline, and W. C. Reynolds. "An Experimental Investigation of the Flow Structure of the Turbulent Boundary Layer." Report MD-8. Stanford University: Thermosciences Div., Dept. of Mech. Engr., 1963.

(33) Schraub, F. A., and S. J. Kline. "A Study of the Turbulent Boundary Layer With and Without Longitudinal Pressure Gradients." Report No. MD-12. Stanford University: Thermosciences Div., Dept. of Mech. Engr., 1965.

(34) Sirkar, K. K., and T. J. Hanratty. "Relation of Turbulent Mass Transfer to a Wall at High Schmidt Numbers to the Velocity Field." J. of Fluid Mech., Vol. 44 (1970), pp. 589-603.

(35) Virk, P. S. et al. "The Toms Phenomena: Turbulent Pipe Flow of Dilute Polymer Solutions." J. of Fluid Mech., Vol. 30 (1967), p. 205.

(36) Wallace, J. M., H. Eckelmann, and R. S. Brodkey. "The Wall Region in Turbulent Shear Flow." J. of Fluid Mech., Vol. 54 (1972), p. 39.

(37) Wells, C. S., and J. G. Spangler. "Injection of a Drag-Reducing Fluid into Turbulent Pipe Flow of a Newtonian Fluid." The Physics of Fluids, Vol. 10, No. 9 (1967), p. 1890.

(38) White, W. D., and D. M. McEligot. "Transition of Mixtures of Polymers in a Dilute Aqueous Solution." Trans. ASME, J. Basic Eng., Vol. 92 (September, 1970), pp. 411-418.

APPENDIX A

VISUAL OBSERVATIONS IN TRANSITION FLOWS

This appendix deals with visual observations made during the transition experiments described in Chapter III. These observations were made in both a water flow and polymer flows of 50, 100 and 200 p.p.m AP-273.

For the 100 p.p.m AP-273 solution, previously undisturbed dye injected along the center line of the channel from the upstream settling chamber, began a small amplitude, long wavelength ($\tilde{=}$ 0.3 m) oscillation at Re $\tilde{=}$ 4300. As flow rate was increased, the previously well-ordered motion underwent brief periods of eratic and violent oscillation. At Re $\tilde{=}$ 7800 the first disturbances in the near-wall region were observed. No real significance should be attached with this number since disturbances may have occurred near the wall at a lower Reynolds number, had we observed much farther downstream. The interesting observation at this flow rate was the existence of a bulge in the centerline dye associated with and near a local disturbance in the wall dye. The view as seen from the movie is illustrated in Figure 30. It is not known in this case if the bulge was two or three-dimensional, although it was most likely three-dimensional. This bulge should not be confused with the long wavelength oscillations mentioned earlier. The bulge and wall disturbance entered the field of view at the same time and moved downstream at the same velocity ($\tilde{=}$ 1.26 U). This velocity was determined by measuring the distance traveled downstream per movie frame by each event.

The perturbed dye left behind the moving disturbance collected very quickly into two well-ordered streaks which slowly migrated downstream. Viewing through the end of the channel, the initially two-dimensional motions in the centerline dye periodically became three-dimensional and swept down on the wall creating a local disturbance in the dye. At higher flow rates larger patches of turbulence occurred (Figure 31) in the wall region with an increase in the number of streaks observed. In this study, movies and direct visual observations strongly suggest that a wallward moving disturbance is responsible for the initiation of turbulent spots.

As mentioned previously, both the water and polymer flows were fully turbulent near Re = 10,000. It does not appear as though transition is delayed by the addition of drag reducing additives when the Reynolds number is based on solution viscosity.

Patterson and Abernathy (29) and Virk et al. (35) also concluded that transition generally is not delayed by drag-reducing additives. Delayed transition has been noted by Giles and Pettit (14), White and McEligot (38), Castro and Squire (6), Gupta et al. (13), and Metzner and Park (25). In a majority of these studies, transition was said to occur with departure from the laminar flow friction factor relation. However, transition may occur at a lower Reynolds number and the friction factor may simply be adhering to Virk's "maximum drag reduction asymptote." Inferring the physics of non-Newtonian flow from non-dimensionalized data based on trends in Newtonian flow can be misleading. The effects of polymer additives on observed departure from the laminar flow relation with small diameter pipes also may be influenced by shear induced molecular degradation, leading to erroneous conclusions.

Identification from films, of the laminar, transitional and fully turbulent flow regimes, allowed these regions to be identified with friction factor versus Reynolds number data. Figure 32 serves to identify these visually observed flow regimes with the friction factor versus Reynolds number data. Friction factor results in the laminar and transitional regimes may have been influenced by a hydraulic diameter effect or by too short an entry length for fully developed laminar flow. In any event, the channel flows were fully turbulent for a Reynolds number greater than 10,000.

APPENDIX B

COMMENTS ON STREAK BURSTING

This appendix will explain some of the difficulties encountered when using the wall dye slot technique to obtain the time between wall ejections in drag-reducing flows.

Visualization of Ejections

Visualization of streak ejections was made using the dual-view mirror arrangement and back lighting technique shown in Figure 33. The arrangement was the same as used by Donohue (8). The camera was located 1 - 2 meters from the channel where it was able to view the dye near the wall from two orthogonal directions simultaneously. The upper portion of the camera field views a side profile of the near-wall region from which events occurring in the x-y plane are seen. The dye seen in this view is back lighted with a 160 watt light source covered with a frosted Plexiglas plate. The lower portion of the camera's field of view sees a taped off portion of the dye slot which allows only one or two streaks to be visualized by the dye, and is back lighted with a 160 watt light source. The dye used was a dilute food coloring solution consisting of one volume each of red and green concentrated dye to twenty volumes of water.

When viewing in the plane of the wall, low-speed streaks lifted slightly away from the wall before interacting with the buffer region.

When these streaks interact, small patches of fluid are ejected away from the wall. Kim et al. (18) have shown that the period between wall ejections is directly related to the wall-shear stress.

The concept of obtaining a period between ejections using wall dye slot visualization requires that the following criteria be satisfied: (1) All streaks that pass over the dye slot must be marked at the slot or in a very short distance downstream from the slot. (2) Dye cannot collect into streaks farther downstream from the slot such that ejections from those streaks are counted. (3) The field of view must be long enough that during the "life time" of a streak all ejections are observed. The "life time" of a streak will be that time from the beginning of its formation until its eventual breakdown when it is no longer identifiable as a longitudinal structure. When the filming time is long as compared to the time between ejections, the spatially averaged ejection rate (F) may be obtained by counting the number of ejections observed in a finite time span. The time between ejections from an individual streak is then given by $\overline{T}_E = 1/F\overline{\lambda}$.

When viewing the movie films, ejected patches of dyed fluid would broaden and mix with the surrounding fluid as they moved farther away from the wall. Viewing the movie films in reverse was found to be the most efficient way of identifying the ejection events. Using this procedure, the ejected patch of fluid away from the wall became narrower as the wall was approached. The ejected patch appeared to "focus down" to a narrow patch at the wall. The location downstream from the dye slot where the ejected patch "focused down" or appeared to originate from was called the "virtual origin" of the ejection. The length of viewing downstream from the dye slot was approximately 23 cm.

Bursts and Ejections

Offen and Kline (28) are perhaps the first to make a distinct difference between bursts and ejections, with a quantitative estimate of the interrelation between the two. An ejection is a small patch of fluid that leaves the near-wall region with a high velocity component normal to the wall, and an axial velocity less than the local mean velocity. The resultant effect is about a 75% contribution to the average production of turbulent kinetic energy. The word burst describes a period when one or more ejections are separated by a quiescent period greater than or equal to approximately 1/6 the average time between bursts. It is associated with the breakdown of a streak, by the ejection of fluid elements from within the streak, some time after its formation. The time span between breakdown of successive streaks is associated with the bursting period, $\overline{T}_B$, although a streak may burst more than one time during its "life time." For the water flows observed in this study, most streaks are destroyed after bursting one time. The breakdown of the streak during bursting takes place in a relatively short period as compared to the "life time" of the streak. In this case, the time between bursts is nearly equal to the streak "life time," since the period between streak breakdown and the formation of a successive new streak is small. In drag-reducing flows, the "life time" of the streaks is greater than for a water flow at the same wall-shear stress. Streaks may burst more than one time before losing their identity; therefore care must be taken when associating the bursting period with the time from formation to breakdown of a streak. Streak bursts do not necessarily terminate the existence of a streak.

During streak breakdown, a burst may contain several ejections. Kim et al. (18) did not treat ejections separately from bursts and it is highly probable that Kim measured the time between ejections $\overline{T}_E$ rather than $\overline{T}_B$. The average time between bursting events is called the "bursting period," while the time between ejection events is called the "ejection period." Offen and Kline (28) observed 41 bursts and 81 ejections at a fixed point in the flow over a period of approximately 230 seconds, indicating that on the average two ejections occur during every bursting period. Multiple ejections during periods of bursting have also been noted by Corino and Brodkey (7).

Donohue et al. (9) observed the spatially averaged ejection rate in drag-reducing flows, and found that the time between ejections had adjusted to the production levels associated with the reduced wall-shear values. Attempts to obtain the ejection period for both 50 and 100 p.p.m AP-273 solutions in this study did not satisfy at least two of the required criteria previously mentioned. These were: (1) dye may not collect into streaks farther downstream from the slot such that ejections from those streaks are counted, and (2) the field of view must be large enough that during the "life time" of a streak all ejections are observed. Figures 35 and 36 clearly illustrate the problem associated with drag-reducing flows. By viewing the motion pictures in reverse the ejected fluid elements marked by dye may be traced to their "virtual origin." Superimposing 2.5 cm divisions on the screen, "virtual origins" of ejected fluid were identified, and a histogram of "virtual origins" of ejections from streaks marked at the dye slot was obtained. Results given in this section are for cases when dye marks the outer portions of the viscous sublayer such that $M < 16$. Only a small portion of the dye

collects into streaks resulting in nearly all ejections in the field of view being marked. For the water flow (Figure 34) all ejections from streaks marked at the dye slot were seen in the field of view. As seen in Figure 35 the marking of nearly all ejections allowed calculation of the rate of ejections per unit area. For this case the value was 41.3 ejections/s-m^2. The rate of ejections per unit area could be found for most drag-reducing flows.

The data of Donohue et al. (9) and Achia and Thompson (1) tend to indicate that the time interval between ejections has decreased to the Newtonian level at a lower wall-shear stress. However, the field of view was limited in these studies, leading to the possibility that some streaks left the field of view before bursting, and as mentioned earlier, streaks formed downstream from the slot may also have been counted. Based on these observations it is unclear whether the time between wall ejections takes on a value equal to or higher than for a water flow at the reduced wall shear. A future study should be made to resolve this question.

Quantification of the ejection period from near-wall streaks in some drag-reducing flows might possibly be made with a normal wire generating oxygen bubble time lines[1] similar to those of Kim et al. (18). Problems associated with obtaining mean bursting or ejection periods using the

---

[1]Hydrogen bubble time lines could not be generated in any of the polymer solutions used in this study. Oxygen bubble time lines from a 0.025 mm platinum wire were generated in a beaker solution of 100 p.p.m 837-A. Use of oxygen time lines, in light of possible degradation near the generating wire, is justified since fluid motions which dictate the contortions of time lines are large as compared to the region marked by oxygen time lines.

wall dye slot are overcome by generation of time lines from a fixed location.

Streak Breakup

The main feature of the fluorescent dye is that it emits observable light when properly lit. Close observation of water flows in the channel reveal a vortical motion to be associated with fluid elements being ejected from streaks. This vortical motion as viewed from the side of the channel appears to be a "horseshoe" type vortex structure. The event is most easily observed at low flow rates and occurs at the beginning of nearly every ejection event. The "legs" of the structure are inclined at a fairly large angle to the wall and rotation appears to be as shown in Figure 37. Circular planes of dye, of varying diameter, are seen within this structure. As the structure moves downstream it appears to increase in size while losing its identity as marked by the dye (although the structure could still be present). There is no obvious indication of the structure before the ejection event. Photographing the structure is very difficult since the circular planes which reveal the structure are very thin. Close-up high-speed photography moving with the mean flow will reveal more of the details of this structure and the events associated with its occurrence. Offen and Kline (28) have commented on the existence of such a vortex structure being associated with fluid ejections.

In drag-reducing flows, the observed vortical motions associated with Newtonian ejections generally appear with ejections from dominant streaks. Most other streaks were ejected as longitudinal dye structures while displaying lateral waving motions. As mentioned earlier, not all

streaks began to burst in the field of view. For the AP-19 run analyzed, approximately 63% of the streaks burst in the field of view, 14% left without bursting and 23% dissipated or lost their identity without bursting. Offen and Kline (28) have stated that the velocity of an ejected low-speed streak after having left the influence of the wall should be a function of the strain rate along its trajectory. Carpenter (5) found that for drag-reducing flows the Reynolds stresses were greatly reduced from Newtonian values. This might be explained by the solution's ability to resist axisymmetric straining.

In both the AP-19 and SL-4 runs there was a high degree of probability that two to three adjacent streaks would burst at nearly the same time and location downstream from the dye slot. Again, viewing a width of nearly $3\bar{\lambda}$, "groups" of bursts occurred approximately 76% of the time for the water flow and 67% of the time for the drag-reducing flow. This might indicate that the mechanism responsible for bursting dominates a small region larger than the streak spacing.

After the breakdown of a streak there is usually some residual leftover which still can be identified as a streak. In the water flow this residual usually loses its identity a short time after breakdown or is overtaken by a new streak. In the drag-reducing flow a larger portion of the streak is left as a residual. Possibly only the upper portions of the streak are "ripped" away during bursting. Runstadler et al. (32) have also commented on a small residual left after bursting.

A reduced rate of mixing was seen in drag-reducing flows. Dye transported to the center of the channel in a short period of time for a water flow had seldom diffused to the center before reaching the end of

the channel in 100 p.p.m AP-273 flows. Large reductions in eddy diffusivity were noted by Reischman (30) in 100 p.p.m AP-273 solutions.

APPENDIX C

COMMENTS ON FLUORESCENT DYE LIGHTING TECHNIQUE

The fluorescent dye lighting technique employed in this study adds a new dimension to flow visualization. The contortions and motions of the dye marked fluid may be viewed in three dimensions with a high degree of detail. However, both the back light and side light arrangements should be used since each reveals information that the other may not easily detect (i.e., dye contour and relative dye density). Fluorescent dyes other than Rhodamine B may also be used.

When using this lighting technique, fluid should pass through the system only one time and should not be recirculated. The smallest traces of recirculated dye are noticeable and tend to "cloud" the picture. This is important in achieving a high quality photographic reproduction.

APPENDIX D

MIXING TECHNIQUE AND SOLUTION CHARACTERISTICS

Mixing Technique

The procedure used in mixing and preparing the polymer solutions was described in Chapter II. The technique yielded results which were consistently reproducible over a moderate range of temperatures (10-27°C) with the mixing temperature for the concentrated solutions held constant. The solutions also yielded consistent results when the temperature of the solution remained constant and the mixing temperature was varied. Concentrated solutions were mixed at approximately 31°C as part of a consistent procedure. As we will see in Appendix E, these solution characterizations are useful in predicting the level of drag reduction for pipe and channel flows. The correlations are useful provided that solution degradation has not begun to take place.

Solution Characteristics

The drag-reducing characteristics for 100 p.p.m AP-273 solutions are shown in Figure 39. The data shows excellent consistency between solution batch mixes. Data from both the channel and pipes are represented in Figure 39.

The Polyox Coagulant solutions tested rapidly degraded after mixing at the 100 p.p.m level. Characterizations made at 2 hours and 11 hours after mixing showed approximately 10% decrease in drag reduction with

only a small decrease noted at 24 hours. A solution mixed with 0.17% Formaldehyde to retard degradation yielded an increase of 15% in drag reduction when run at 2 hours after mixing. A 100 p.p.m Polyox solution obtained by injection of a 1000 p.p.m concentrated solution at the pipe inlet showed increases in drag-reduction of 20% to 60% above the characterizations of untreated 100 p.p.m Polyox solutions at 2 hours after mixing. The levels of drag-reduction obtained in this manner yielded nearly the same characterization as obtained by Donohue et al. (9) for a 140 p.p.m Polyox-FRA solution.

APPENDIX E

PRE-RUN AND DATA REDUCTION CALCULATIONS

Pre-Run Calculations

Flow visualization experiments may be run at either constant flow rate, drag reduction, or wall-shear stress. Computation of the desired flow conditions is only required for the latter two. Initial estimates are therefore made before each run and "on-line" adjustments made during the run to achieve the specified shear stress or drag reduction. This procedure eliminates timely and unnecessary adjustments in flow conditions since the total volume of solution available for each run is limited.

Constant Wall-Shear Stress

Flow rates for water runs at constant wall-shear stress are obtained in a relatively straightforward manner. For Reynolds numbers less than 10^5 the friction factor may be expressed by the Blasius relation:

$$f = 0.316\ Re^{-.25} \tag{E.1}$$

From the definition of friction factor and applying a simple force balance between the fluid and its surroundings, the wall-shear stress may be expressed as:

$$\frac{U_\tau}{U} = 0.2\ Re^{-.125} \tag{E.2}$$

For a given channel geometry or pipe diameter and fluid properties, the wall-shear stress may be expressed explicitly as a function of the mass-average velocity. Conversely, the average velocity required to achieve the specified wall-shear stress may be obtained directly. After the flow rate has reached steady state conditions, minor adjustments may be needed to obtain the required wall-shear stress.

Experiments in drag reducing flows may also be run at a specified wall-shear stress; however, the method is not so straightforward. An initial estimate of the average velocity necessary for these conditions require that the drag-reduction characteristics (Figure 39) of the solution be known. Once these are known from a single experiment, then future experiments may be designed. The procedure begins with calculation of the solvent shear velocity from Equation (E.2) using an initial estimate (best guess) of the required average velocity. The level of drag reduction may then be obtained from the experimentally determined characteristics (Figure 39). The wall-shear velocity under drag-reducing conditions may then be computed through the following definition,

$$(U_\tau)_p = (U_\tau)_s \, (1 - \% \text{ D.R.})^{\frac{1}{2}} \tag{E.3}$$

where the wall-shear stress is given as:

$$\tau_w = \rho U_\tau^2 \tag{E.4}$$

If this is not the desired wall-shear stress, then the procedure is repeated with a new flow rate estimate. Not more than three iterations should be required. During the data run final adjustments in flow rate may be required to obtain the desired wall-shear stress.

Constant Drag Reduction

Experiments where the level of drag reduction is specified may require "on-line" calculations for flow rate corrections. The solvent friction velocity is obtained from the solution drag-reduction characteristics and applied to Equation (E.2), yielding an estimate of the flow rate at the required drag reduction. Utilizing the Blasius friction factor relation, the level of drag reduction may be calculated at each flow rate through the relation,

$$\% \text{ D.R.} = 1 - 6.33 \left(\frac{D_H}{\nu_s}\right)^{0.25} \left(\frac{g \rho' D_H}{L \rho_s}\right) \frac{\Delta h_p}{U^{1.75}} \qquad \text{(E.5)}$$

where

$$6.33 \left(\frac{D_H}{\nu_s}\right)^{0.25} \left(\frac{g \rho' D_H}{L \rho_s}\right)$$

is a constant (B) dependent on fluid properties and channel geometry.

$$\% \text{ D.R.} = 1 - B \, \Delta h_p / U^{1.75} \qquad \text{(E.6)}$$

The total change in elevation of the two-fluid manometer interface during the run, as indicated by the micrometer, is given as Δh. The density difference of the two fluids in the micromanometer is given as ρ', and the length between pressure taps as L. An estimate of the level of drag reduction during the run requires that only pressure drop and flow rate measurements be made. The weir height is measured to determine the flow rate from an experimentally determined correlation. Final adjustments in flow rate are then made to achieve the desired level of drag reduction. Accurate measurements are then made of flow rate and fluid temperature.

Post-Run Calculations

Immediately following the run an accurate measurement of the flow rate was calculated from the timed weir bucket collection. Knowing the fluid temperature, a solvent Reynolds number is then calculated, from which the solvent friction factor was obtained from Figure 8. The drag-reducing friction velocity is obtained directly from measured pressure drop,

$$U_\tau = \left(\frac{g\,\rho'\,D_H\,\Delta h}{4L\rho_s}\right)^{\frac{1}{2}} \tag{E.7}$$

from which a drag-reducing friction factor may be calculated from the relation:

$$f = 8\left(\frac{U_\tau}{U}\right)^2 \tag{E.8}$$

Finally the level of drag reduction is obtained through the relation,

$$\%\ \text{D.R.} = 1 - f_p/f_s \tag{E.9}$$

and the corresponding solvent friction velocity is found using Equation (E.8).

APPENDIX F

UNCERTAINTY ESTIMATES

All experimental data is subject to a certain degree of error, the error being defined as the difference between the true value and the observed value. Errors may arise in three forms: fixed errors, random errors, and human errors. Fixed errors in experiments are minimized by comparison with data from other investigators whose results are well accepted in the literature. This data is classified as qualifying data for the experimental apparatus or technique and is an essential step before proceeding further into an investigation. Human errors are attributed to mistakes in taking and recording data. These errors are minimized by comparing the data to known correlations. Comparing the measured flow rate to that obtained using the weir height calibration curve is one example. Comparisons with previous data eliminates, to a large degree, the human error factor. Random errors are those errors which vary from reading to reading or between experiments, and their effect can be reduced by taking the average of a large amount of data.

Fixed and random errors were accounted for by uncertainty estimates following the methods outlined by Kline and McClintock (20). Uncertainties in the following quantities were estimated at 20:1 odds.

Volume flow rate collected	$\pm$ 3%
Elapsed time of collection	$\pm$ 2%
Channel cross-sectional area	$\pm$ 3%

Micromanometer reading (Δh) $U_\tau \cong 0.016$ m/s	$\pm$ 10%
Micromanometer reading (Δh) $U_\tau \cong 0.010$ m/s	$\pm$ 20%
Effective fluid density in micromanometer (ρ')	$\pm$ 5%
Solution viscosity	$\pm$ 10%

The uncertainties in average flow rate ($\dot{Q}$) and velocity (U) were then estimated to be $\pm$4% and $\pm$5%, respectively. The uncertainties in wall-shear velocity and friction factor were then estimated.

$$U_\tau = \text{constant } (\Delta h\, D_H\, \rho')^{\frac{1}{2}}$$
$$f = \text{constant } (\Delta h\, D_H\, \rho'\, U^{-2}) \quad \text{(See Appendix B.)}$$

$$U_\tau \pm 6\% \quad (\cong 0.016 \text{ m/s})$$
$$f \pm 13\%$$

$$U_\tau \pm 10\% \quad (\cong 0.010 \text{ m/s})$$
$$f \pm 22\%$$

The corresponding uncertainties in the level of drag reduction were $\pm$18% and $\pm$ 30%, respectively.

An estimate of the streak spacing error was made using the following statistical relation,

$$\bar{\lambda} - t\,\sigma/\sqrt{N} \leq \mu \leq \bar{\lambda} + t\,\sigma/\sqrt{N}$$

with μ given as the true mean and t taken at the 95% confidence level from a "t distribution" for N statistically independent samples. The scaling error when measuring distance between adjacent streaks was estimated at $\pm$2%. The resultant error in non-dimensional streak spacing was typically $\pm$15%.

The number of statistically independent samples required for a given streak spacing accuracy may be estimated through the following relation:

$$N = [t\ (\sigma/\overline{\lambda})\ (\overline{\lambda}/\Delta\overline{\lambda})]^2$$

Taking $\sigma/\overline{\lambda} = 0.36$ when measuring the distance between streaks and assuming a normal distribution, approximately 207 samples are required for a 5% uncertainty in the mean, while only 52 samples are needed for a 10% uncertainty. These values correspond to the sampling of approximately 10 to 30 statistically independent movie frames for these experiments.

APPENDIX G

FIGURES AND ILLUSTRATIONS

This appendix contains the figures and illustrations referred to in the text of this thesis.

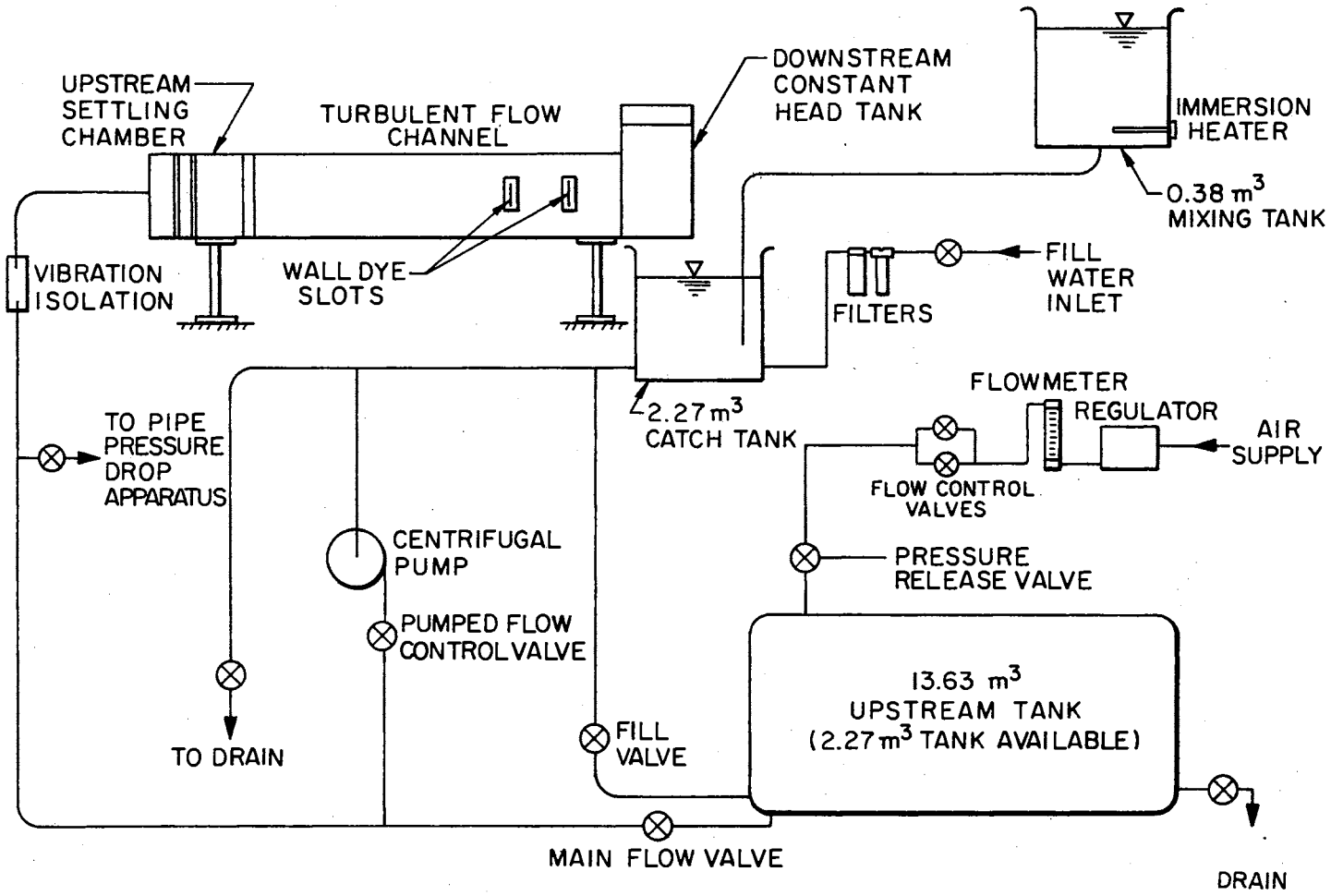

Figure 1. Schematic of Two-Dimensional Channel and Circulation System

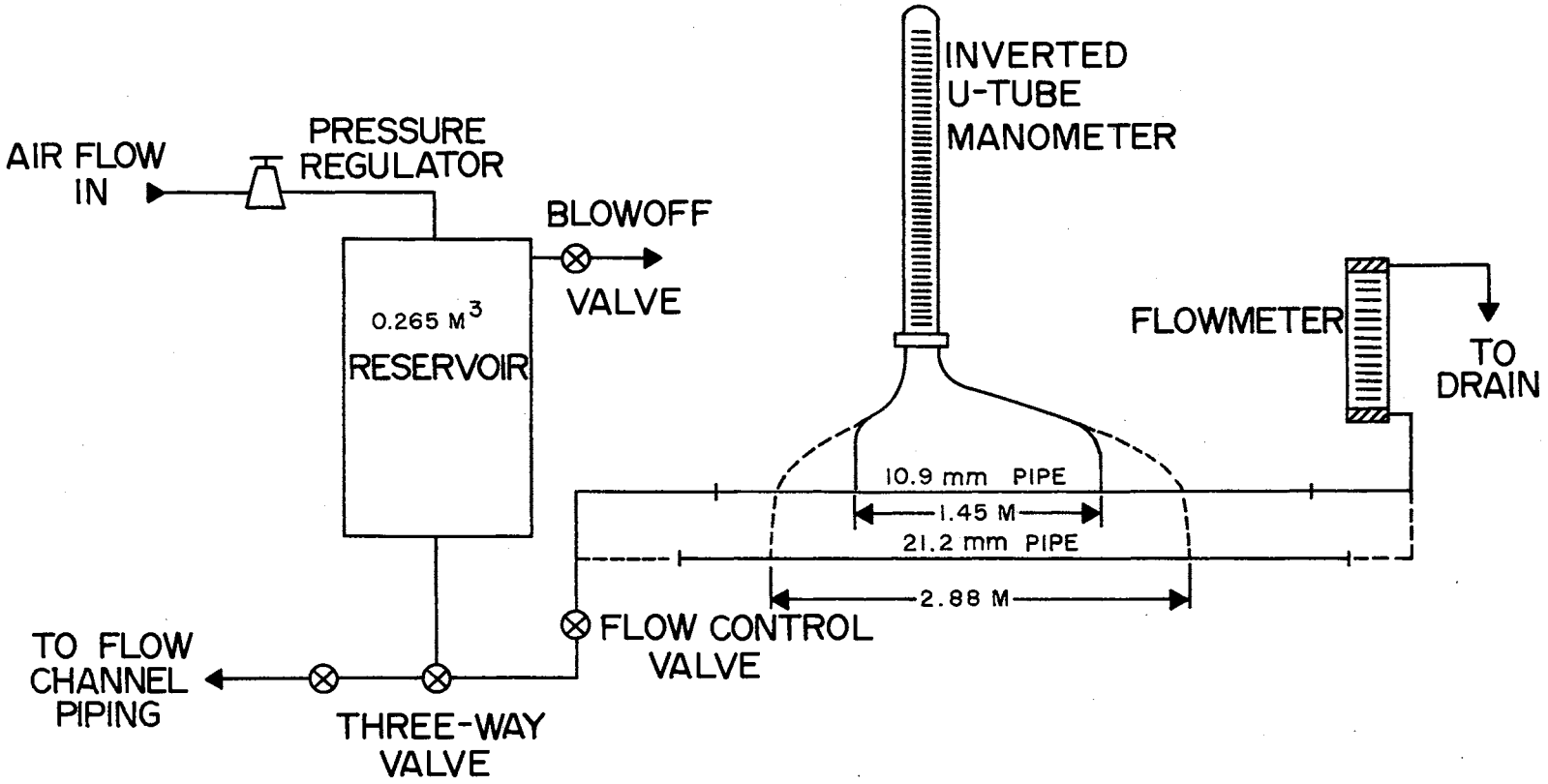

Figure 2. Line Diagram of Pipe Pressure Drop Apparatus

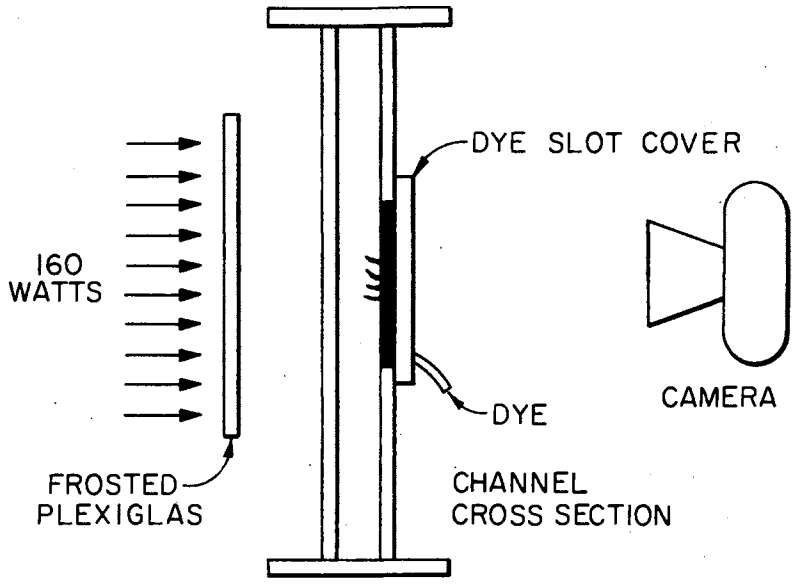

Figure 3. Back Lighting Technique for Visualization of Low-Speed Streaks

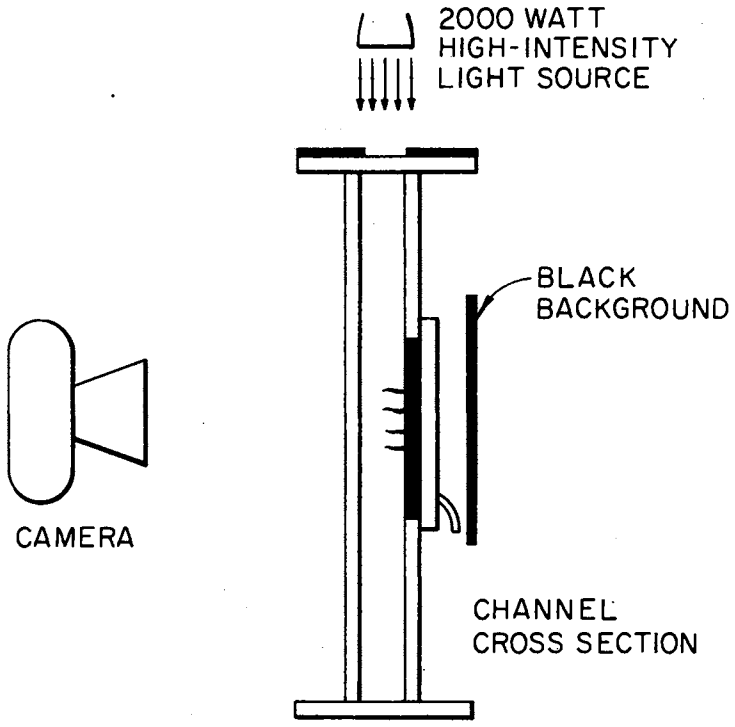

Figure 4. Side Lighting Technique for Visualization of Wall Region

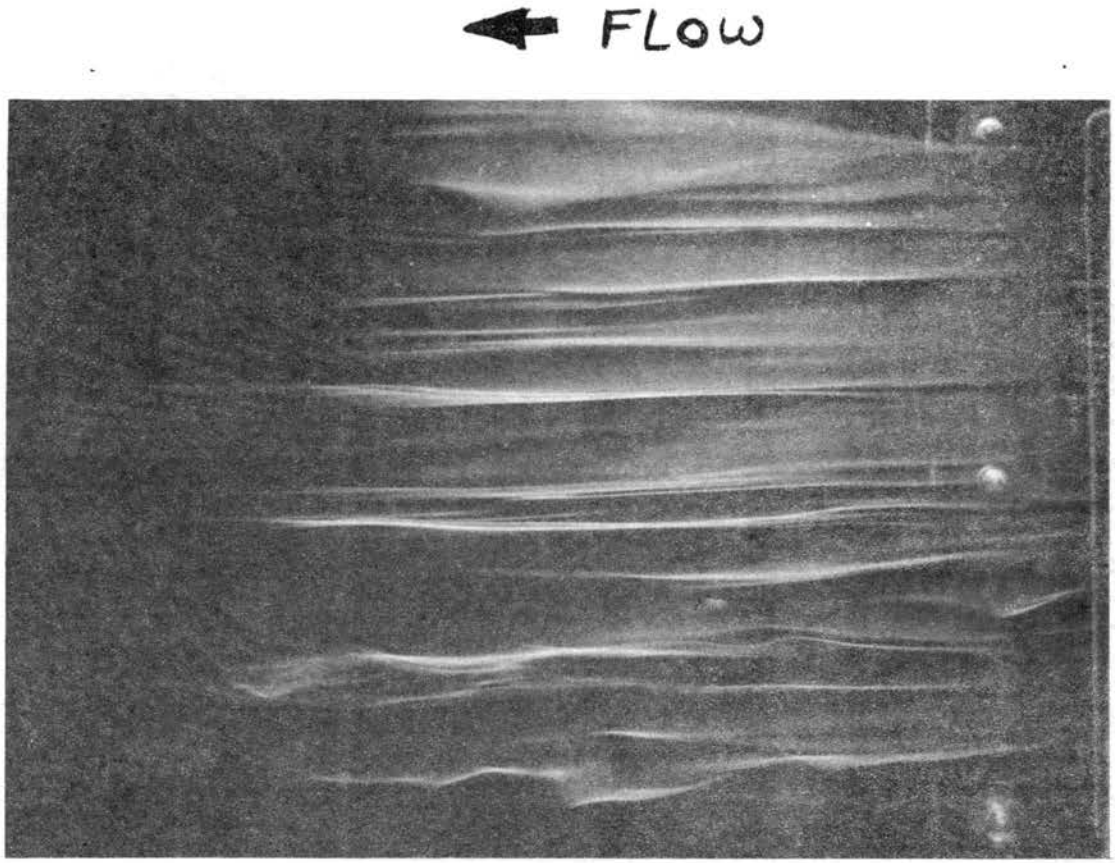

Figure 5. Near-Wall Flow Structure as Revealed Using the Side Lighting Technique (Water Flow, Re ≅ 6000)

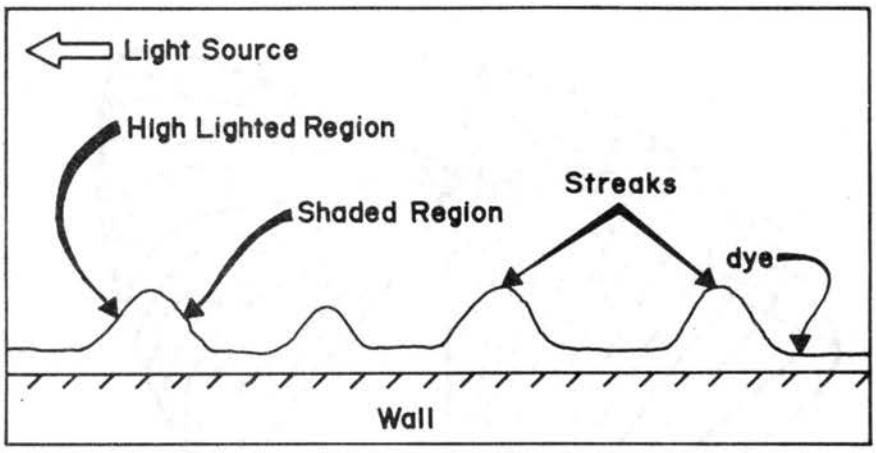

Figure 6. End-View Cross Section of the Near-Wall Streak Structure as Viewed With the Side Lighting Technique

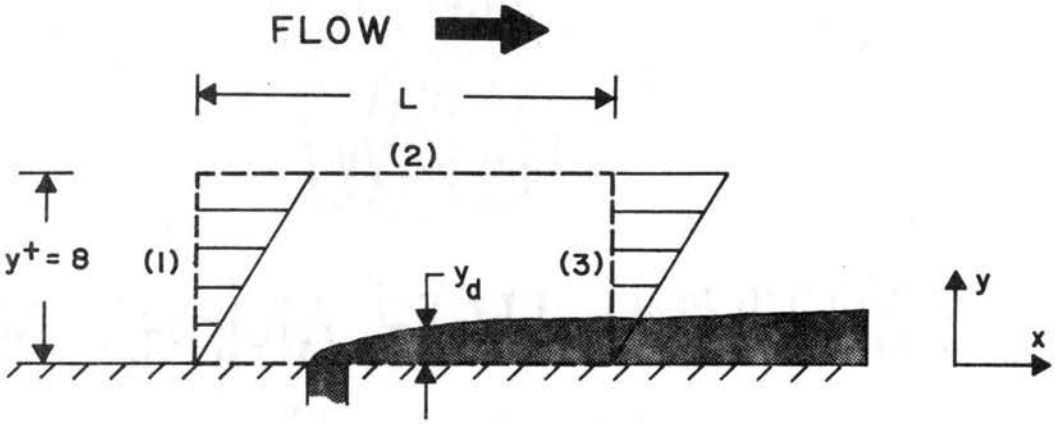

Figure 7. Control Volume for Analysis of the Outer Bounds of Dye Seeping Into a Laminar, Constant Shear Flow

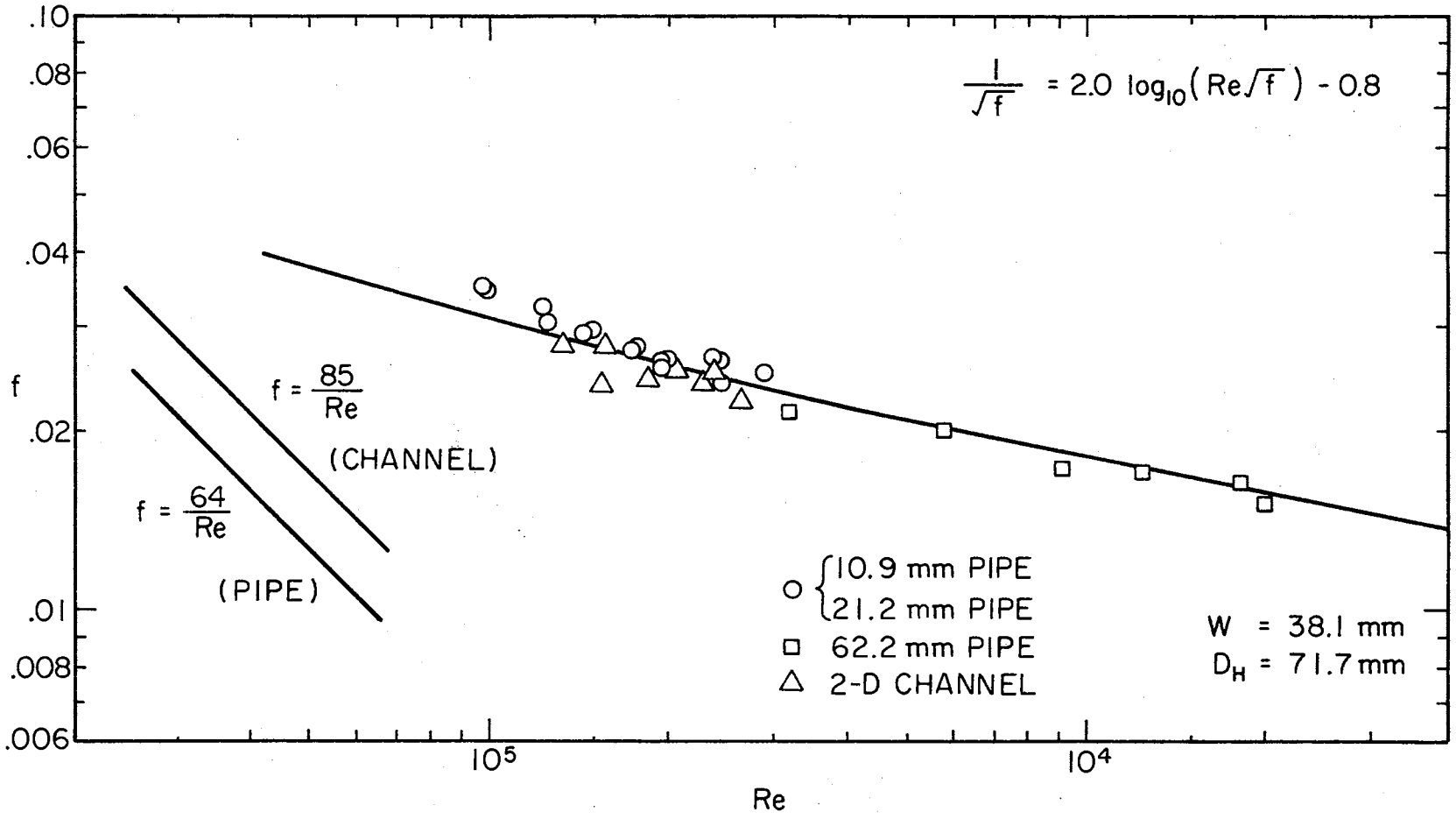

Figure 8. Universal Friction Correlation for Internal Turbulent Flow

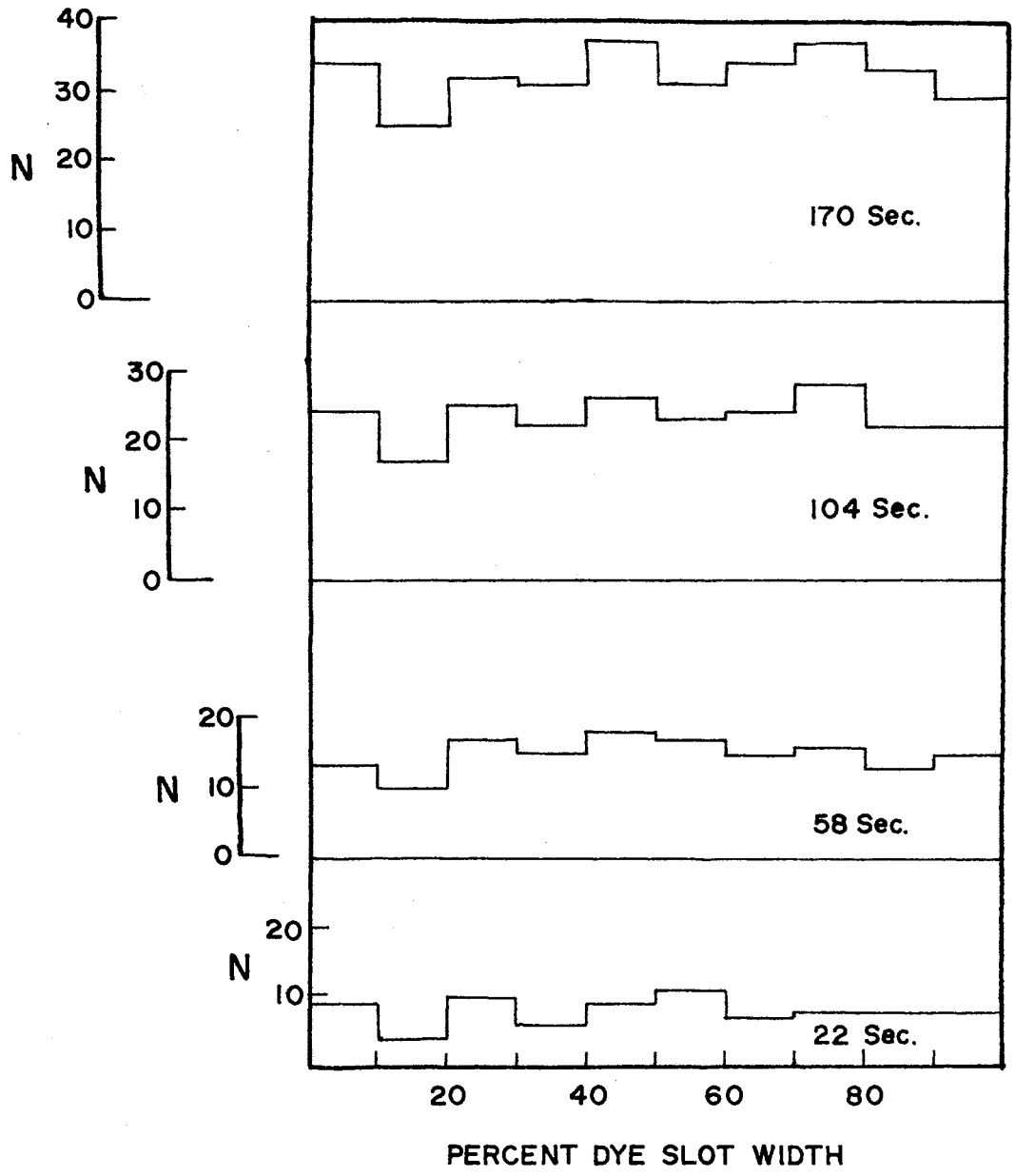

Figure 9. Histogram of Transverse Location of Low-Speed Streaks for a Drag-Reducing Flow (Re = 10,280)

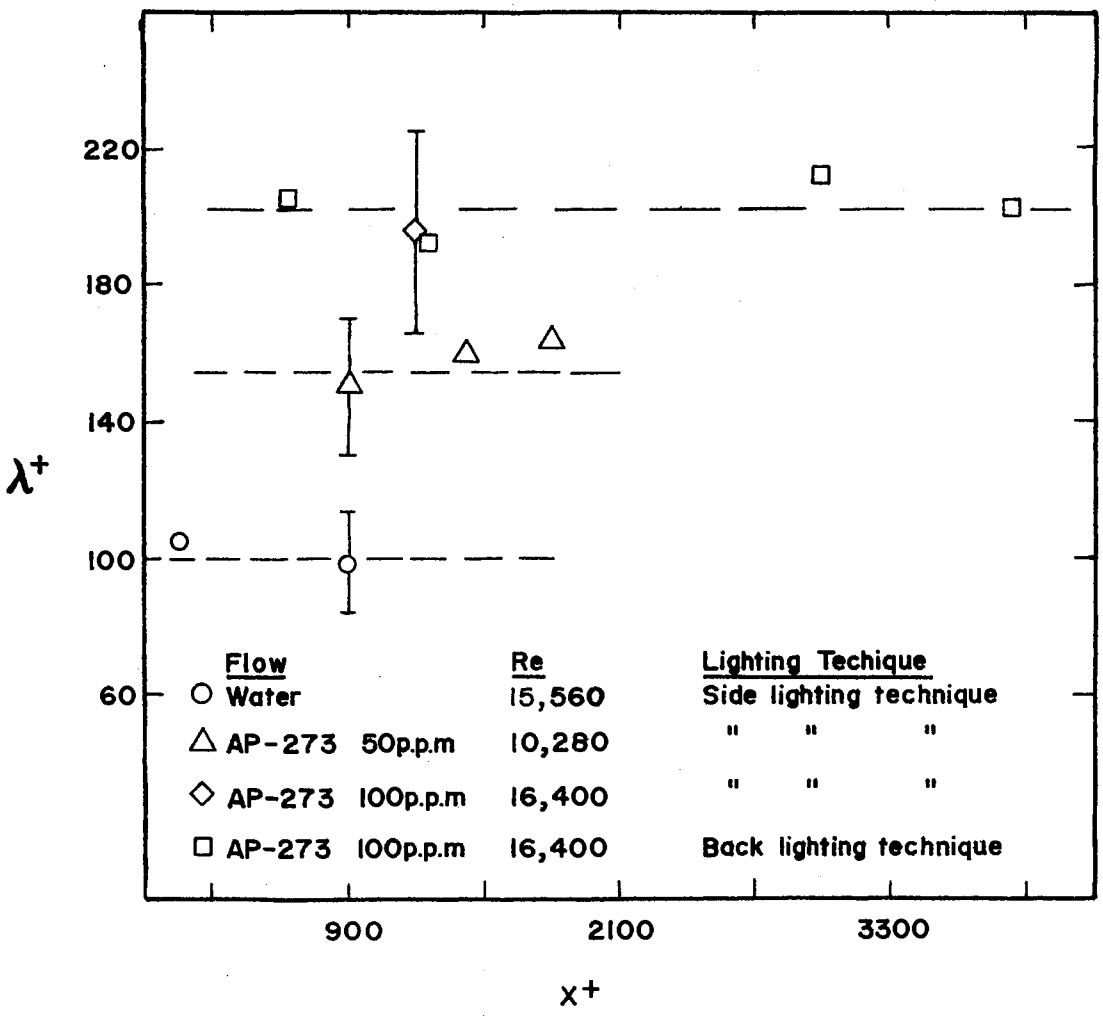

Figure 10. Longitudinal Distribution of the Spanwise Streak Spacing

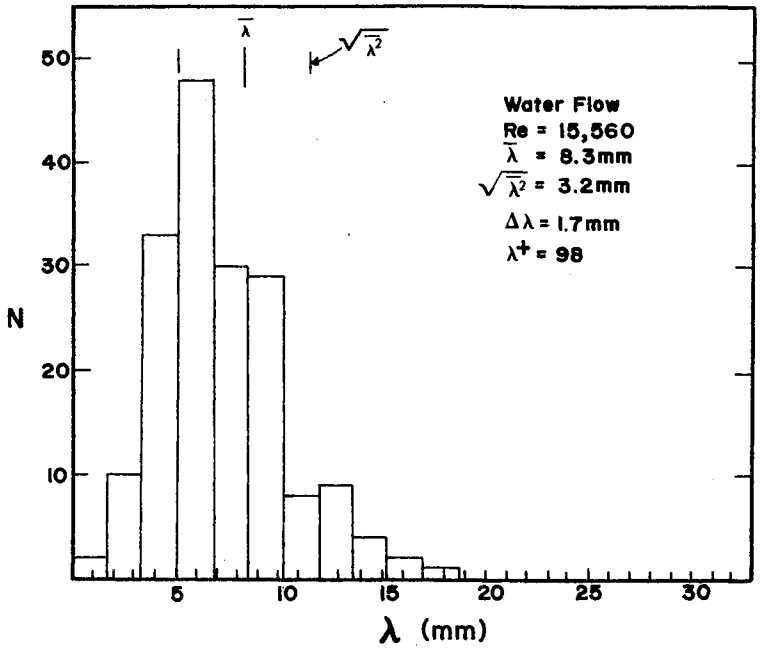

Figure 11. Streak Spacing Histogram for Solvent Flow (Re = 15,560)

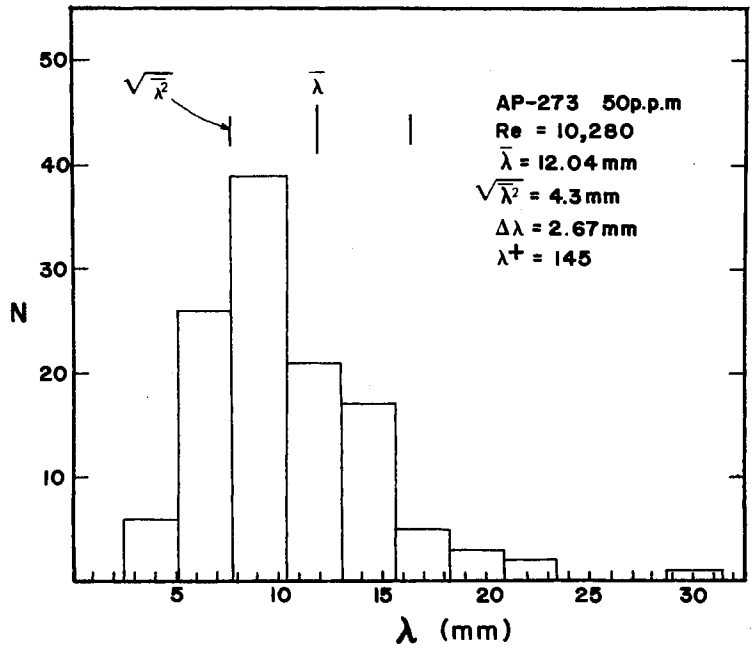

Figure 12. Streak Spacing Histogram for a Drag-Reducing Flow (Re = 10,280)

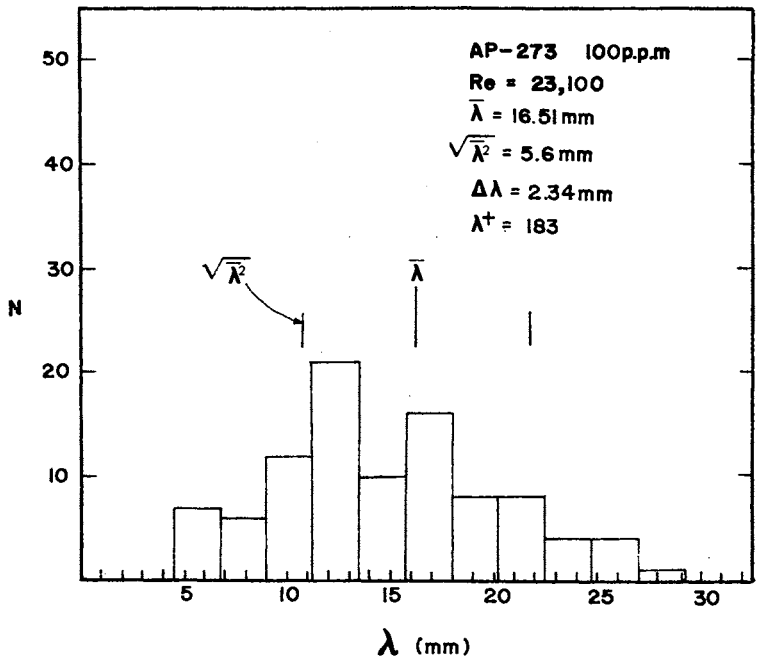

Figure 13. Streak Spacing Histogram for a Drag-Reducing Flow (Re = 23,100)

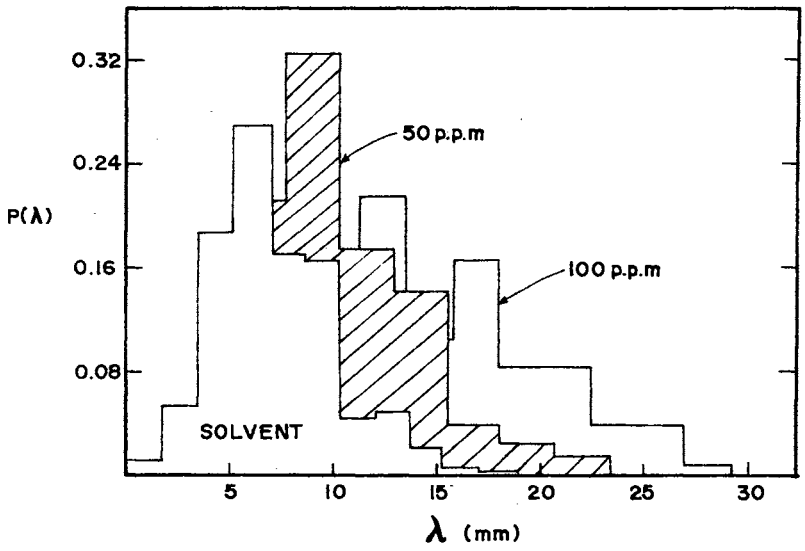

Figure 14. Comparison of Drag-Reducing Streak Spacing Histograms to Solvent Histogram

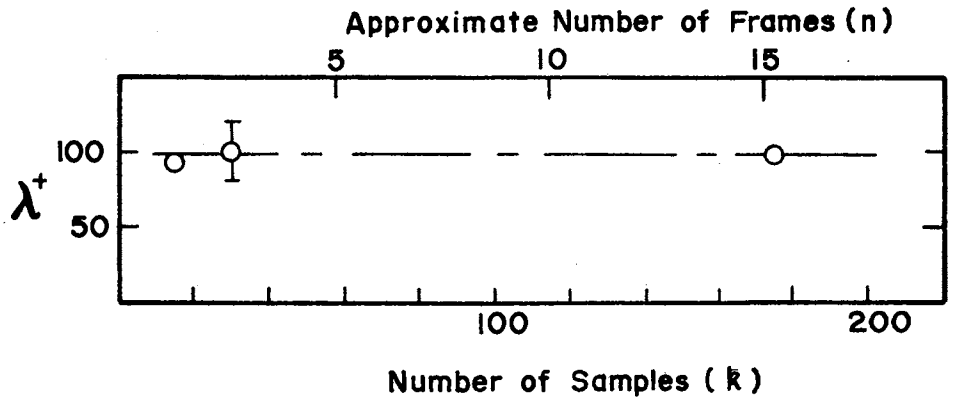

Figure 15. Number of Samples Required to Determine $\overline{\lambda}$ in a Water Flow (Re = 15,560)

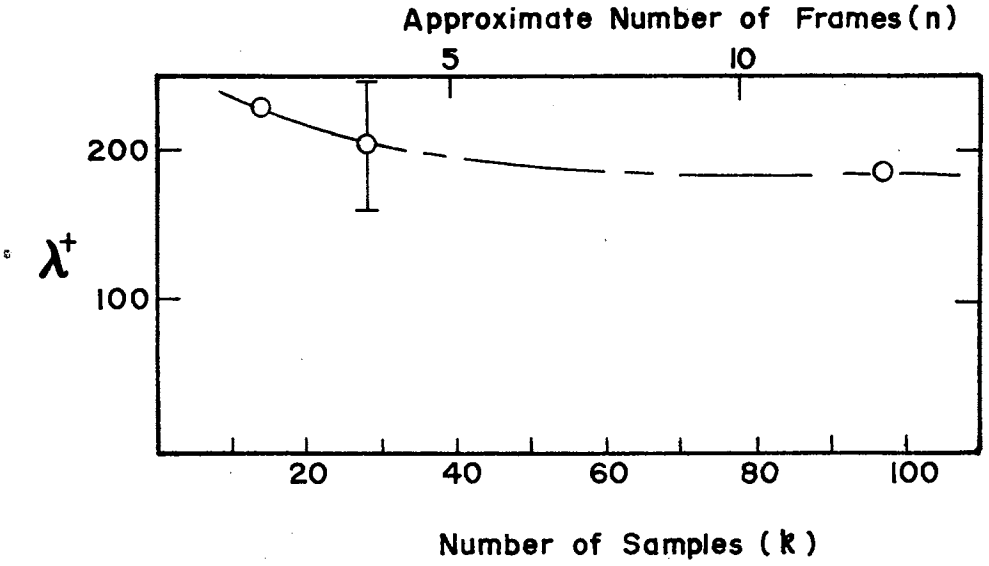

Figure 16. Number of Samples Required to Determine $\overline{\lambda}$ in a Drag-Reducing Flow (Re = 23,100)

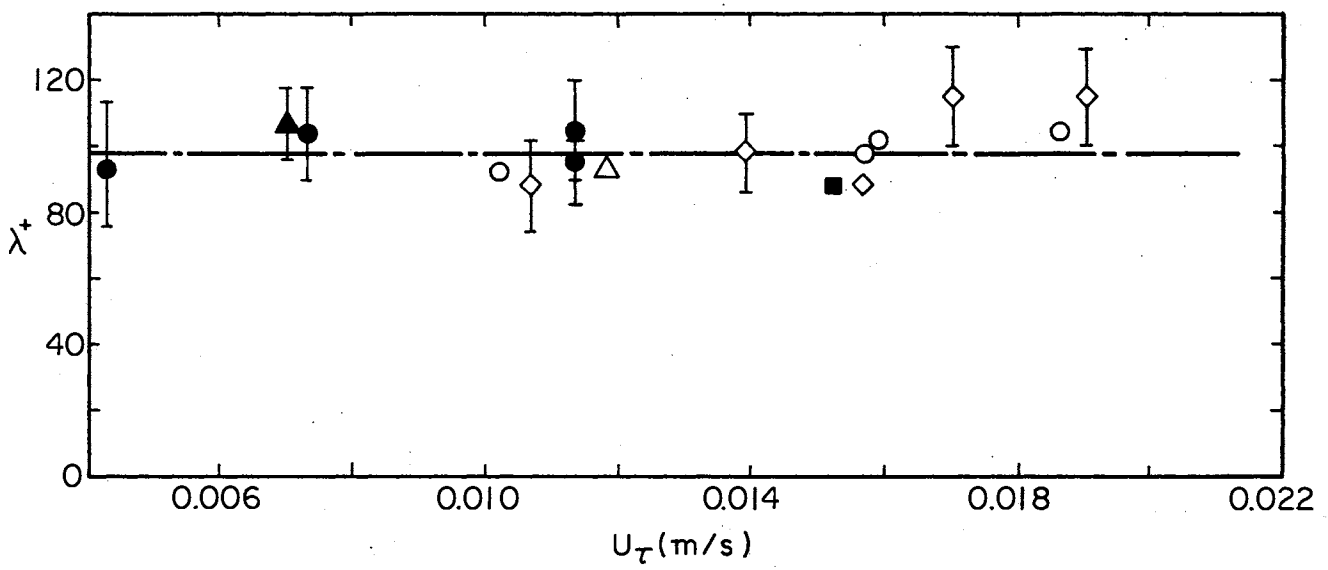

Figure 17. Non-Dimensional Streak Spacing for Non-Drag-Reducing Flows

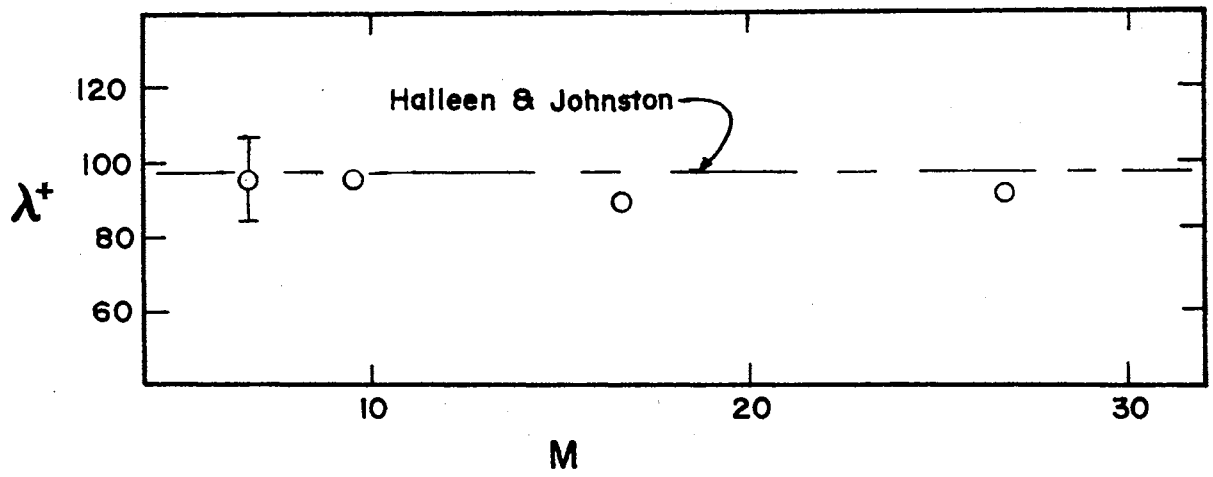

Figure 18. Variation in Non-Dimensional Streak Spacing With Sublayer Dye Flow Rate Ratio for a Water Flow (Re = 15,200)

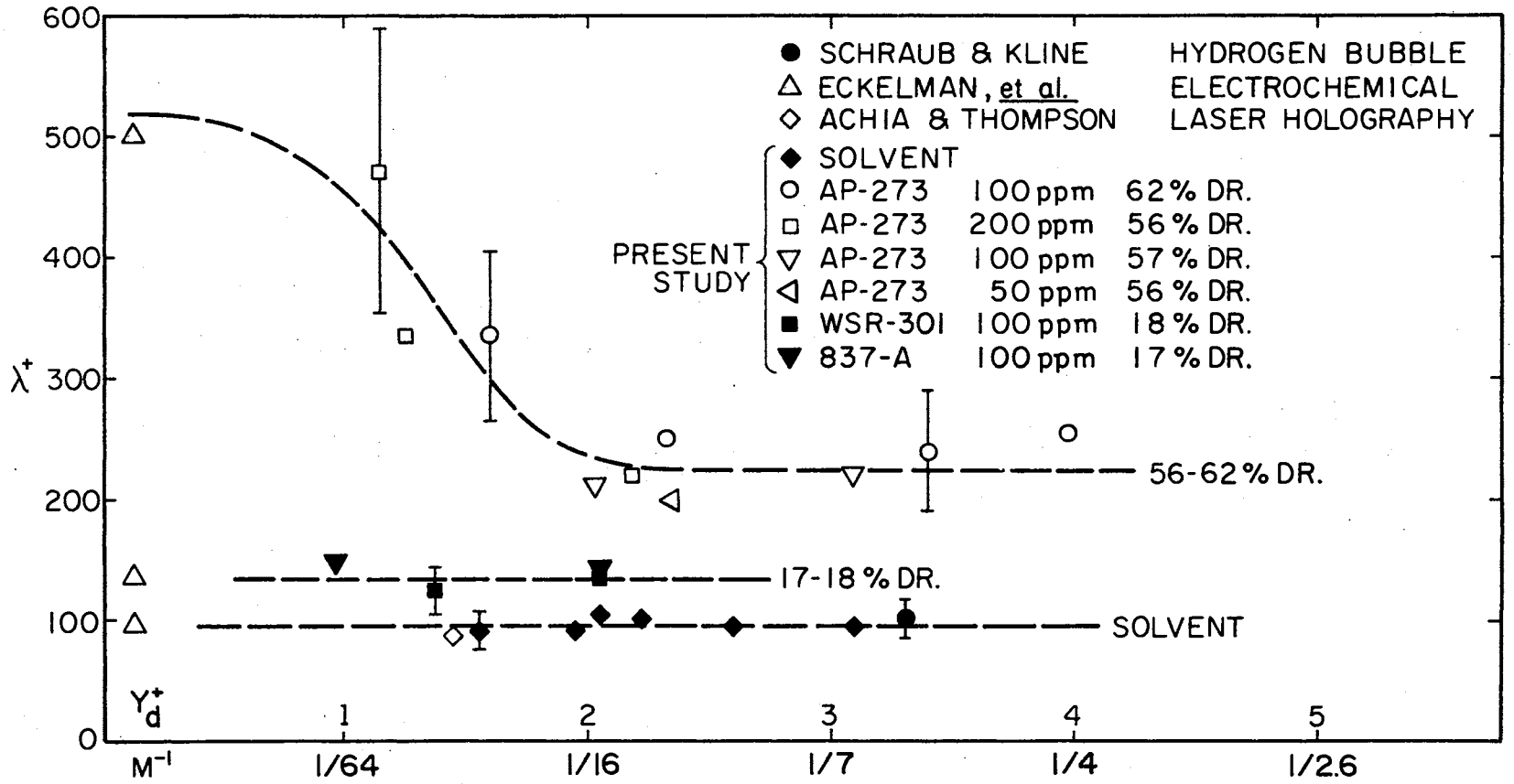

Figure 19. Effect of Sublayer-Dye Flow Rate Ratio on Non-Dimensional Streak Spacing

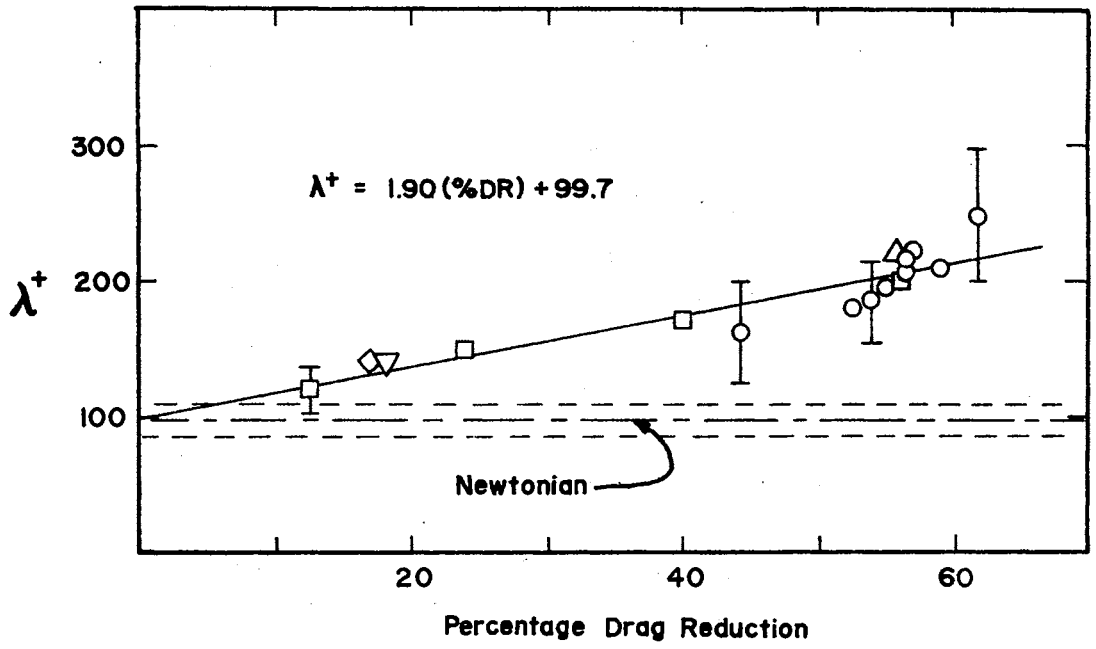

□	AP-273	50 p.p.m
○	AP-273	100 p.p.m
△	AP-273	200p.p.m
◇	Magnifloc 837-A	100 p.p.m
▽	Polyox WSR-301	100 p.p.m

Figure 20. Non-Dimensional Streak Spacing for Drag-Reducing Solutions (Counting Technique I) $4 < M < 16$

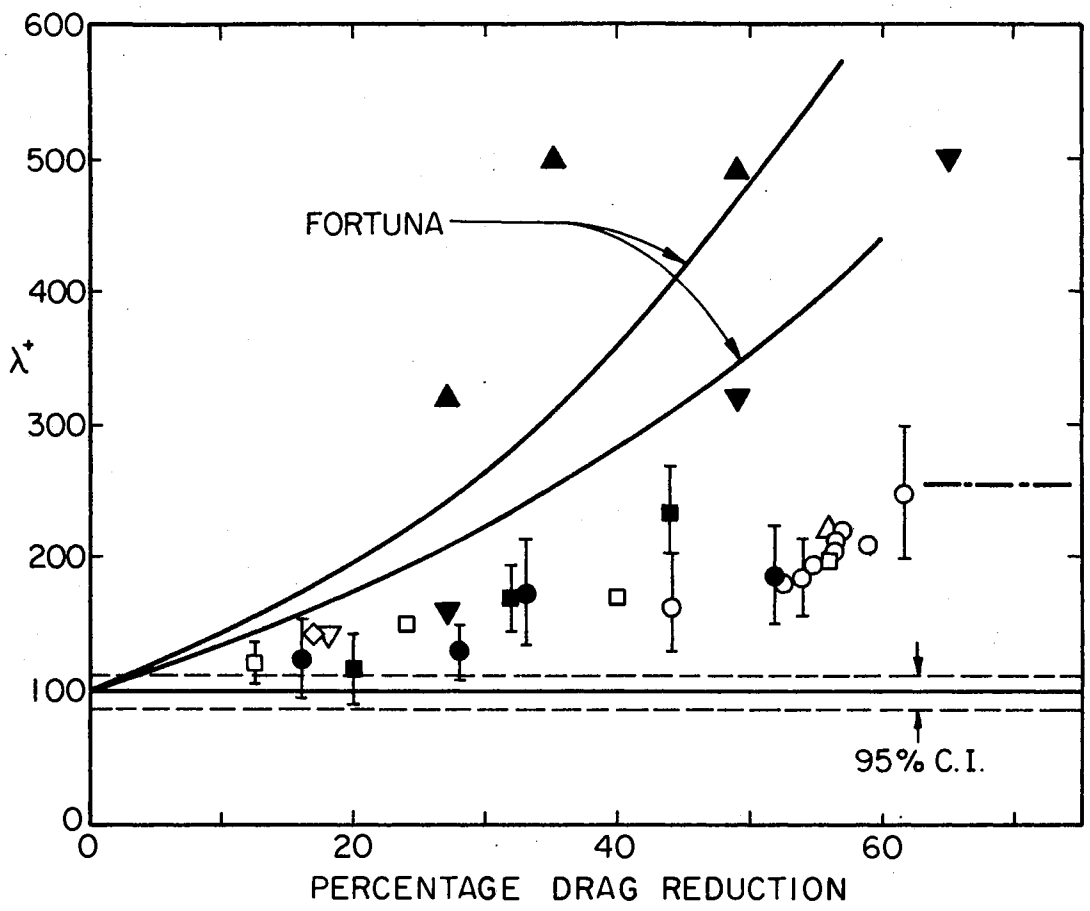

● DONOHUE, et al., 140 ppm POLYETHYLENE OXIDE
▲ FORTUNA & HANRATTY 160 ppm AP-30
▼ ECKELMAN, et al., 160 ppm AP-30
■ ACHIA & THOMPSON 50 ppm AP-30
MORETTI & KAYS
SCHRAUB & KLINE
} RELAMINARIZATION LIMIT dP/dx≪0

PRESENT STUDY

□ AP-273 50 ppm
○ AP-273 100 ppm
△ AP-273 200 ppm
◇ MAGNIFLOC 837-A 100 ppm
▽ POLYOX WSR-301 100 ppm
} COUNTING TECHNIQUE I

Figure 21. Comparison of Non-Dimensional Streak Spacing With Other Investigators ($4 < M < 16$)

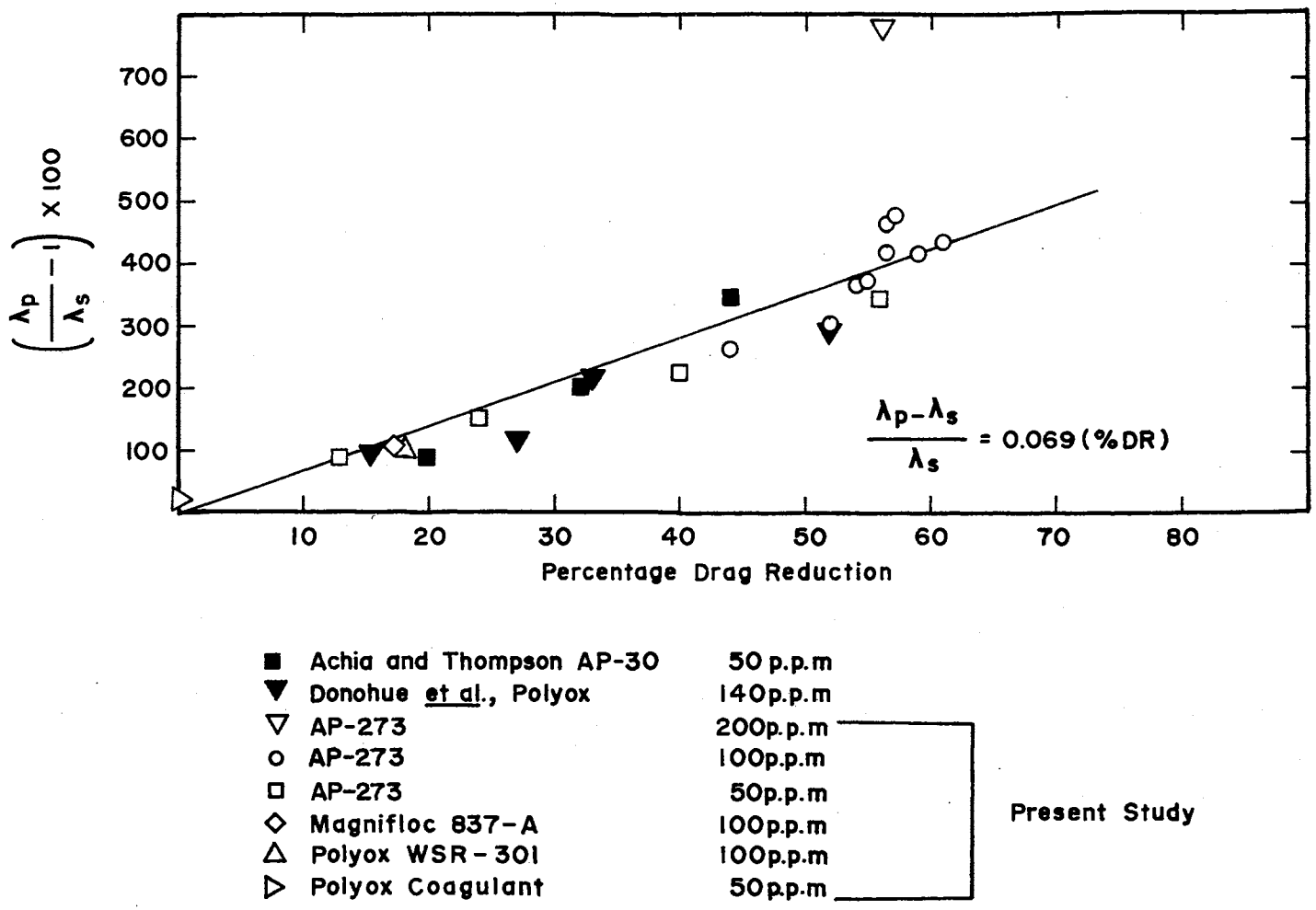

Figure 22. Percentage Increase in Dimensional Spacing Between Streaks for Drag-Reducing Flows ($4 < M < 16$)

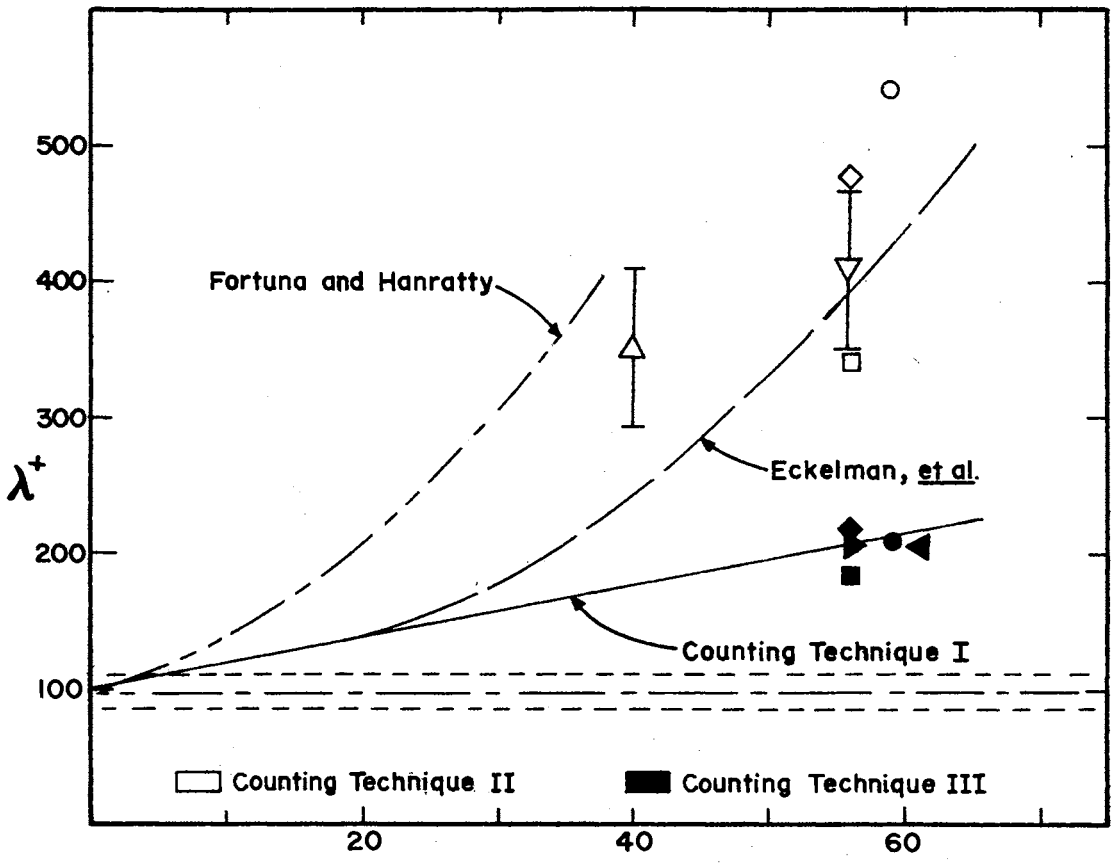

△	AP-273	50 p.p.m	Re = 22,900	M = 11.6
▽	AP-273	50 p.p.m	Re = 31,800	M = 11.6
○	AP-273	100 p.p.m	Re = 22,200	M = 20.0*
◁	AP-273	100 p.p.m	Re = 33,400	M = 25.2
▷	AP-273	100 p.p.m	Re = 23,100	M = 15.6
□	AP-273	200p.p.m	Re = 18,400	M = 13.6
◇	AP-273	200p.p.m	Re = 17,600	M = 48.0

* Estimated M ± 5

Figure 23. Non-Dimensional Streak Spacing for Drag-Reducing Solutions (Counting Techniques II and III)

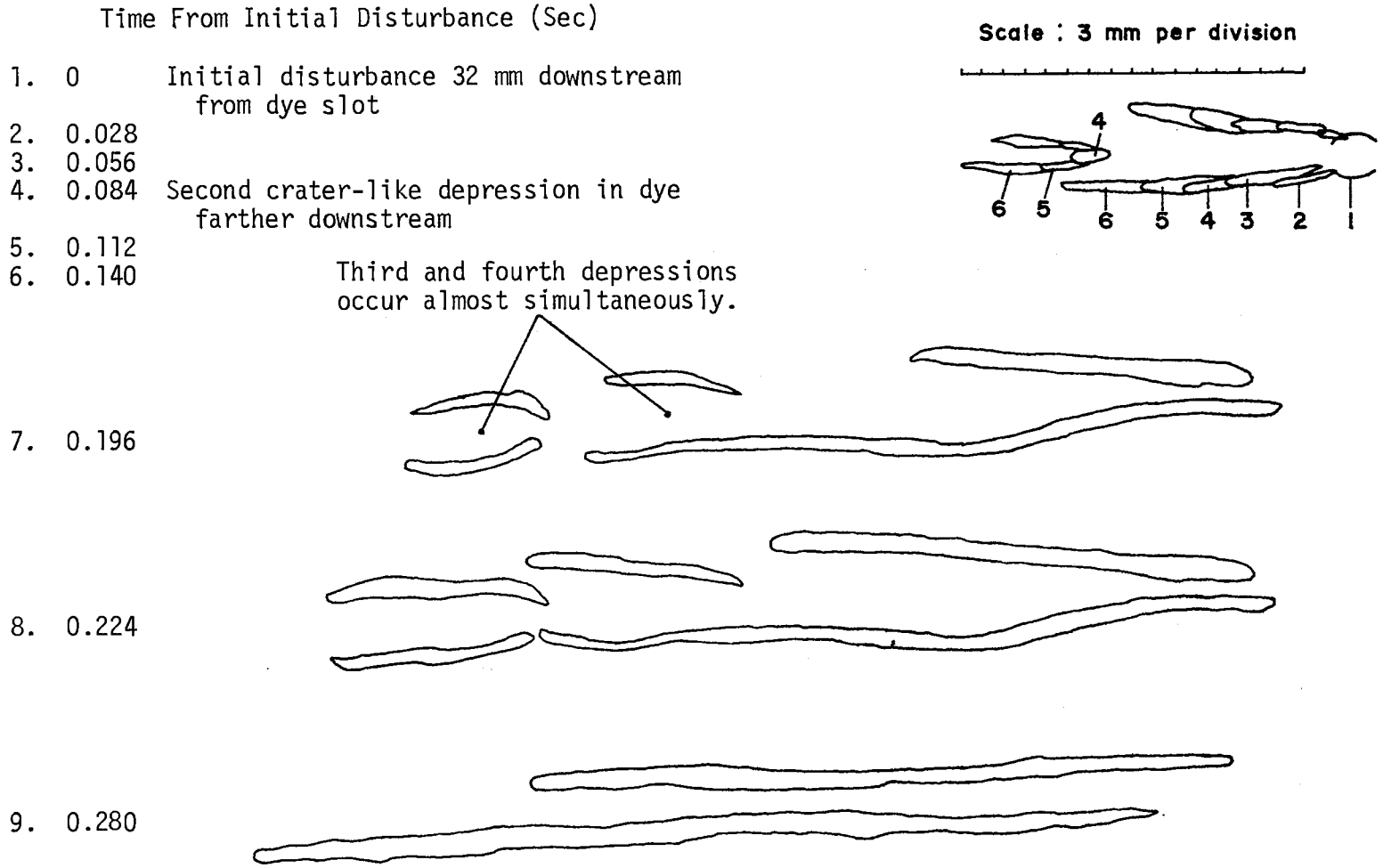

Figure 24. Formation and Growth of a Streak Pair (AP-273, Re = 18,400, M = 13.6)

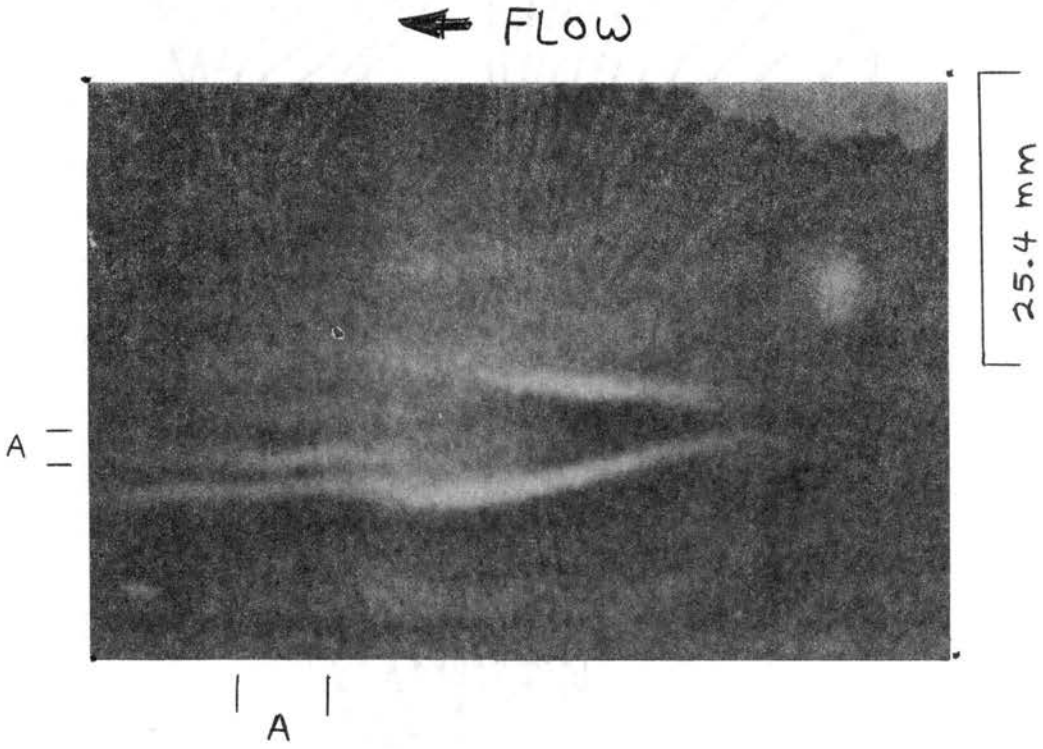

Section A--Second crater-like depression in wall dye

Figure 25. Growth of a Streak Pair 0.112 Seconds After Initial Disturbance to Wall Dye (AP-273, Re = 18,400)

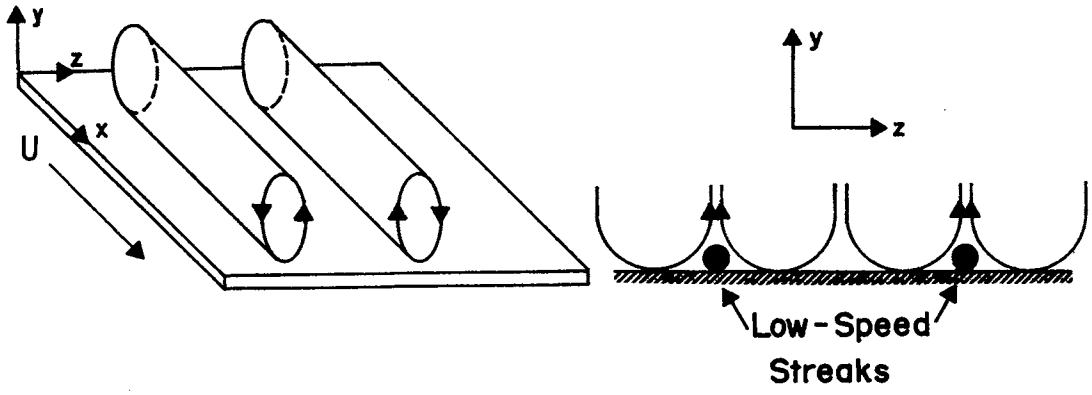

Figure 26. Near-Wall Large Eddy Structure as Proposed by Bakewell et al. (2) and Sirkar et al. (34)

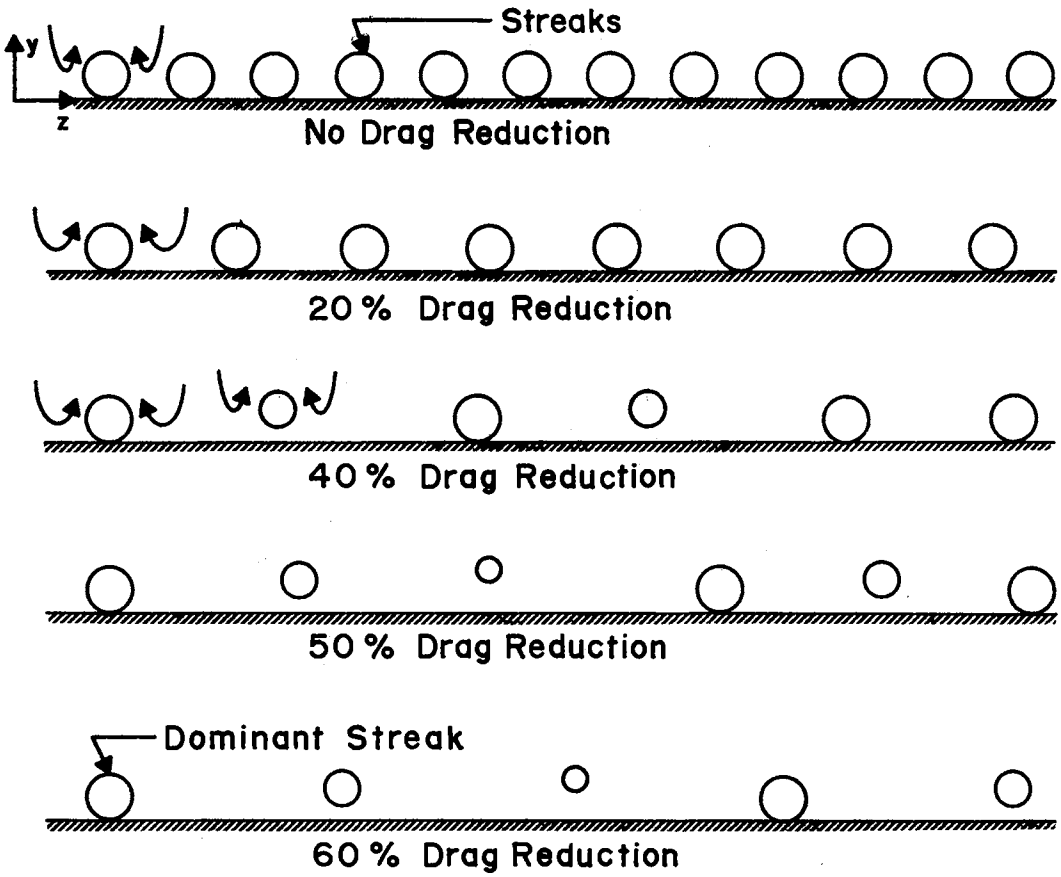

Figure 27. Proposed Near-Wall Eddy Structure Under Drag-Reducing Conditions

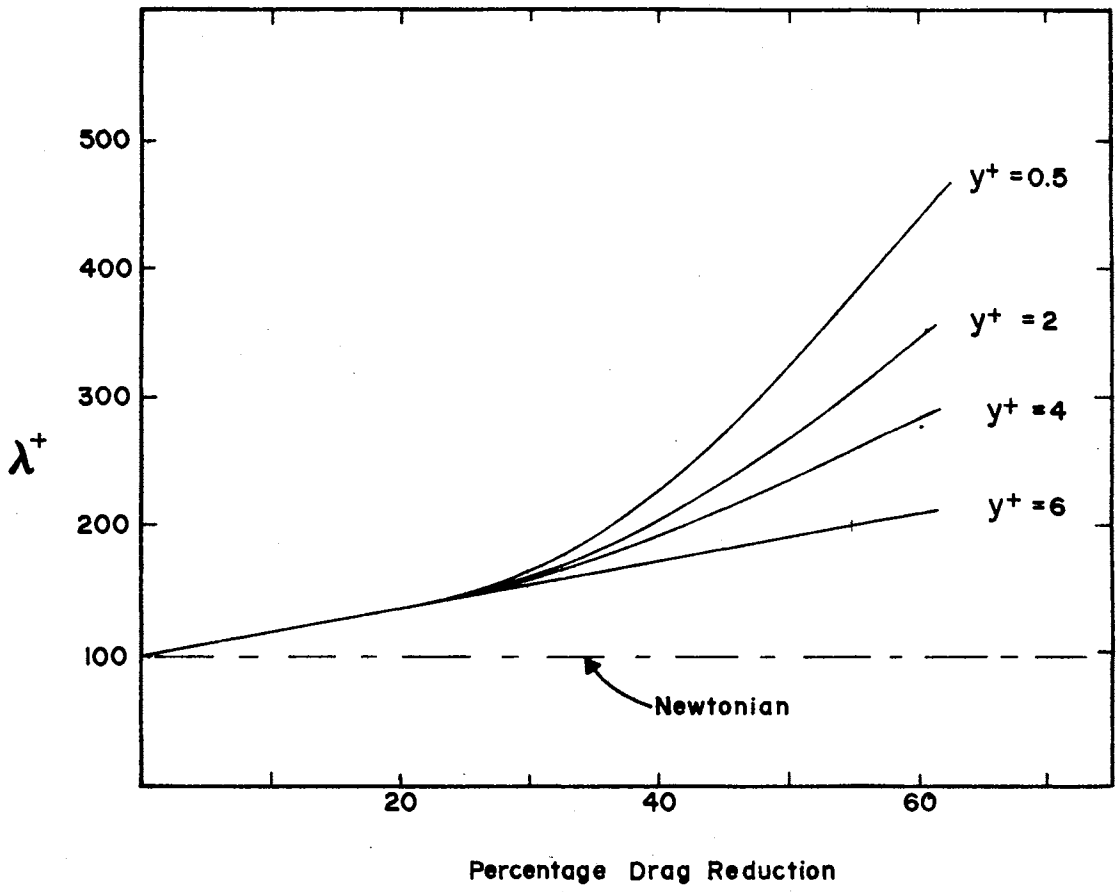

Figure 28. Expected y^+ Variation in Non-Dimensional Streak Spacing at Various Values of Drag Reduction

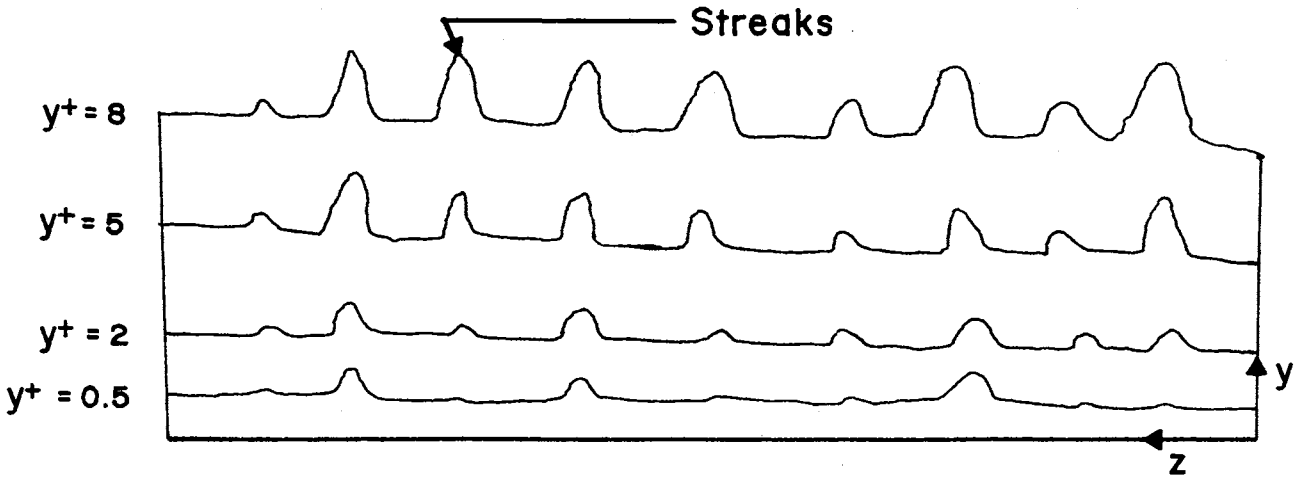

NOTE: Not to scale

Figure 29. Proposed Near-Wall Streak Structure at Large Values of Drag Reduction

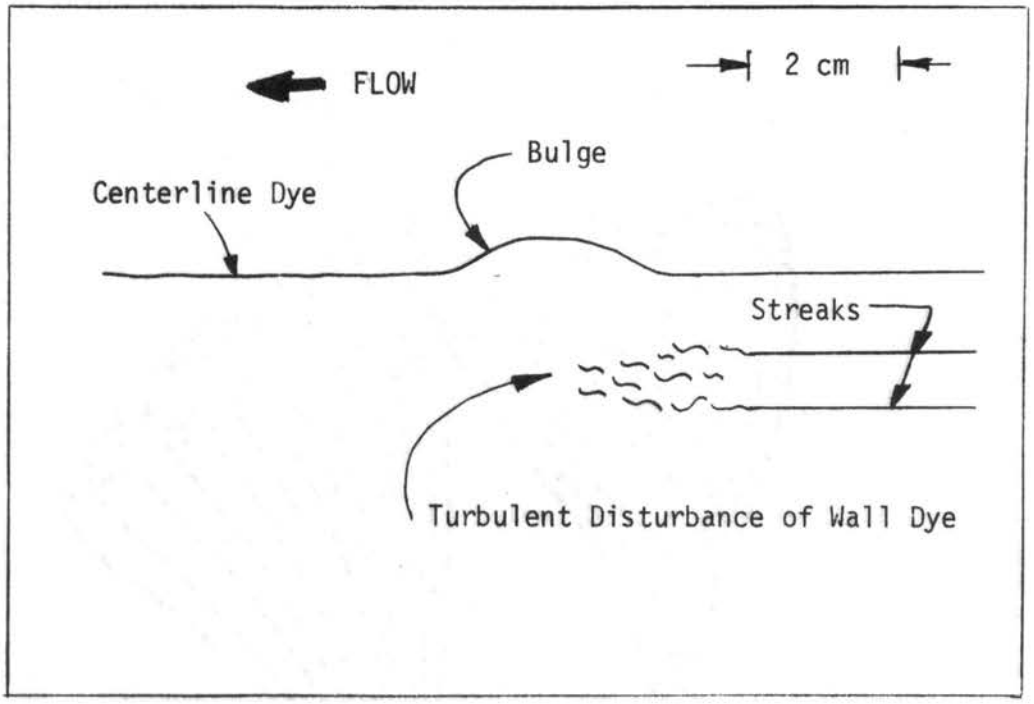

Figure 30. Sketch of the Relation Between Centerline Dye Bulge and Turbulent Wall Disturbance During Transition (AP-273, Re ≅ 7,800)

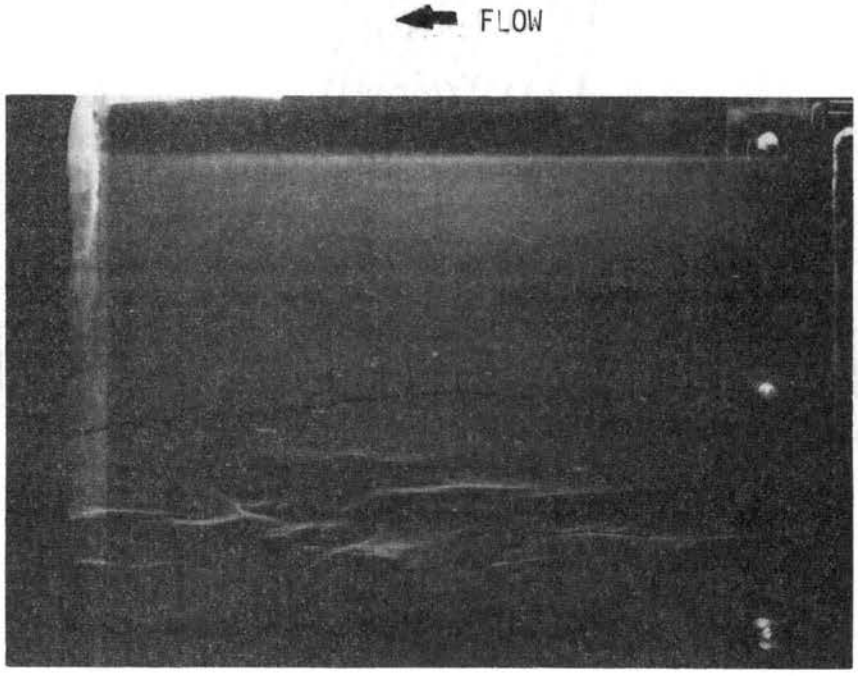

Figure 31. Patch of Wall Turbulence During Transition (AP-273, Re ≅ 8,000)

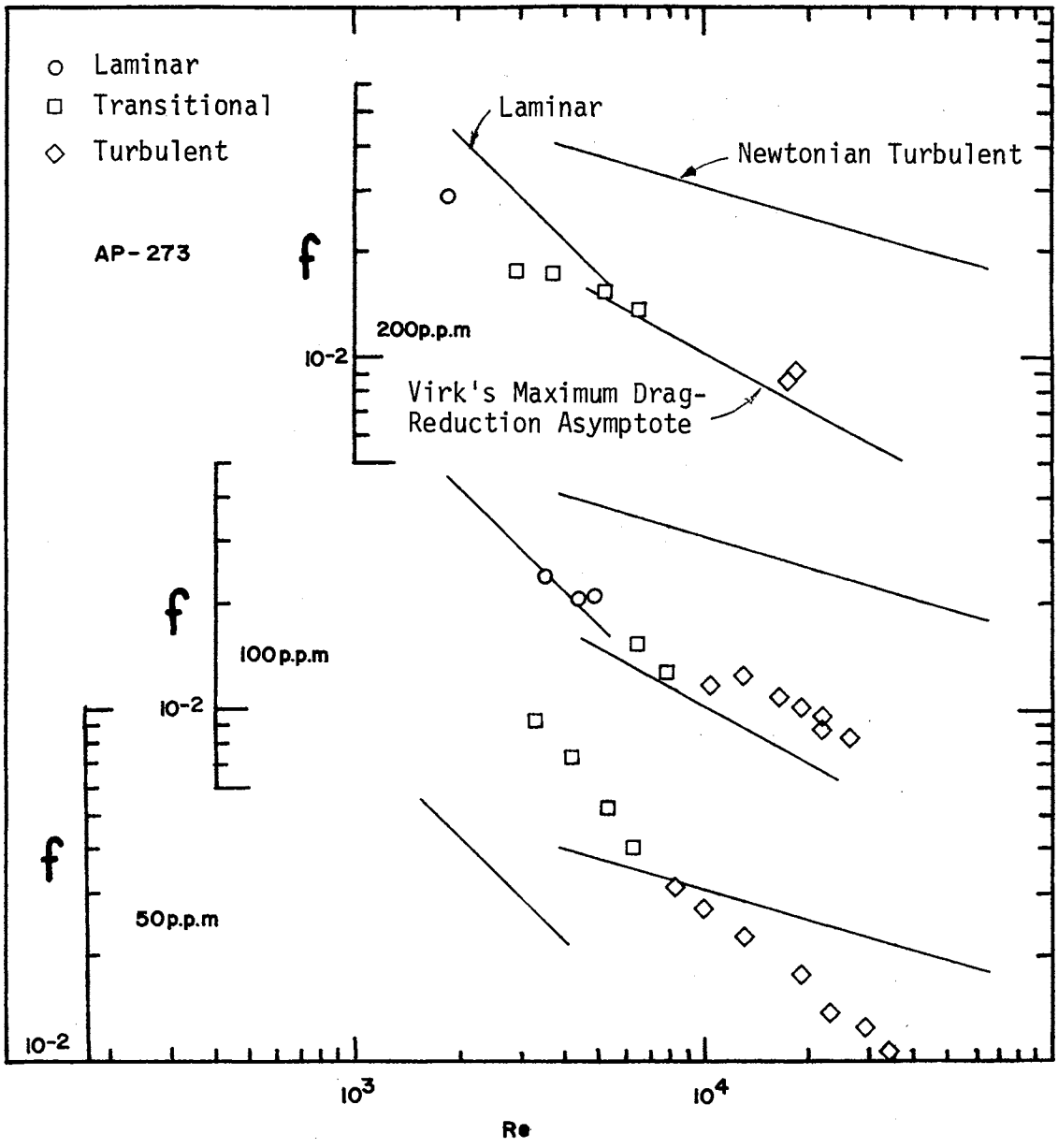

Figure 32. Visually Observed Flow Regimes Corresponding to Friction Factor Data

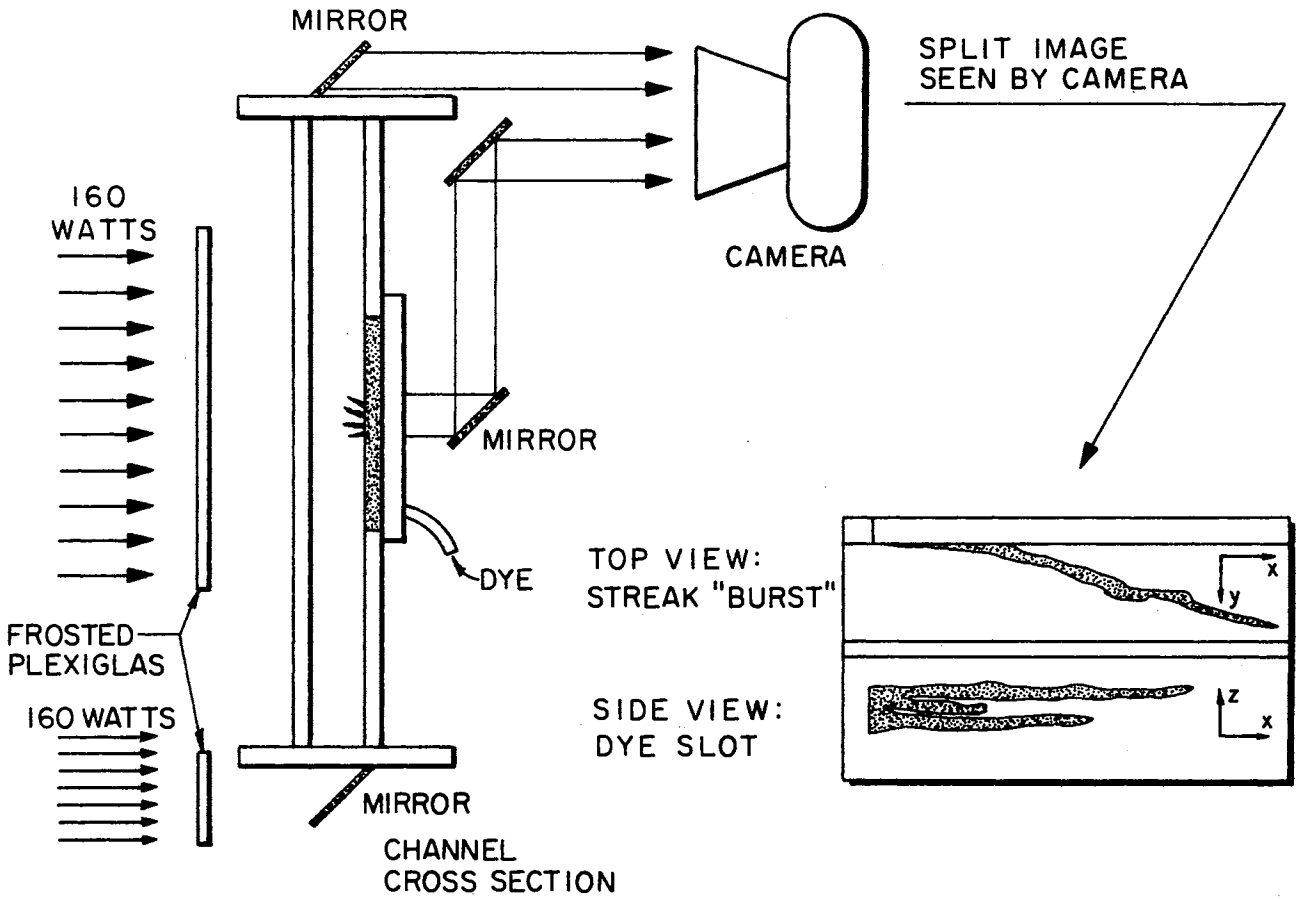

Figure 33. Back Lighting Technique for Dual View Visualization of Wall Region

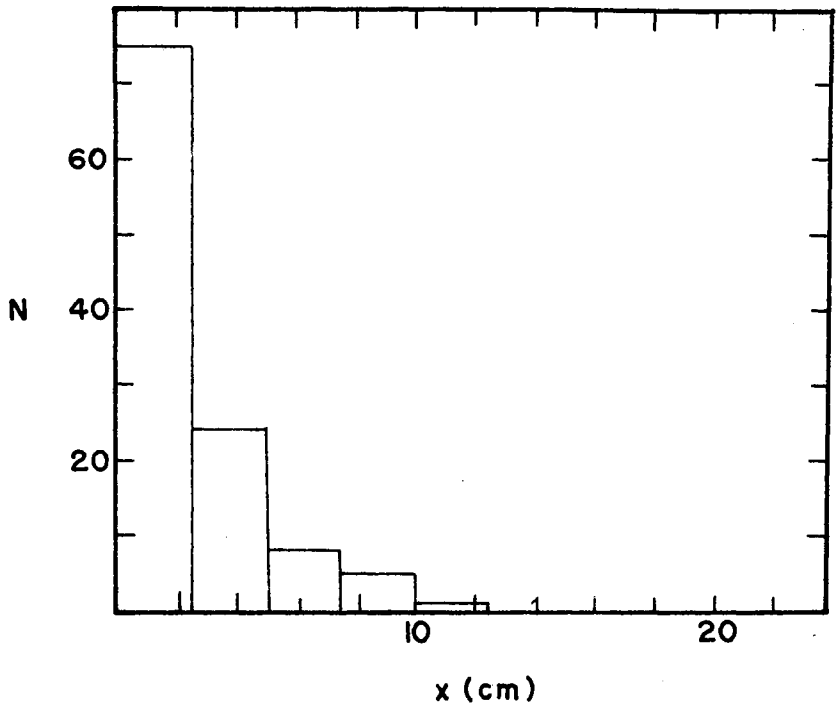

Figure 34. Streak Ejection Distribution for a Water Flow (Re = 15,400)

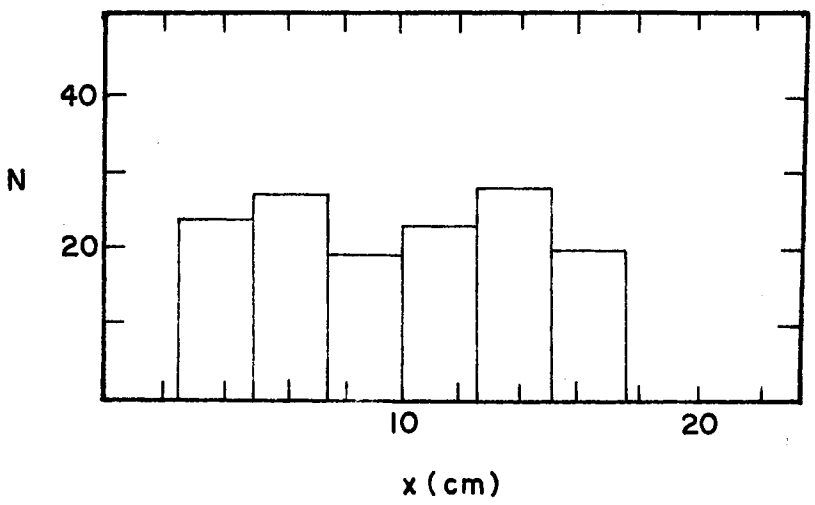

Figure 35. Streak Ejection Distribution for a Drag-Reducing Flow (Re = 10,000)

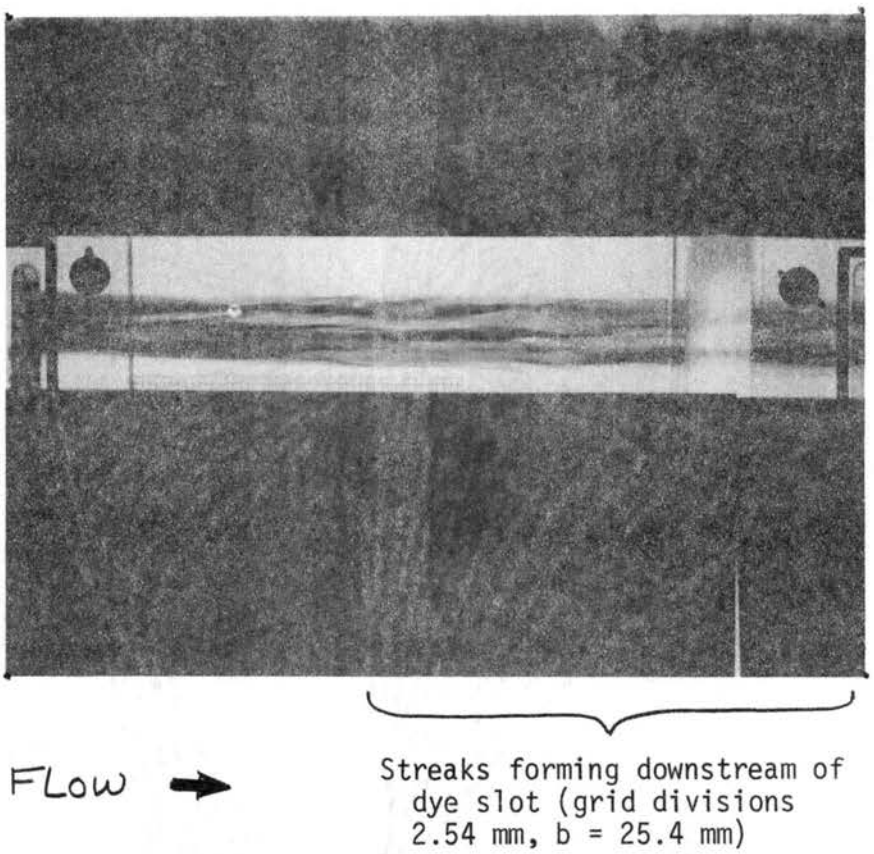

Figure 36. Near-Wall Streak Structure as Visualized Using the Back Lighting Technique (AP-273, Re = 13,000)

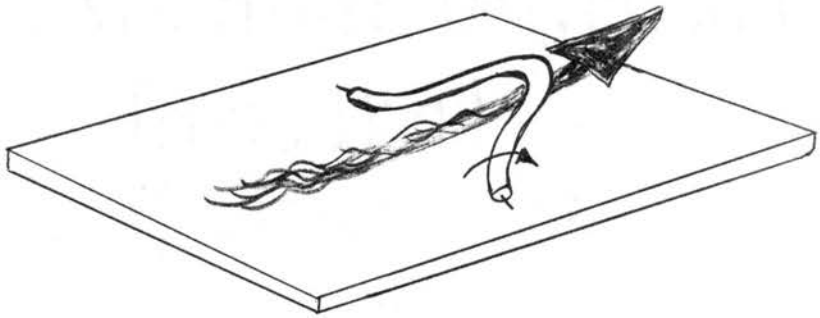

Figure 37. Vortical Motion Associated With Newtonian Streak Bursting

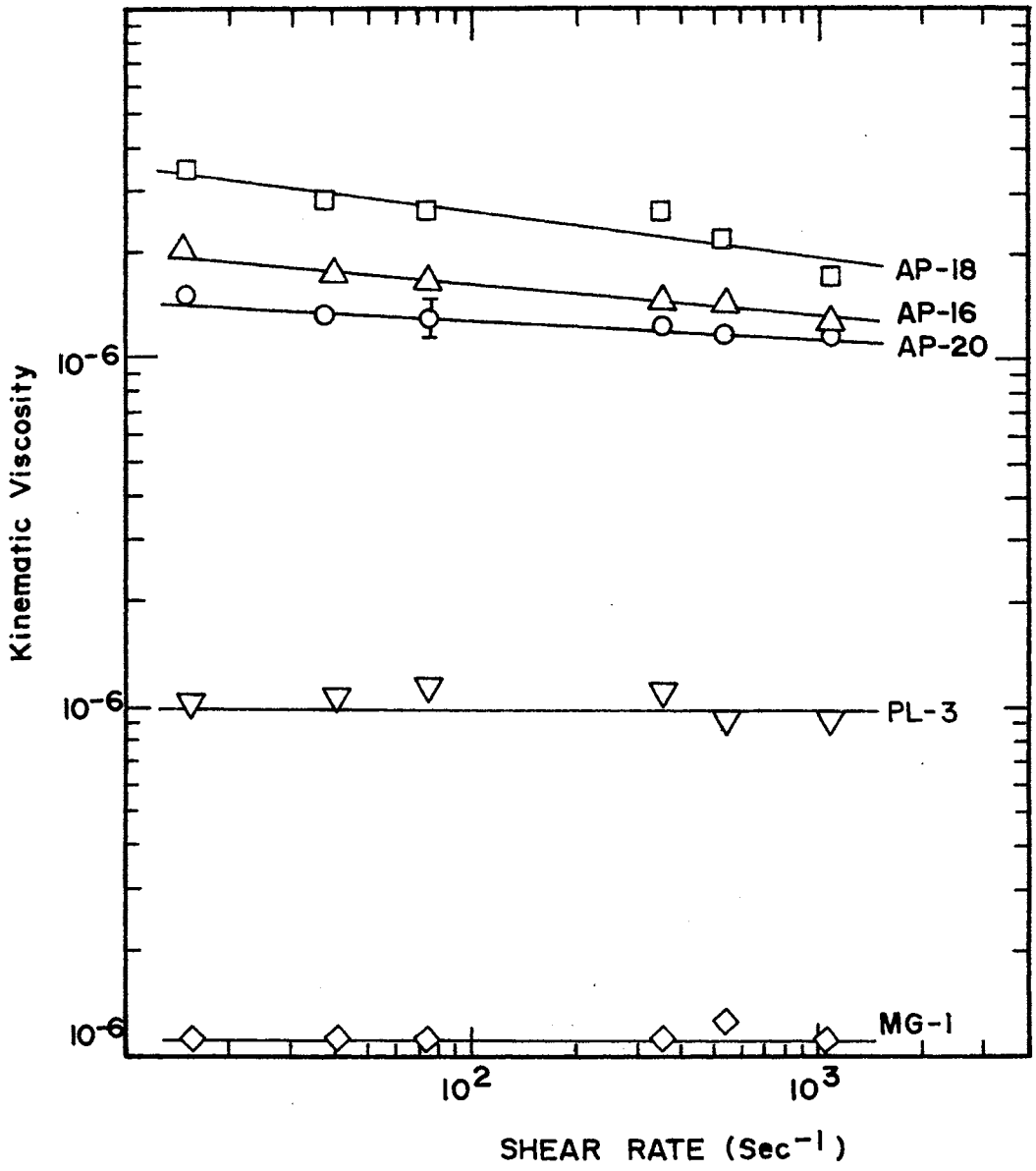

Figure 38. Viscosity-Shear Rate Dependence of the Drag-Reducing Solutions

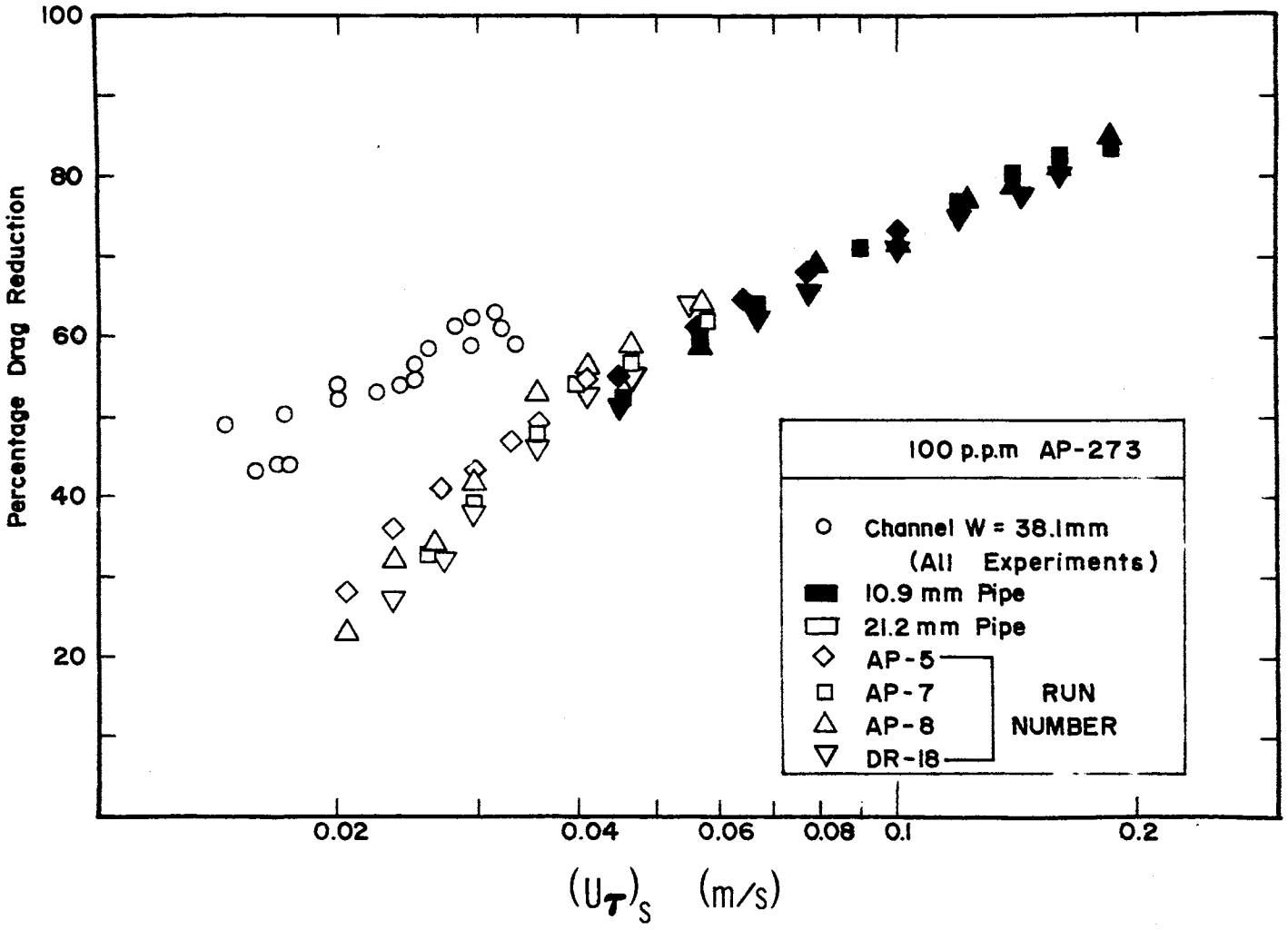

Figure 39. Drag-Reducing Characteristics of 100 p.p.m, AP-273

VITA

David Kenyon Oldaker

Candidate for the Degree of

Master of Science

Thesis: AN EXPERIMENTAL INVESTIGATION OF THE NEAR-WALL FLOW STRUCTURE DURING DRAG REDUCTION

Major Field: Mechanical Engineering

Biographical:

Personal Data: Born in Oakland, California, August 2, 1949, the son of Mr. and Mrs. C. R. Oldaker.

Education: Graduated from Oklahoma Military Academy, Claremore, Oklahoma, in May, 1970; received the Bachelor of Science degree in Mechanical Engineering from Oklahoma State University, July, 1973; completed the requirements for the Master of Science degree at Oklahoma State University in December, 1974.

Professional Experience: Commissioned Second Lieutenant, U. S. Army in July, 1973; graduate research assistant under National Science Foundation Grant GK-40609, School of Mechanical and Aerospace Engineering, Oklahoma State University, 1973-1974.